Харківський національний університет
імені В.Н. Каразіна

Фізична інженерія поверхні

Физическая инженерия поверхности

Том 11, № 3

Physical surface engineering

Vol. 11, No. 3

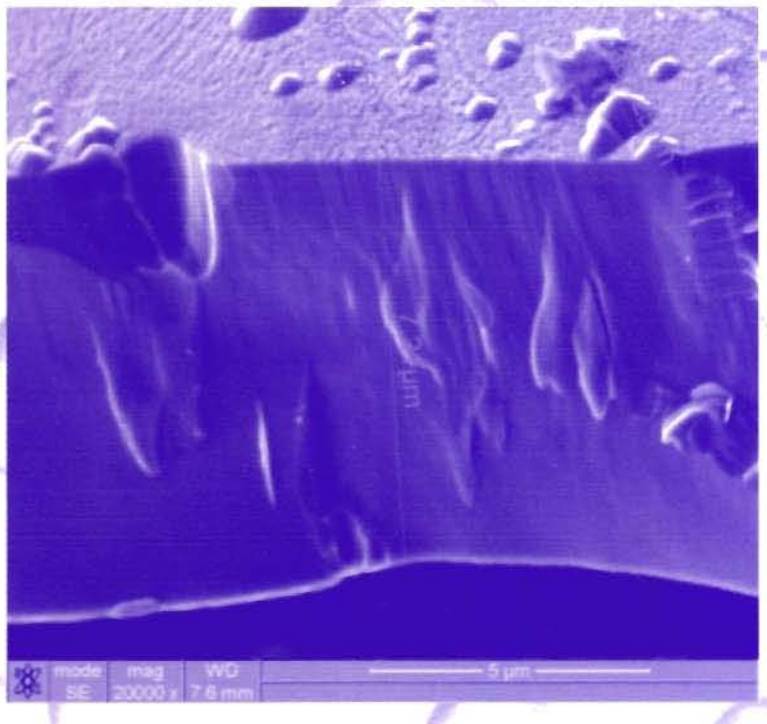

2013

ISSN 1999-8074

МІНІСТЕРСТВО ОСВІТИ І НАУКИ УКРАЇНИ
НАЦІОНАЛЬНА АКАДЕМІЯ НАУК УКРАЇНИ

ХАРКІВСЬКИЙ НАЦІОНАЛЬНИЙ УНІВЕРСИТЕТ імені В.Н. КАРАЗІНА
НАУКОВИЙ ФІЗИКО-ТЕХНОЛОГІЧНИЙ ЦЕНТР МОНМС та НАН УКРАЇНИ
КОНЦЕРН "ЦЕНТР НОВИХ ТЕХНОЛОГІЙ"
ХАРКІВСЬКИЙ ФІЗИКО-ТЕХНІЧНИЙ ІНСТИТУТ
"ЦЕНТР НАУКОВО-ТЕХНІЧНИХ ДОСЛІДЖЕНЬ"

НАУКОВИЙ ЖУРНАЛ

Фізична інженерія поверхні

Физическая инженерия поверхности

ЗАСНОВАНИЙ У 2002 РОЦІ

ВИДАЄТЬСЯ 4 РАЗИ НА РІК

Physical surface engineering

Том 11, № 3, липень – вересень 2013

ХАРКІВ 2013

Затверджено до друку рішенням
Вченої ради Харківського національного університету імені В.Н. Каразіна, (протокол № 9 від 28 жовтня 2013 р.),
Вченої ради Наукового фізико-технологічного центру, (протокол № 8 від 24 жовтня 2013 р.)

Статті пройшлм внутрішнє та зовнішнє рецензування.
Свідоцтво про державну реєстрацію КВ № 9214 від 29.09.04.

Фізична інженерія поверхні

Физическая инженерия поверхности

Physical surface engineering

Зміст
Содержание
Contents

Dzubenko M.I., Kolpakov S.N., Popov I.V., Pryyomko A.A. Use of the determined properties of a roughness of a surface in measurement of a geometrical form of object 254

Sapaev I.B. The injection photo diode on the basis of *n*Si-*n*CdS-n^+CdS heterostructures 260

Kaverin M.V., Zhollybekov B. Structure, properties and morphology of nanostructured coatings solid Ti-Si-N 263

Pylypenko M.M., Drobyshevskaya A.A. Purification of hafnium from oxygen and nitrogen 270

Guliamov G., Sharibaev N.Y., Erkaboev U.I. Definitions of localized energy states on the quasi-fermi level with changing times 275

Sayenko S.Yu., Shkuropatenko V.A., Tarasov R.V., Prudyvus K.A., Savina S.A., Zykova A.V. Analyses of fluorapatite prepared by both chemical precipitation and solid phase reaction methods 279

Sayenko S.Yu., Svitlychniy Eu.O., Lobach K.V. Application of electroconsolidation of powder components for production of ultradenced ceramics Al_2O_3 and ZrO_2(3% Y_2O_3) 285

Guliamov G., Erkaboev U.I., Sharibaev N.Y. The temperature dependence of the band GAPSi 289

Lytovchenko S.V., Beresnev V.M., Chyshkala V.A., Dmytrenko A.Ye., Nyemchenko U.S., Burkovska V.V. Silicide coatings structure optimization based on multiscale approach 293

Torianik I.N., Beresnev V.M., Pogrebnjak A.D., Sobol O.V., Beresneva Ye.V., Podcherniaieva I.A., Kropotov A.Yu., Stiervoiedov N.G., Turbin P.V., Kolesnikov D.A., Grankin S.S., Nyemchenko U.S., Srebniuk P.A., Novikov V.Yu. Magnetron sputtering of high temperature composite ceramics AlN-TiB_2-$TiSi_2$ 299

Tabatadze I.G., Jabua Z.U., Gigineishvili A.V. Optical properties of dysprosium monoantimonide thin films 304

Правила оформления рукописей 309

Правила оформлення рукописів 310

Information for authors 311

UDC 53.06

USE OF THE DETERMINED PROPERTIES OF A ROUGHNESS OF A SURFACE IN MEASUREMENT OF A GEOMETRICAL FORM OF OBJECT

M.I. Dzubenko, S.N. Kolpakov, I.V. Popov, A.A. Pryyomko

Usikov institute of radiophysics and electronics NAS of Ukraine (Kharkiv)
Ukraine

Received 01.07.2013

Classification of surfaces as roughness is carried out. The roughness can have the determined, stochastic or chaotic character, depending on a method of their forming. In the work the problem of finding of normal vector to a surface and coordinates of a point of lighting by a laser beam for the case of approximation of a roughness by a flat reflective diffraction grating is solved.
Keywords: surface, roughness, diffraction grating, coherent radiation.

ИСПОЛЬЗОВАНИЕ ДЕТЕРМИНИРОВАННЫХ СВОЙСТВ ШЕРОХОВАТОСТИ ПОВЕРХНОСТИ В ИЗМЕРЕНИИ ГЕОМЕТРИЧЕСКОЙ ФОРМЫ ОБЪЕКТА

М.И. Дзюбенко, С.Н. Колпаков, И.В. Попов, А.А. Приёмко

Проведена классификация поверхностей по типу шероховатостей. Шероховатость в зависимости от метода возникновения может иметь детерминированный, стохастический или хаотический характер. В работе решена задача нахождения вектора нормали к поверхности и координаты точки освещения лучом лазера для случая аппроксимации шероховатости плоской отражательной дифракционной решёткой.
Ключевые слова: поверхность, шероховатость, дифракционная решетка, когерентное излучение.

ВИКОРИСТАННЯ ДЕТЕРМІНОВАНИХ ВЛАСТИВОСТЕЙ ШОРСТКОСТІ ПОВЕРХНІ У ВИМІРІ ГЕОМЕТРИЧНОЇ ФОРМИ ОБ'ЄКТУ

М.І. Дзюбенко, С.Н. Колпаков, І.В. Попов, А.А. Приемко

Проведена класифікація поверхонь за типом шорсткостей. Шорсткість залежно від методу виникнення може мати детермінований, стохастичний або хаотичний характер. У роботі вирішено завдання знаходження вектора нормалі до поверхні і координати точки освітлення променем лазера для випадку апроксимації шорсткості плоскими відбивними дифракційними гратками.
Ключові слова: поверхня, шорсткість, дифракційні грати, когерентне випромінювання.

Surface of objects can have various character of a roughness (fig. 1). The roughness, as a rule, is formed as a result of external mechanical (or another) impacts on object, for example, polishing. The surface with the determined roughness turns out by impact on object of the determined process. For example, diffraction gratings possess such surface. The surface with a stochastic roughness is formed at action on object of several processes some of which are determined, and others are casual. The surface with a chaotic roughness turns out at impact on object of chaotic process, for example, a polishing by a sand stream. In many cases it is possible to present a roughness of surfaces of the first two types as a combination of several diffraction gratings with various options of their relative positioning (fig. 2).

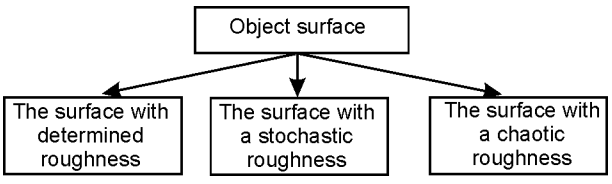

Fig. 1. Object surfaces classification.

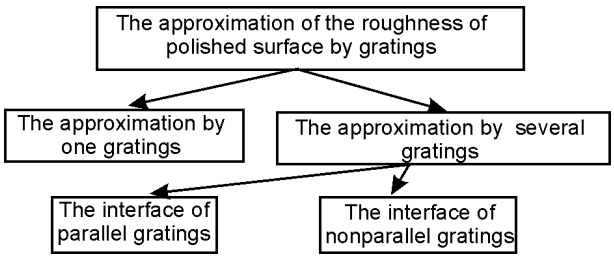

Fig. 2. The approximation of the roughness of polished surfaces by gratings.

The simplest case – one diffraction grating use. At approximation by several gratings there are options of their relative positions, there is need to enter concept of conjugation of gratings. Conjugation defines mechanical ways of their imposing at each

other. So, the diffraction pattern, received at interaction of coherent radiation with similar surfaces, represents quite determined structure (fig. 3) [1].

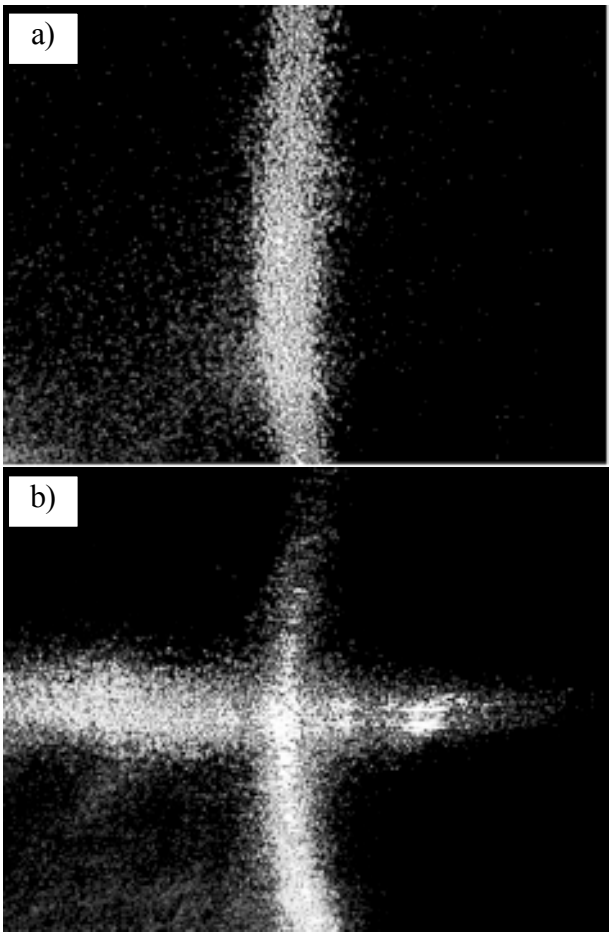

Fig. 3. Diffraction patterns received from surfaces after mechanical machining. a) – one polishing direction, b) – polishing was made in two directions.

Diffraction maxima from each of gratings form a diffraction curve. The quantity of diffraction curves in a diffraction pattern corresponds to the quantity of the diffraction gratings which have taken part in formation of a roughness of this surface. The considered model of roughness gives the grounds to apply the diffraction methods based on approach of Fresnel-Kirchhoff [2, 3]. For the solution of a number of tasks, as well, the geometrical theory of diffraction is used [4].

The result of diffraction depends on a ratio of the spatial sizes of a beam and object. When a diameter of a beam is much smaller then the spatial extent of object, the result of section of a beam and a surface represents the tangent plane to this surface. In this case the object surface unambiguously is defined by a set of the tangent planes in each point of a surface. For this case the primary measuring information in the analysis of a geometrical form are parameters of a normal to a surface in a point of lighting and coordinate of this point.

In this work the theoretical and experimental research of the diffraction picture, received as a result of interaction of coherent radiation with a surface, was made for the purpose of measurement of parameters of a normal and coordinates of a point of lighting.

Two options of the achievement of objective point are possible. The first: the diffraction picture in the aperture plane of the receiver is analyzed. In this case the contradiction between the sizes of the receiver and the picture demands permission. The second option assumes formation of a diffraction picture on the coordinate screen. In this work the second case, as more interesting from the practical point of view, is considered.

Let's consider diffraction of coherent radiation on one-dimensional reflecting grating for inclined falling of a beam. Thus, the beam is focused arbitrarily in relation to strokes of a grating (fig. 4). The flat wave, which direction of distribution is defined by corners θ and φ, falls on a grating. The angular spectrum of diffracted light is described by the following expression [5]:

$$F(k_x,k_y)=\frac{1}{(2\pi)^2}\int_{-\infty}^{\infty}\int u(x,y,0)\exp[-i(k_x x+k_y y)]dxdy. \quad (1)$$

There $u(x, y, 0)$ – an intensity of electric field in a point $(x, y, 0)$;

$k_x = k\cdot\cos\theta$, $k_y = k\cdot\cos\varphi$, $k = 2\cdot\pi/\lambda$;

λ – wave length of the used radiation.

The angular range of a falling flat wave looks like:

$$F_1(k_x, k_y) = \delta(k_x)\cdot\delta(k_x). \quad (2)$$

The angular spectrum of a field after diffraction on a grating is equal to convolution of an angular spectrum of a falling wave F_1 and function of reflection amplitude coefficient of a grating $\Phi(x)$ [5]:

$$F(k_x,k_y)=\int_{-\infty}^{\infty}\int F_1(\xi,\eta)\Phi(k_x-\xi,k_y-\eta)d\xi d\eta. \quad (3)$$

For infinite uniform periodic structure the range of coefficient of reflection is:

$$\Phi(k_x,k_y)=\sum_{n=-\infty}^{n=\infty}a_n\delta(k_y)\delta\left(k_x-\frac{2\pi\cdot n}{d}\right), \quad (4)$$

where n – a number of a diffraction order; d – a

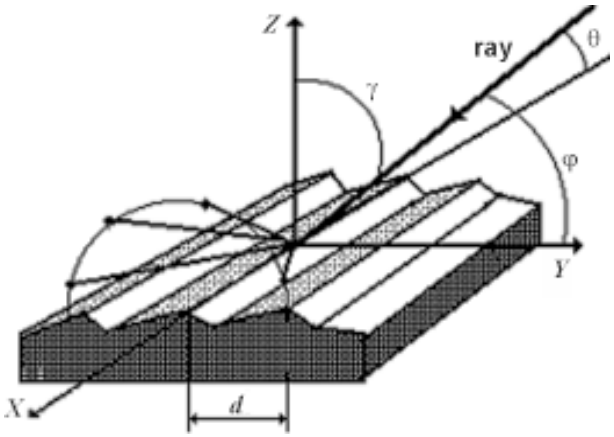

Fig. 4. Diffraction on a grating.

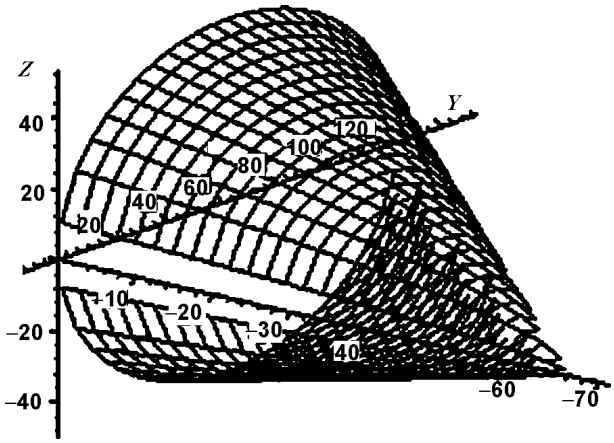

Fig. 5. Surface, formed by diffraction orders.

grating period; a_n – coefficient of Fourier number of amplitude coefficient of reflection of a grating:

$$a_n = \frac{1}{d}\int_{-d/2}^{d/2} R(x)\exp\left[-i\frac{2\pi\cdot n\cdot x}{d}\right]dx.$$

$R(x)$ – is defined by concrete model of diffraction structure of a surface and the direction of beam falling on it. Substituting (2) and (4) in (3) and carrying out integration, we will receive an angular spectrum of a field after diffraction on a grating [6]:

$$F(k_x,k_y) = \sum_{n=-\infty}^{\infty} a_n \delta\left(k_y - k\left(\cos\varphi - \frac{2\pi\cdot n}{d}\right)\right)\cos(k_x - k\cos\theta).$$

From the last expression we define directing cosines of diffraction orders:

$$\cos\theta_n = \cos\theta,\ \cos\varphi_n = \cos\varphi - n\lambda/d,$$

$$\cos\eta_n = \sqrt{\sin^2\theta - \left(\cos\varphi - \frac{n\lambda}{d}\right)^2}. \qquad (5)$$

Apparently from (5), next ratio is true for any orders: there k_n – a single vector of n – order of diffraction in the direction of distribution, $i(1, 0, 0)$ – ort in the direction of the OX axis (fig. 4).

Thus, at normal falling of a beam on a surface the diffraction maxima lie on a straight line. In this case formation of diffraction orders is described by classical laws of diffraction of a beam on a grating [7, 8]. At diffraction of randomly focused beam all diffraction orders lie on a surface of the circular angle, which axis coincides with the OX axis, and the corner at top is equal $2\cdot\beta$ (fig. 5). It was confirmed completely by experimental check [9].

Section of a similar surface by the plane of the screen leads to that diffraction orders on the plane of the receiver form diffraction maxima as the curve of the second order (fig. 6).

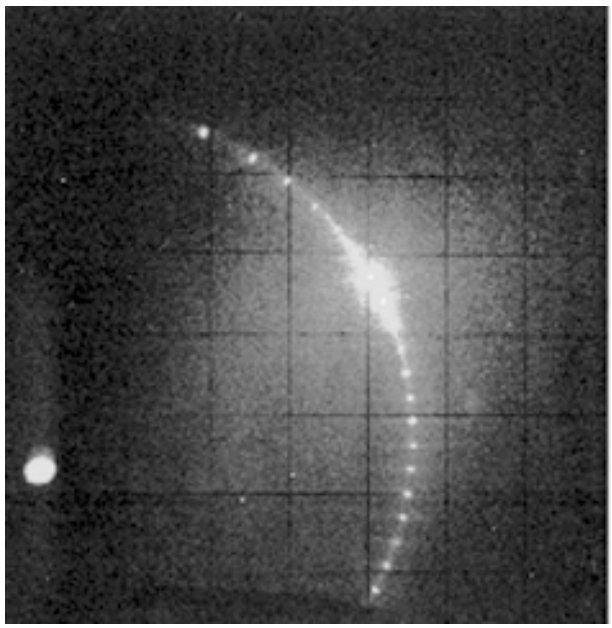

Fig. 6. Diffraction maxima at arbitrary falling of a beam on a grating.

The third formula in (5) defines the quantity of diffraction orders at a beam assumed position concerning grating strokes. Recognizing that a radicand shouldn't be negative, the maximum number of diffraction orders is defined by the following expression:

$$N = \frac{d}{\lambda}(\sin\theta + \cos\varphi).$$

The system of coordinates, in which it is necessary to define the position of a normal to a surface and coordinates of a point of lighting, is formed by the plane of the screen, on which the diffraction pattern is formed, and a perpendicular to it. The position of a beam in this system of coordinates is described by the straight line equation:

$$\frac{x-x_b}{u_{xb}}=\frac{y-y_b}{u_{yb}}=\frac{z-z_b}{u_{zb}},$$

there x_b, y_b, z_b – coordinates of a point of the falling of a beam on the screen; u_{xb}, u_{yb}, u_{zb} – directing cosines of the straight line, containing a beam.

The perpendicular to the screen forms an axis X, the beginning of coordinate lies on the screen. Therefore $x_b = 0$. Directing cosines of diffraction orders (5) are found in the system of coordinates formed by a diffraction grating. The analysis of a diffraction pattern is kept in system of coordinates formed by the screen. The equations of the plane, that is tangent to a surface, also are in this coordinate system. Therefore for the processing of a diffraction pattern it is necessary to find coordinates of directing vectors of diffraction orders in screen system of coordinates.

The solution of this task assumes the definition of a matrix of transition from one system of coordinates to another. Thus, some properties of the diffraction curves should be noted, allowing connect coordinates of diffraction maxima on the screen with coordinates of a point of lighting and parameters of the tangent plane to a surface. As it was already noted, diffraction orders form a circular conic surface in space. As a result of a section of this surface by a flat screen diffraction curves represent second order curves. In this task the spatial position of a beam was set so that diffraction curves have ellipse forms. Cases of a parabola, hyperbole and straight line are almost unrealizable. The parabolic form turns out in case of a screen arrangement strictly parallel to a forming conic surface, hyperbolic – strictly parallel to a cone axis, the straight line turns out only when the projection of an incident beam to a grating is parallel to its strokes.

For transformation of coordinates of directing vectors of diffraction orders the oblique-angled system of coordinates formed by the screen and a beam of the laser was interpolated. At first coordinates were transformed from the system of coordinates connected with a grating in system of coordinates, connected with a beam, and then from this system of coordinates to system of coordinates formed by the screen. Such two-level approaching allowed us considerably reduce time of computing procedures.

The matrix of transition T_{b0} from the oblique-angled system of coordinates, formed by a beam and the screen, in rectangular system, formed by the screen and a perpendicular to it, is:

$$T_{b0}=\begin{bmatrix}\cos\delta_x & \cos\delta_y & \cos\delta_z\\ 0 & 1 & 0\\ 0 & 0 & 1\end{bmatrix}.$$

There δ_x, δ_y, δ_z – the angles between a falling beam and axes of rectangular system of coordinates.

The following step is calculation of a matrix of transition T from system of coordinates of a grating in system of coordinates of a beam. For this purpose it is necessary to find the equation of the straight line containing diameter of an ellipse on the screen. The ellipse, as a second order curve, unambiguously is defined by coordinates of five points. The beam is generator of conic surface. Therefore its point of intersection with the screen lies on a considered ellipse. Thus, for a complete definition of an ellipse it is necessary to measure coordinates of four maxima on a diffraction curve. The equation of the ellipse passing through five points with coordinates (y_1, z_1), (y_2, z_2), (y_3, z_3), (y_4, z_4), (y_5, z_5) looks like [10]:

$$\begin{vmatrix} y^2 & yz & z^2 & y & z & 1\\ y_1^2 & y_1z_1 & z_1^2 & y_1 & z_1 & 1\\ y_2^2 & y_2z_2 & z_2^2 & y_2 & z_2 & 1\\ y_3^2 & y_3z_3 & z_3^2 & y_3 & z_3 & 1\\ y_4^2 & y_4z_4 & z_4^2 & y_4 & z_4 & 1\\ y_5^2 & y_5z_5 & z_5^2 & y_5 & z_5 & 1 \end{vmatrix}=0$$

Calculation of determinant of this matrix gives the ellipse equation.

There A, B, C, D, E – equation coefficients. Passing simple, but quite bulky mathematical calculations, we will write down a matrix of transition T from rectangular system of coordinates of a grating to the oblique-angled system of coordinates formed by a beam and the plane of the screen, consisting of directing cosines of the axes, that form system of coordinates, connected with a grating, in the system of coordinates, connected with a beam:

$$T_{gb}=\begin{bmatrix}u_{xx} & u_{xy} & u_{xz}\\ u_{yx} & u_{yy} & u_{yz}\\ u_{zx} & u_{zy} & u_{zz}\end{bmatrix}.$$

To find coordinates of directing vectors of diffraction orders in the system of coordinates, formed by the plane of the screen and a perpendicular to it, the following equation must be solved

$$X=T_{b0}^{-1}\left[T_{gb}^{t}\cdot X_g\right]. \qquad (6)$$

There $X(u_x, u_y, u_z)$ – a required directing vector;

$X_p(u_{xg}, u_{yg}, u_{zg})$ – a directing vector of diffraction orders in system of grating coordinates, it is defined by expressions (5).

Angles θ and φ, which define the position of a normal to a surface in a lighting point, are in the equation (6). Knowing coordinates (y_n, z_n) of n-th diffraction maximum on the screen, it is possible to write down the equation of n-th diffraction order

$$\frac{x}{u_x(\varphi,\theta,n)} = \frac{y-y_n}{u_y(\varphi,\theta,n)} = \frac{z-z_n}{u_y(\varphi,\theta,n)}. \quad (7)$$

The point of illumination of a surface with coordinates (x_b, y_b, z_b) belongs to a straight line (7), therefore the following equalities have to be carried out

$$\frac{x_b}{u_x(\varphi,\theta,n)} = \frac{y_b-y_n}{u_y(\varphi,\theta,n)} = \frac{z_b-z_n}{u_y(\varphi,\theta,n)}. \quad (8)$$

From expression (8) it follows that coordinates of three diffraction maxima completely define the equation of the plane tangent to a surface in a lighting point, and coordinates of this point. I.e. the system decision

$$\begin{cases} \dfrac{x_b}{u_x(\varphi,\theta,n)} = \dfrac{y_b-y_n}{u_y(\varphi,\theta,n)}, \\ \dfrac{x_b}{u_x(\varphi,\theta,n)} = \dfrac{z_b-z_n}{u_z(\varphi,\theta,n)}, \\ \dfrac{x_b}{u_x(\varphi,\theta,m)} = \dfrac{y_b-y_m}{u_y(\varphi,\theta,m)}, \\ \dfrac{y_b-y_m}{u_y(\varphi,\theta,m)} = \dfrac{z_b-z_m}{u_z(\varphi,\theta,m)}, \\ \dfrac{y_b-y_h}{u_y(\varphi,\theta,h)} = \dfrac{z_b-z_h}{u_z(\varphi,\theta,h)}, \end{cases}$$

there n, m, h – the numbers of diffraction maxima, allows to calculate (x_b, y_b, z_b) and φ, θ – angles.

Substituting the found values of θ and φ angles in the equation (6) we find coordinates (u_{xk}, u_{yk}, u_{zk}) of directing vector of a normal to the tangent plane. The required equation of the tangent plane is.

Thus, the measured coordinates of three diffraction maxima in a diffraction pattern allow calculate the coordinates of laser lighting point on a surface and directing cosines of a vector of a normal to a surface in a lighting point.

The roughness of a surface is approximated by a reflective diffraction grating. As model the reflective diffraction grating with the period of 5 microns was used. Ne-Ne LG-208 laser forms a beam with a diameter of 1.5 mm and divergence 1.2 mrad. Wave length of the laser radiation is 0.6328 microns. The screen represents diffusely reflecting plane, with the coordinate grid put on it. In the experiment the graph paper pasted on glass was used. The screen size is 350 to 280 mm.

The laser beam incidence was normal to the screen. It allowed create in space three-dimensional system of coordinates in which all measurements have been carried out. The point of a beam incidence on the screen corresponded to the origin of coordinates (fig. 7).

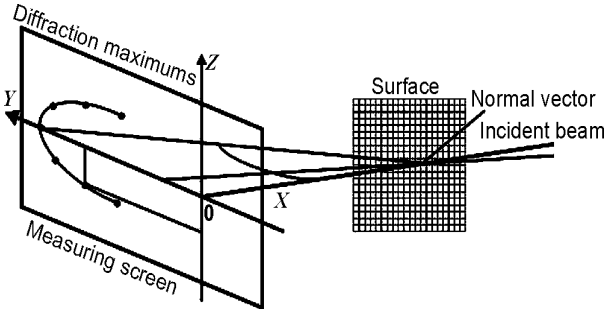

Fig. 7. Scheme of experiment.

The diffraction grating was located on a small rotary table perpendicular to the XOY plane. The angle г was fixed by means of indication of a small rotary table. It allowed install a grating with exact knowledge of its spatial parameters. At this relative positioning of a beam and the screen the attitude of a point of lighting is defined completely by distance l from the origin of coordinates to it. Thus, the point of lighting has coordinates (l, 0, 0).

The true attitude of the grating plane is defined by the equation.

True coordinates of a point of illumination on a grating surface $B(141.5, 0, 0)$.

As a result of diffraction the diffraction curve is formed on the screen. The measured coordinates of diffraction maxima are specified in tab. 1.

Table 1

Y, mm	144.5	203.7	210	142.5
Z, mm	82.5	31.5	0	–82.5

On the basis of these points coordinates and a point of intersection of a beam with the screen the equation of the ellipse approximating a diffraction curve (fig.8) was received

$$-0.444y^2 + 0.018yz - 0.623z^2 + 93.32y - 2.236z = 0.$$

The algorithm of restoration of the equation of the plane is based on theoretical conclusions produced above.

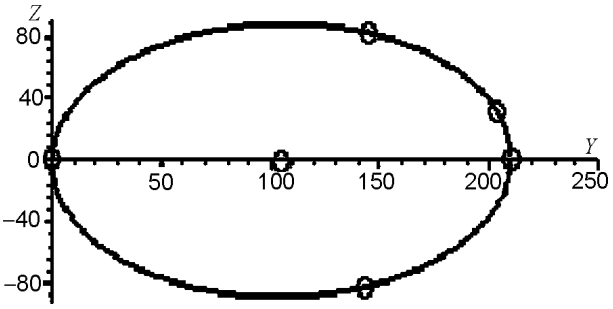

Fig. 8. Diffraction curve.

As a result the following equation of the plane of a grating (fig. 9) has turned out. The values of the measured coordinates of a point of lighting are (139.2, 0, 0). So, the relative error of measurement of coordinates was 1,6%. For the estimation of an error of the restored plane position next corners were calculated:

– between the true position of the plane and measured one – 0.36, 0;

– between the restored plane and the plane of coordinates XOY (the true plane is perpendicular to XOY plane) – 90.29, 0.

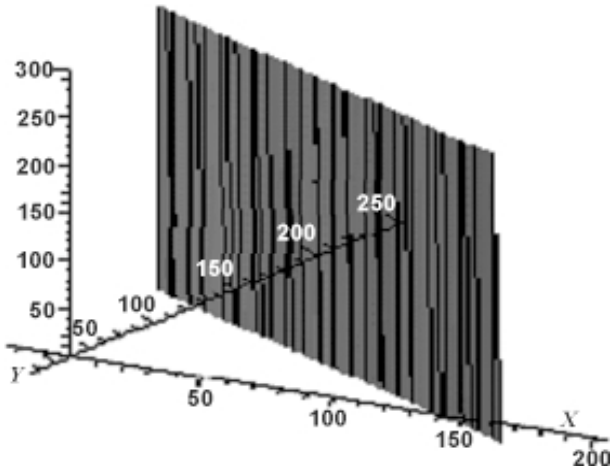

Fig. 9. Restored plane.

The made experiments on restoration of the equation of the plane in space completely confirmed theoretical conclusions. Distinctions in spatial positions of the true and restored planes are caused by the following factors:

– inaccuracy of measurement of coordinates of diffraction maxima on the screen because of their ellipticity;

– divergence of laser radiation wasn't considered in calculations;

– intensity distribution in diffraction maxima wasn't considered in calculations;

– inaccuracy of measurement of true position of a grating.

CONCLUSION

Approximation of roughness of a surface by integration of reflective diffraction gratings allowed to measure normal parameters in a point of lighting by a beam of the laser and coordinate of this point. Measurements were made on the basis of the analysis of the diffraction field, received as a result of interaction of coherent radiation with a surface. These data from all surface of object allow measure its geometrical form unambiguously.

The material presented in article can be of interest for developers of monitoring systems of a geometrical form of products of mechanical engineering, for example shovels of gas-turbine engines.

REFERENCES

1. Dzubenko M.I., Kolpakov S.N., Popov I.V., Pryyomko A.A. Diffraction of coherent radiation on surfaces having non Gaussian statistics of roughness//Radiophysics and electronics. – Vol.17, № 4. – P. 92-97.
2. Nasarov V.N., Lin'kov A.E. Diffraction methods of control of geometric parameters and spatial positioning of objects//Optical magazine. – 2002. – Vol. 69, № 2. – P. 76-81.
3. Born M., Vol'f E. Basis of optics. – M.: Science, 1970.
4. Borovikov V.A., Kinber B.E. Geometric theory of diffraction. – M.: Communication, 1978. – 247 p.
5. Vinogradova M.B., Rudenko O.V., Suhorukov A.P. Theory of waves. – M.: Science, 1979. – 384 p.
6. Volkov V.V. et al. Measuring of dimensions of integrated circuits taking into account real profile of etching by diffraction pattern//Microelectronics. – 1984. – Vol.13, ed.1. – P. 64-72.
7. Shestopalov V.P., Kirilenko A.A., Masalov S.A., Sirenko Yu.K. Resonant scattering of waves. V. 1. Diffraction gratins. – K.: Scientific mind, 1986. – 232 p.
8. Andrenko S.D., Evdokimov A.P., Sidorenko Yu.B., Shestopalov V.P. Features of scattering of waves from skew grating. – Kharkiv: AS USSR Preprint №244, 1984. – 40 p.
9. Lahno V.I., Priyomko A.A. Speckle method of measuring of configuration of industrial products //Col. Of Sci. Articles KhStTURE. – 1999. – Vol. 1. – P. 105-108.
10. Korn G., Korn T. Reference book on mathematics. – M.: Science, 1984. – 831 p.

УДК 53.043;53.023;539.234.

THE INJECTION PHOTO DIODE ON THE BASIS OF *n*Si-*n*CdS-n^+CdS HETEROSTRUCTURES

I.B. Sapaev

Physical Technical Institute of the Academy of Sciences of the Republic of Uzbekistan (Tashkent) Uzbekistan

Received 02.07.2013

It is shown that the *n*Si-*n*CdS-n^+CdS heterostructures in operative (carrying) direction of current, while being exposed to low intensity radiation, operate as injection photodiodes. Their current sensitivity is $S_\lambda \approx 2.12$ A/W at $\lambda = 0.625$ μm, which effectively represents a 4.2 increase in compare to spectral sensitivity of the ideal photo receiver at small wavelength of irradiation.

Keywords: heterostructure, film, spectrum, injection.

ИНЖЕКЦИОННЫЙ ФОТОДИОД НА ОСНОВЕ *n*Si-*n*CdS-n^+CdS ГЕТЕРОСТРУКТУРЫ

И.Б. Сапаев

Показано, что гетероструктуры *n*Si-*n*CdS-n^+CdS в пропускном направлении тока при малых уровнях освещения работают как инжекционный фотодиод. Они обладают токовой чувствительностью $S_\lambda \approx 2.12$ A/W при $\lambda = 0.625$ μm, что в 4.2 раза превышает спектральную чувствительность идеального фотоприемника при этой длине волны излучения. Высокие значения S_λ обеспечивают высокую эффективность превращения световой энергии в электрическую при малых уровнях освещенности.

Ключевые слова: гетероструктура, пленка, спектр, инжекционный.

ІНЖЕКЦІЙНИЙ ФОТОДІОД НА ОСНОВІ *n*Si-*n*CdS-n^+CdS ГЕТЕРОСТРУКТУРИ

І.Б. Сапаєв

Показано, що гетероструктури *n*Si-*n*CdS-n^+CdS у пропускному напрямку струму при малих рівнях освітлення працюють як інжекційний фотодіод. Він має струмову чутливість $S_\lambda \approx 2.12$ A/W при $\lambda = 0.625$ μm, що в 4.2 разів перевищує спектральну чутливість ідеального фотоприймача при цій довжині хвилі випромінювання. Високі значення $S_л$ забезпечують високу ефективність перетворення світлової енергії в електричну при малих рівнях освітленості.

Ключові слова: гетероструктура, плівка, спектр, инжекційний.

Injection photodiodes based on n^+-n transitions or Schottky barrier are normally made of high resistance semiconductors characterized by large length of diffusive displacement, whereas thickness of the base area (distance from the injected contact to the second one) tremendously exceeds (several times) the diffusive displacement length – "long diodes" [1]. Such type photodiodes operate in the mode of high levels of injection. The carrying capacity of their base area is determined by injected carriers. The injection photodiodes are developed and investigated on various types of semiconductors (doped Germanium and Silicon, Gallium Arsenide and Indium Antimonide, solid alloys of A^2B^5 compounds and other materials) [2]. However, there is virtually no information in the literature on how to develop injection photodiodes based on Si-CdS heterostructures. Such structures are characterized by astonishing interrelation of electrical and photoelectrical properties both of pertinent Si and CdS. Such structures are characterized also by direct optical transitions that help to obtain a high efficiency of generation of electron-hole pairs.

The photosensitive n^+CdS-*n*CdS-*n*Si structure has been created by dusting of CdS-powders (in quasi-closed system in vacuum 10^{-5} torr) on the surface of silicon plate of *n*-type with the specific resistance $\rho \approx 15$ Ohm·cm and thickness of 300 – 400 мм. Thus the source temperature was (CdS) $T_{source} \approx 800 - 850$ °C, and on the substrate (*n*Si) it was supported in limits $\approx 250 - 270$ °C. The carried out researches by means of microscope MII-4 have shown, that films CdS consist of columnar grains to be focused in the direction of the films growth and disarranged on an azimuth. It has been established, that the size of crystallites strongly depends on technological modes and first of all on temperature of Si substrate. For example, made at $T_{substrate}$ =

250 °C films CdS had the size of crystallites ≈0,8 – 1 мм which completely penetrated all thickness of films $d \approx 1$ μm. Thus, grown up CdS films were high-resistant with specific resistance $\rho \geq 10^8$ Ohm·cm. Further, on CdS film was formed n^+CdS layer by thickness ~500 Å and current-collecting "П" – figurative contact by means of vacuum evaporation In.

The spectral distribution of the photocurrent of such structure consists of two parts and its spectral range stretches from $\lambda \approx 460$ nm to $\lambda \approx 1200$ nm (fig. 1). In the first and the second parts of spectral distribution the photocurrent has different polarity that is caused with return inclusion of the barriers created between n^+CdS-nCdS and nCdS-nSi.

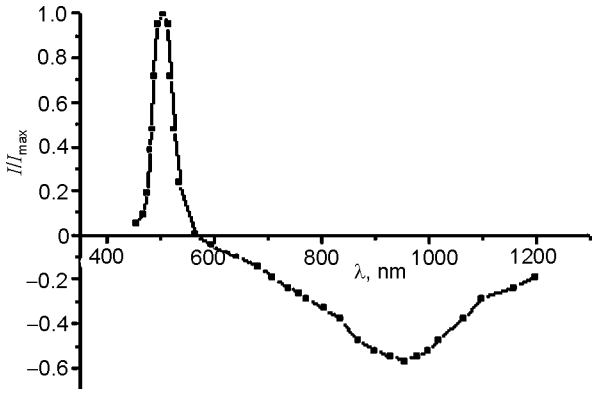

Fig. 1. Spectral distribution of a photocurrent of n^+CdS-nCdS-nSi heterostructure.

Besides the curve of spectral distribution of photosensitivity shows, that between sulphide of cadmium and of silicon with electronic conductivity is available an isotype heterojunction containing a small density of superficial conditions on section border. Acknowledgement to that is that the structure has the straightening factor of more than two orders, and occurrence of maximum in curve dependence I/I_o, λ at $\lambda \approx 955$ nm; and tangent, made to it on recession in long-wave area of the spectrum cuts on abscissa axis the length of the wave, corresponding to width of the forbidden zone of silicon.

The developed n^+CdS-nCdS-nSi – heterostructure is characterized by rectification properties, whereas the rectification coefficient defined as a ratio of direct and reverse current at fixed voltage – $K = I_{forward}/I_{back}$ ($V = 5$ V) makes up 2 orders (refer to fig. 2). The direct direction of current in the structure is deemed to occur when "+" potential is applied on the contact of Silicon surface whereas "–" potential is applied on the reverse surface. The analysis of the direct line of dark current-voltage of n^+CdS-

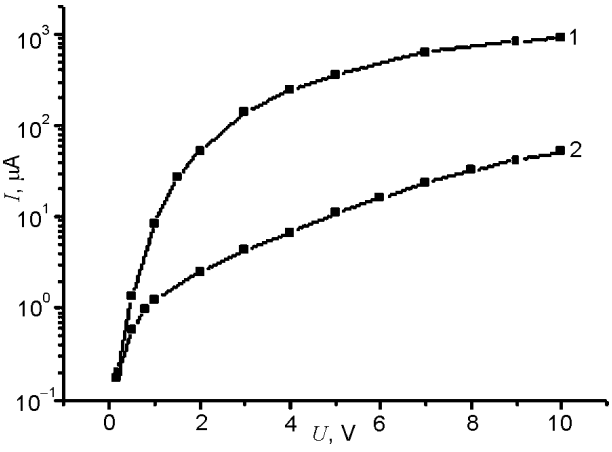

Fig. 2. Conventional direct (1) and reverse (2) sections of current-voltage characteristics of nSi-nCdS-n^+CdS heterostructure in semi-log scale at room temperatures.

nCdS-nSi heterostructures [3] clearly demonstrates that the base of the structure is of high-resistance and the ratio of thickness of base to the length of diffusion of the minority current carriers amounts ~4 at base thickness of (nCdS) ~ 1 μm, that corresponds to the diffusive length of minor carriers – electrons 0.26 μm. Thus, it is determined that n^+CdS-nCdS-nSi – heterostructures meet the requirements set out for injection photodiodes [4]. Besides, the structure investigated is photo-sensitive.

Research of their current-voltage characteristics in direct and reverse directions shows that there is the strengthening of photocurrent. As one can judge from fig. 3, the direct line of current-voltage characteristics obtained in darkness and while exposed to light, practically do not differ from one another judging by the shape of the line. However, the values of photocurrent and dark current do indeed differ.

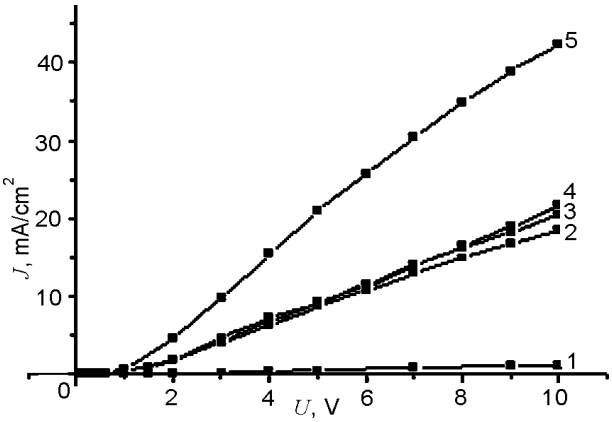

Fig. 3. Dark and light current-voltage line of nSi-nCdS-n^+CdS heterostructure: 1 – dark, 2 – 0.05 Lux, 3 – 1.25 Lux, 4 – 4 Lux, 5 – 20 mW/cm^2.

Comparing values of photocurrent and dark current was done at the same voltage ($V = 10$ V). They are reflected in tabl. 1. This table also reflects

Table 1

Dependences of the photocurrent (I_{Ph}) and integrated sensitivity ($S_{current\ sensitivity}$) from light exposure (E_{lux})

E, 10^{-2} lux	I_{dark}, mA/cm^2	I_{Ph}, mA/cm^2	$S_{current\ sensitivity}$, A/lm	$S_{current\ sensitivity}$, A/W
0	0.91	–	–	–
5	–	18.6	3720	$4.1 \cdot 10^5$
125	–	20.5	164	$1.8 \cdot 10^4$
400	–	22	55	$6 \cdot 10^3$

the photocurrent values and the current sensitivity ($S_{current\ sensitivity}$) at different levels of illumination (E, lux). The data in the tabl. 1 clearly demonstrates that the integrated sensitivity in the investigated heterostructures has a high value. Moreover, it has a maximum value at luminous flux of $E = 0.05$ Lux, wherby $S_{current\ sensitivity} = 3720$ A/Lm. For comparison we should mark that the best industrial photo receivers FD-7, FD-11 are characterized by $S_{current\ sensitivity} = (4 – 5)$ mA/lm [5].

Nevertheless, the current sensitivity still remains high even at illumination with monochromatic light of laser with the wavelength of $\lambda = 0.625$ μm and power of 20 mW/cm^2 , reaching ~2.1 A/W. One can incidentally conclude that we are actually witnessing the photocurrent strengthening. This is further evidenced by the fact that the current sensitivity of such structure tends to be ≈2.1 A/W, whereas the ideal photo receiver at similar wavelength has the current sensitivity of ≈0.5 A/W [5]. Under the ideal photo device, we understand the one, which is free of effect of reflection from surface, has the internal quantum efficiency ≈1 and all generated carriers participate in the process of photocurrent formation. Usually such photo receivers are absent as they are idealized. That is why it is possible to think that *n*Si-*n*CdS-*n*$^+$CdS – heterostructure has high spectrum sensitivity in the result of inner strengthening of photocurrent.

REFERENCES

1. Vikulin I.M., Stafeeyev V.I. Physics of semiconductor devices. – M.: The Soviet Radio, 1980. – 296 p.
2. Stafeeyev V.I. FGUP Scientific Production Amalgamation. – M.: Orion, 2008. – 103 p.
3. Stafeeyev V.I. Influence of resistivity of the thickness of semiconductor on shape of current-voltage characteristics of diode//JTF. – 1958. – № 8. – P. 1631.
4. Mirsagatov Sh.A., Aytbayev B.U., Rubinov V.M. //FTP. – 1996. – Vol. 30, №.3. – P. 550.
5. Ambrozyak. Design and technology of semiconductor photoelectric devices. – M.: The Soviet Radio, 1970. – 392 p.

PACS NUMBER: 61.05.CM, 61.46.HK, 62.20.QP.68.37.HK, 81.15.-Z

STRUCTURE, PROPERTIES AND MORPHOLOGY OF NANOSTRUCTURED COATINGS SOLID Ti-Si-N

M.V. Kaverin[1], B. Zhollybekov[2]
[1]*Sumy State University*
Ukraine
[2]*Karakalpak State University (Nukus)*
Uzbekistan
Received 12.08.2013

The work presents a comparative analysis of results obtained from samples of nanostructured Ti-Si-N coatings. Element composition, defect structure, concentration of elements throughout the depth of coating and morphology of films were studied using the techniques of slow positron beam (SPB), X-ray photoelectron spectroscopy (XPS), Rutherford backscattering spectrometry (RBS), proton microbeam (μ-PIXE), X-ray diffraction (XRD), scanning electron microscopy with energy – dispersive analysis (SEM with EDS). Results of mentioned above experiments showed that changing the substrate potential during deposition of coatings the stoichiometry and morphology of obtained coatings changes too. After thermal treatment up to 600 °C the formation of two phases: solid solution of TiN, and amorphous or quasi-amorphous α-SiN_x (Si_3N_4) envelope was observed. During experiments the grain size did not change significantly, while the extra energy was used for the completion of the spinodal (phase) segregation.

СТРУКТУРА, СВОЙСТВА И МОРФОЛОГИЯ ТВЕРДЫХ НАНОСТРУКТУРИРОВАННЫХ ПОКРЫТИЙ Ti-Si-N
М.В. Каверин, Б. Жоллыбеков

В работе представлен сравнительный анализ результатов, полученных на образцах наноструктурированных покрытий Ti-Si-N. Элементный состав, дефектная структура, концентрация элементов по глубине покрытия и морфология пленок были изучены с использованием таких методов как пучок медленных позитронов (SPB), рентгеновской фотоэлектронной спектроскопии (РФЭС), резерфордовского обратного рассеяния (RBS), протонного микропучка (μ-PIXE), рентгеноструктурного анализа (РСА), сканирующей электронной микроскопии с энергодисперсионным анализом (SEM с EDS). Результаты указанных выше экспериментов показали, что изменение потенциала подложки во время нанесения покрытий приводит к изменению стехиометрии и морфологии получаемых покрытий. Кроме того после термической обработки до 600 °С наблюдается образование двух фаз: твердого раствора TiN и аморфной или квазиаморфной фазы α-SiN_x(Si_3N_4). В ходе экспериментов размер зерна не изменился, а дополнительная термическая обработка способствовала завершению спинодальный (фазовой) сегрегации.

СТРУКТУРА, ВЛАСТИВОСТІ ТА МОРФОЛОГІЯ ТВЕРДИХ НАНОСТРУКТУРОВАНИХ ПОКРИТТІВ Ti-Si-N
М.В. Каверін, Б. Жоллибеков

У роботі представлений порівняльний аналіз результатів, отриманих на зразках наноструктурованих покриттів Ti-Si-N. Елементний склад, дефектна структура, концентрація елементів за глибиноюпокриття та морфологія плівок були досліджені з використанням таких методів як пучок повільних позитронів (SPB), рентгенівської фотоелектронної спектроскопії (РФЕС), резерфордівського зворотнього розсіювання (RBS), протонного мікропучка (μ-PIXE), рентгеноструктурного аналізу (РСА), скануючої електронної мікроскопії з енергодисперсійним аналізом (SEM з EDS). Результати зазначених вище експериментів показали, що змінювання потенціалу підкладки під час нанесення покриттів призводить до змінювання стехіометрії та морфології одержаних покриттів. Крім того після термічної обробки при 600 °С спостерігається утворення двох фаз: твердого розчину TiN та аморфної або квазіаморфної фази α-SiN_x(Si_3N_4). У ході експериментів розмір зерна не змінився, а додаткова термічна обробка сприяла завершенню спінодальної (фазової) сегрегації.

INTRODUCTION

One of the most important problems of modern materials science is fabrication and construction of new materials with unique functional properties [1–8]. Nanostructure materials with high hardness, elasticity modulus, thermal stability, wear and corrosion

resistance belongs to such materials [9 – 11]. There is a large variety of different coating's systems, but Ti-Si-N coatings stand separately due to its unique properties and characteristics. That is why it is very important to study such nanostructure coatings and to obtain new information about structure of defects, phase composition, physical and mechanical properties, and this task seems to be an actual problem of modern physics of solids.

It is well known from literature [3, 5], that adding of Si to the TiN coating leads to increasing of the coating's hardness and temperature resistance. At a specified concentration of Si, which equals to (5 ÷ 12)% it also leads to forming of two-phases composite with TiN and α-SiNx phases.

EXPERIMENT DETAILS

We used a Cathodic-Arc-Vapor-Deposition device "Bulat –3T" with HF generator [3, 5]. Potential bias was applied to the substrate from HF generator of pulsed damped oscillations, it frequency was less than 1 MHz. The duration of each pulse was 60 μs; repetition rate was about 10 kHz. The amount of negative self-bias potential of the substrate caused by HF diode effect was 2 ÷ 3 kV. Using steel 3 samples (2 mm thickness, 20 mm diameter, polished surface), we deposited coatings on the device with cathodic vacuum-arc vaporizer in high-frequency discharge (two cathodes, made of Ti and Si). Atomic Nitrogen was injected into the chamber. Thickness of the obtained coating was near 2.2 μm.

For TiN coatings fabrication we used Ti of the grade BT-1-00. Thickness of all coatings was 2.2 μm. Deposition parameters are presented in the tabl. 1.

Table 1

Physical and technical parameters of deposition of coatings

Deposited material	Coating	I, A	P_N, Pa	U_{hv}, V	U_b, B	Remarks
Ti	TiN	90	0.3	200	200	Pulse high-frequency technology
Ti + Si	Ti-Si-N	100	0.3	200	–	Pulse high-frequency technology
Ti + Si	Ti-Si-N	100	0.7	200	–	Pulse high-frequency technology

Phase composition and structure researching were provided on the X-ray diffractometer DRON-3M in CuKα irradiation using graphite monochromator in secondary beam. Diffraction spectrums were obtained in pointwise regime with a scanning step 2 = 0.05 … 0.10. For stress analysis, we used X-ray tensometry ("α-sin^{2}ψ"-method) and its modifications, which are valid for coatings with strong axial type texture [12, 13].

Elementary composition of the coatings was studied using Rutherford backscattering of $^4He^+$ ions with 1.7 MeV energy, detector resolution $E = 13$ keV, dispersion angle ≈1700. Also we used scanning electron microscopy (SEM) with energy dispersion analysis (Jeol 7000F microscope, Japan) in contrast of electrons and in direct and backscattering electron reflection. For surface morphology investigations, we used atomic-force microscopy AFM Objective to obtain 3D image of surface topography, electron-ion scanning microscope Quanta 200 3D with roentgen-fluorescent microanalyzer EDAX with appropriate software, and automatic contact precision profilometer SURTRONIC 25.

Nanohardness and elastic modulus measurements were done using trihedral Berkovich indentor (Nano Indenter G200, TN, USA, Oak Ridge, Nano Instruments Innovation Center). For analysis of vacancy-type defects in the coating we used slow positron beam (Halle, Germany). We measured S-parameter of the Doppler broadening annihilation peak (DBAP) by changing energy of the fallen positron beam from 1 KeV to 30 KeV, and that allowed us to change the analysis depth [14,15].

The bonding states were determined using photoelectron spectroscopy (XPS, Kratos AXIS Ultra) with a monochromatic AlK (1486.71 eV, X-ray radiation 15 kV/10 mA).

EXPERIMENTAL RESULTS AND DISCUSSION

Fragments of diffraction spectrums for Ti-Si-N samples (as deposited and after annealing under the temperature 600 °C for 30 min) are presented on fig. 1. We calculated lattice parameter $a_0 = 0.42462$ A and found strong texture (111) (Ti, Si) N and (222) (Ti, Si) N (see curves 1 and 2).

In addition, we detected small peaks from TiO_2 (JCPDS-19-370). Volume fraction of oxides after thermal annealing in the chamber is low and it is not higher than 5%.

Stresses analysis showed, that there is high compression deformation in (Ti, Si)N hard solution

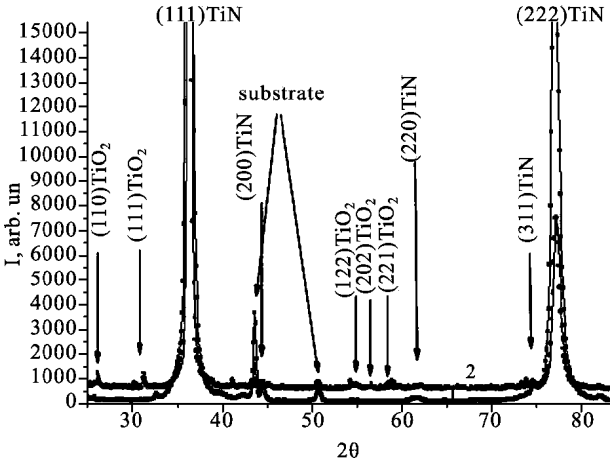

Fig. 1. Ti-Si-N coating's X-ray diffraction patterns: 1) as deposited; 2) after annealing under the temperature 600 °C for 30 min, vacuum $P = 50$ mbar.

(equals to – 2.6%) and it is reduced to the value of – 2.3% after annealing.

Coherent-scattering region evaluation (using Sherrer methodic) showed that size of nanograins increased from 12.5 nm to 13 nm, and when initial size of nanograins is 25 nm, it increased to (28 ÷ 30) nm. In other words, due to annealing under the temperature of 600 °C for 30 minutes, insignificant changing of grain size is observed, and rest part of energy was used on finishing of spinodal segregation process, forming of monolayer α-Si_3N_4.

We can make an interim conclusion, that when compression deformation and order of structuring are high, annealing under the temperature of 600 °C for 30 minutes do not lead to catastrophic changes both in phase composition, structure and mode of deformation. Layer, made of (Ti, Si)N solid solution, is formed, and silicon-nitrogen phase is also formed around nanograins. In according to it, Si concentration is reduced in solid solution; some amount of Ti atoms creates TiO_2 film on the coating's surface. Ti-Si-N coatings structure is characterized by high level of microdeformations of lattice (more than 1%) [9]. High value of microdeformations of lattice probably indicates on inhomogeneity of chemical structure in every phase of the coating. Coatings have strong texture [6]. Condensation compressive stresses leads to (111) texture forming in (Ti, Si)N solid solution films. Using approximation methods we defined average crystallites sizes of the (Ti, Si)N solid solution, and it varies from 12.5 to 25 nm. The obtained coatings have next hardness: TiN ($H = 28$ GPa, $E = 312$ GPa); Ti-Si-N ($H = 38 \div 39$ GPa, $E = 356$ GPa).

In tabl. 2, we summarized results of tribological investigations. It is clearly seen from this results, that

Table 2

Tribological properties of nanocomposite coatings

Coating	Temperature, °C	Wear factor, coating, mm^3/nm	Wear counter body mm^3/nm	Friction coefficient
Ti-Si-N	30	$7.69 \cdot 10^{-5}$	$3.28 \cdot 10^{-5}$	0.88
	300	$2.63 \cdot 10^{-5}$	$3.49 \cdot 10^{-5}$	0.82
	600	$1.95 \cdot 10^{-5}$	$2.75 \cdot 10^{-5}$	0.69
TiN	30	$6.75 \cdot 10^{-5}$	$3.30 \cdot 10^{-5}$	0.81
	300	$3.62 \cdot 10^{-5}$	$3.51 \cdot 10^{-5}$	0.87
	600	$5.16 \cdot 10^{-5}$	$3.83 \cdot 10^{-5}$	0.91

wear coefficient for TiN coating increases with temperature increasing, but for Ti-Si-N coating wear coefficient decreases to 0.69 ($T = 500$ °C), which is approximately on 25% less, than under room temperature.

Elementary analysis results are presented on fig. 2, it was obtained using RBS method and EDS (energy-dispersion spectroscopy). As it is clearly seen from fig. 2a), Si concentration is less than 5 at.%, N concentration ≈ (35 ÷ 40) at.%, rest one is Ti, and for fig. 2b) N concentration ≈ 50 at.%, Ti ≈ 44 at.%, Si ≈ 5.5 at.%. Coating's thickness equals to 2.18 ± 0.01 μm in according to RBS data.

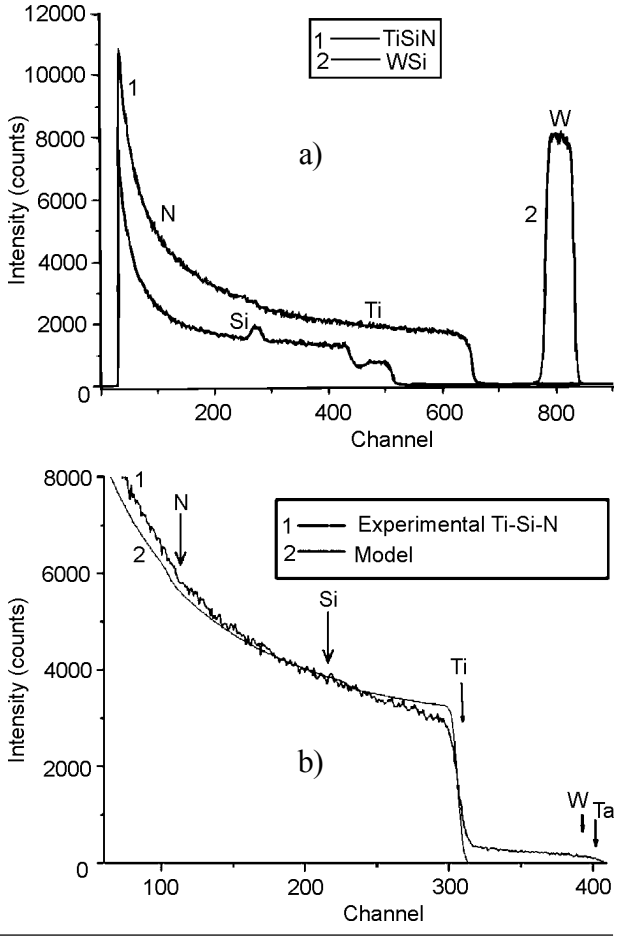

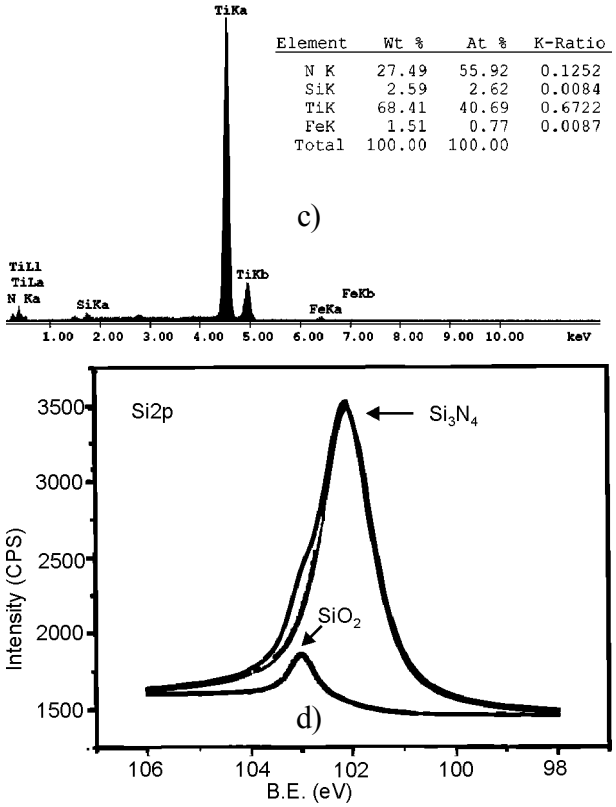

Fig. 2. Energy spectrums for samples with Ti-Si-N coatings; (a) bias potential –50 V, *PN* = 0.5 Pa (RBS), second curve corresponds to etalon SiW curve (for comparing); (b) bias potential –100 V, *PN* = 0.7 Pa (RBS); (c) bias potential –50 V, *PN* = 0.5 Pa (EDX); (d) XPS spectra obtained from Ti-Si-N coating.

RBS data confirms by EDX results, see fig. 2c). Concentration of Si in the coating is 2.62 at.%, Ti ≈40.69 at.%, N ≈ 55.92 at.%. For another series of samples (with Si concentration ≥ 5.8 at.%) we provided investigations of Si-Nx connection using XPS analysis. It showed high peak on 101.9 eV, and it points directly on forming of Si-Nx connection in this sample. But also we had a small peak, which points on forming of a very few amount of Si-O on 103.9 eV (after annealing in the air under the temperature of 600 °C for 30 min). Additional μ-PIXE investigations showed SiN forming on TiN nanograins borders.

Images of the coating's surface before and after annealing, under the temperature 600 °C (for 30 min.) are presented on fig. 3. We can observe flat "drops" of melted phase, no matter of HF stimulation. We should note that part of plasma jet consists of drop fractions, and we did not make analysis of such fractions.

To obtain a real thickness of Ti-Si-N nanostructure coating and to norm the depth of slow positron beam analysis, we cut a circle hole, through the coating thickness. As it is seen from fig. 3c), coating's thickness equals to 2.39 ÷ 2.41 μm. Calculation of positrons penetration depth shows that E_{max} = 20 keV, it corresponds to 2.11 μm of thickness. Even if we will take into account diffusion of thermalized positrons (it length is $L \approx 100$ nm), we will see that positron beam cannot reach interface between coating and substrate. That is why profiles of mean positron's penetration depths give us information about vacancy-type defects on the whole thickness of Ti-Si-N coating, but the interface border is not really achieved by them.

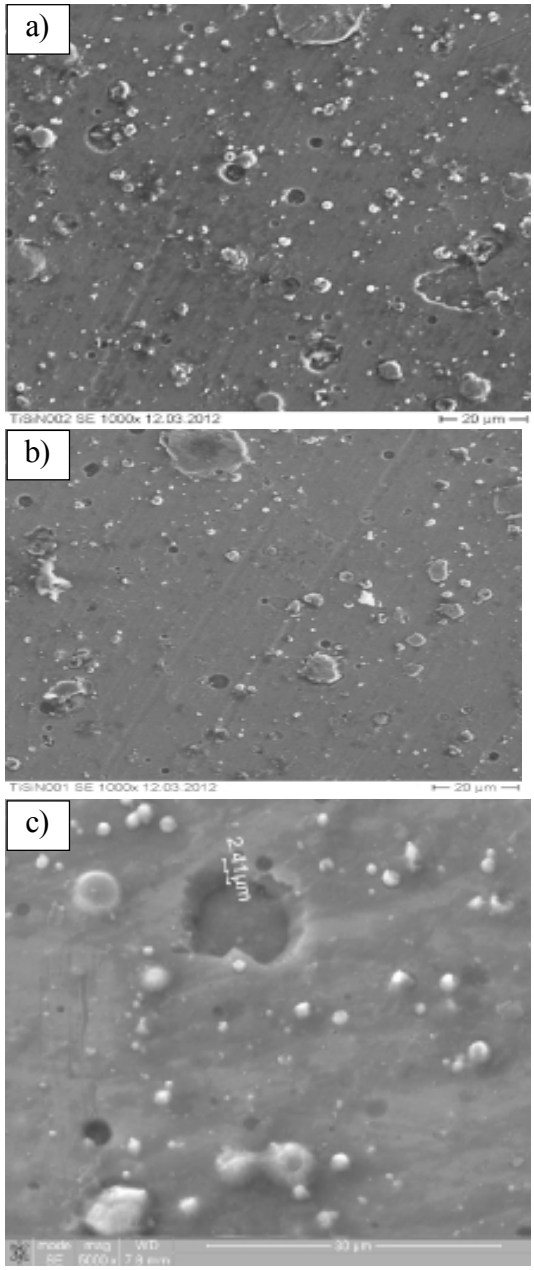

Fig. 3. Surface topography of the Ti-Si-N coating; (a) as deposited state; (b) after annealing under the temperature of 600 °C; (c) SEM-analysis of circle cross-section, which was obtained using ion beam cutting.

Positron annihilation method is the most effective, responsive and reliable method of analysis of free volumes in nanocrystalline materials (it has possible interval of defect's analysis in the range $10^{-6} \pm 10^{-3}$ defects per atom) [14, 15]. Part of positrons can be captured on the interface of two neighboring nanograins or on boundary junction of three neighboring nanocrystals. It gives us good opportunity to solve one of the most complicated and interesting problems of nanomaterials to understand structure (including electron structure) of the interfaces between nanograins, because length (volume) of such interfaces influences a lot on properties of nanocomposite coatings [1 – 9].

Fig. 4 shows dependence of S-parameter on energy, in other words, we can see profiles of defects in Ti-Si-N coating before (black curve) and after (red curve) thermal annealing under the temperature of 600 °C (30 min).

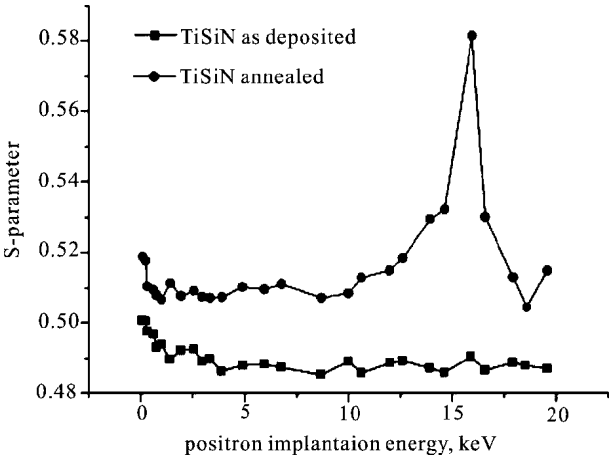

Fig. 4. Dependence of S-parameter on energy of positron microbeam (black curve as deposited coating, red curve annealed coating).

Significant changes in electron and defect structure of the coating is clearly seen from this figure. We should note, that defects concentration increases on the whole thickness of the coating, all positrons locates and annihilates on defects, which are situated on the boundaries of nanograins. Depth of diffusion of thermalized positrons is ≈100 nm, size of nanograins is (12.5 ÷ 13) nm, so we can say that almost all positrons are captured on interface's defects. As approaching to the interface between coating and substrate, *S*-parameter significantly increases, i.e. defects also migrate to the interface between coating and substrate due to thermal diffusion. Thickness of this transition layer of defects is no more than 250 nm. Calculation of vacancy defects concentration was done using positron capture model with two types of vacancy defects [12], and it showed that defects concentration increases after annealing from $5 \cdot 10^{16}$ to $7.5 \cdot 10^{17}$ cm^{-3}, thermally activated vacancies concentration also increases from $1 \cdot 10^{16}$ to $5 \cdot 10^{18}$ cm^{-3} (see red curve).

Loading and unloading curves are presented on fig. 5.

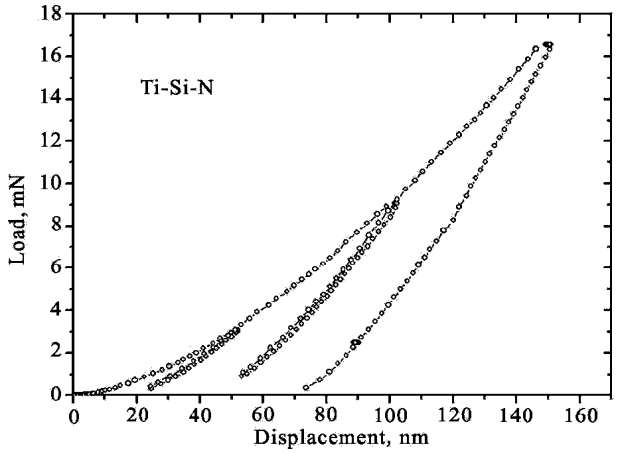

Fig. 5. Loading and unloading curves, obtained for Ti-Si-N coating ($U = -100$ V, $Pn = 0.7$ Pa), indentation on 50, 100 and 150 nm depth.

Nanoindentor penetrates on the surface layer of the Ti-Si-N coating (three different loadings). As it is seen from calculations, based on Oliver-Pharr methodic, an average hardness for such deposition regimes is 38.7 GPa, elasticity modulus is 370 ± 12 GPa. Annealing under the temperature of 600 °C in vacuum leads to increasing of elasticity modulus to values (430 – 448) GPa, it is connected with finishing of process of spinodal segregation on the boundaries of nanograins, i.e. with forming of thin SiN (Si_3N_4) interlayer (amorphous and quasi amorphous phases).

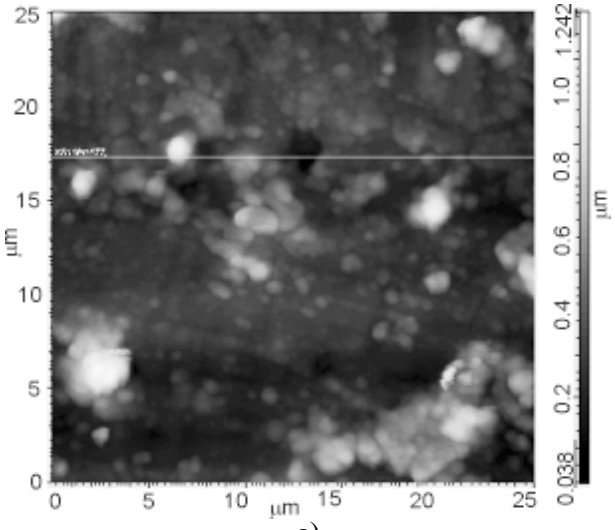

a)

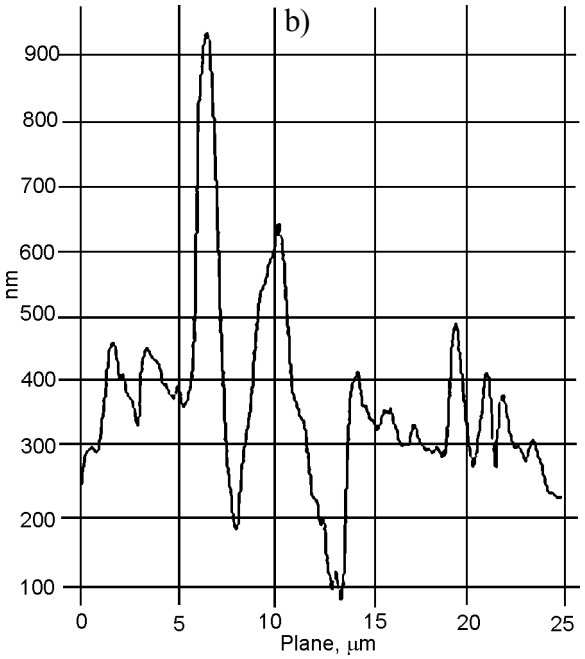

Fig. 6. An image of the surface topography of Ti-Si-N coating: a) – the surface area of 25×25 мм; b) – profilogram of Ti-Si-N coating from 100 to 900 nm roughness.

Fig. 6 shows a surface topography of Ti-Si-N nanostructured coatings. On the surface region of 25×25 μm can be seen a variation in depths.

Moreover, thermal annealing under the temperature of 600 °C in vacuum also changes Ti-Si-N coating's surface morphology (fig. 7).

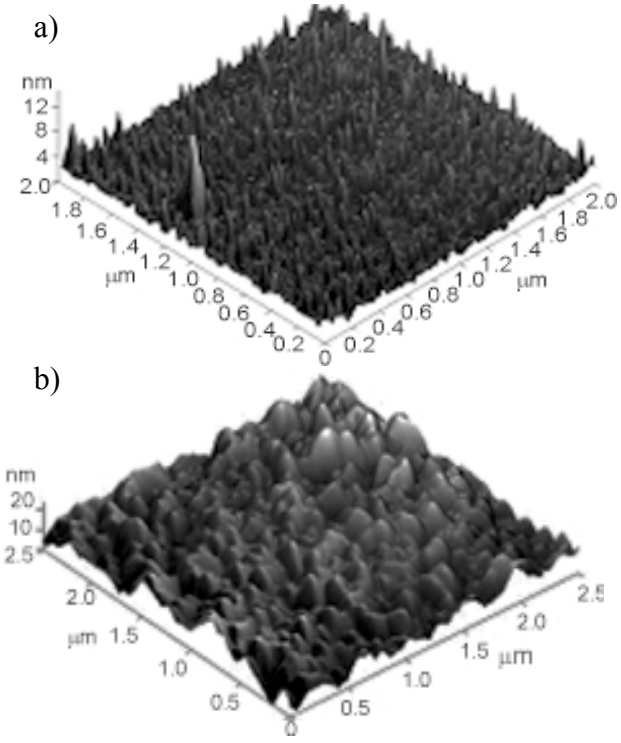

Fig. 7. Ti-Si-N coating's surface morphology: (a) 3d AFM image; (b) after annealing under the temperature of 600 °C.

We observed decreasing of an average roughness size, increasing of amount of defects (it is obvious from fig. 6).

After analysis we can say, that structure of defects changes on nanograins interfaces due to annealing, average roughness size decreases, nanohardness increases on 20% (in comparison with as deposited state) and it correlates with our previous works [13, 16]. Friction ratio decreases on 25% it is the main difference as opposed to works [17 – 19].

ACKNOWLEDGEMENTS

Authors thanks A.D. Pogrebnjak (Sumy, Ukraine) for measuring of profiles defects using slow positron beam, G. Abrasonis (Dresden, Germany) for elements' composition studies using RBS-analysis, V.M. Beresnev (Kharkov, Ukraine), D.A. Kolesnikov (Belgorod, Russia) and R. Krause-Rehberg (Halle, Germany). The work was done under financial support of Ministry of Education and Science of Ukraine (state program, order No. 411), and in collaboration with NIMS (Tsukuba, Japan) and Martin-Luther University (Dresden, Germany). The work was supported by Ministry of Education and Science of Ukraine (project No. 011U001382). Authors are grateful to the staff of the Joint Research Center "Diagnostics of Structure and Properties of Nanomaterials" (Belgorod State University, Russia) for their assistance with instrumental analysis.

REFERENCES

1. Gleiter H. Nanocrystalline materials//Progress in Materials Science. – 989.– Vol. 33.– P. 233-315.
2. Siegel R.W. Cluster-Assembled Nanophase Materials//Annual Review of Materials Science. – 1991. – Vol. 21. – P. 559-579.
3. Veprek S., Reiprich S.A. Concept for the design of novel superhard coatings//Thin Solid Films. – 1995. – Vol. 268. – P. 64-71.
4. Pogrebnyak A.D., Shpak A.P., Azarenkov N.A., Beresnev V.M. Structures and properties of hard and superhard nanocomposite coatings//Physics-Uspekhi. –2009. – Vol. 52. – P. 29-54.
5. Mayrhofer P.H., Mitterer C., Hultman L., Clemens H. Microstructural design of hard coatings //Progress in Materials Science. – 2006. – Vol. 51. – P. 1032-1114.
6. Musil J. Hard and superhard nanocomposite coatings//Surface and Coatings Technology. – 2000. – Vol. 125. – P. 322-330.

7. Andrievski R.A. Nanomaterials based on high-melting carbides, nitrides and borides//Russian Chemestri Reviews. – 2005. – Vol. 74. – P. 1061-1072.
8. Musil J. Hard nanocomposite coatings: Thermal stability, oxidation resistance and toughness// Surface and Coatings Technology. – 2012. – Vol. 207. – P. 50-65.
9. Pogrebnjak A.D., Ponomarev A.G., Shpak A.P., Kunitskii Yu.A. Application of micro- and nanoprobes to the analysis of small-sized 3D materials, nanosystems, and nanoobjects//Physics-Uspekhi. – 2012. – Vol. 55. – P. 270-300.
10. Pogrebnjak A., Danilionok M., Uglov V., Erdybaeva N., Kirik G., Dub S., Rusakov V., Shypylenko A., Zukovski P., Tuleushev Y. Nanocomposite Protective Coatings Based on Ti-N-Cr/Ni-Cr-B-Si-Fe, Their Structure and properties//Vacuum. – 2009. – Vol. 83. – P. 235-239.
11. Pogrebnjak A.D., Uglov V.V., Il'yashenko M.V., Beresnev V.M., Shpak A.P., Kaverin M.V., Erdybaeva N.K., Kunitskii Yu.A., Tyurin Yu.N., Kolisnichenko O.V., Makhmudov N.A., and Shypylenko A.P. Nano-Microcomposite and Combined Coatings on Ti-Si-NAA/C-Co-Cr/Steel and Ti-Si-N/$(Cr_3C_2)_{75}$-$(NiCr)_{25}$Base: Their Structure and Properties. Nanostructured Materials and Nanotechnology IV//Ceramic Engineering and Science Proceedings. – 2010. – Vol. 31. – P. 127-138.
12. Lavrent'ev V.I., Pogrebnyak A.D., Shandrik R. 'Evolyuciya vakansionnyh defektov v poverhnostnyh sloyah metalla pri impul'snom vozdejstvii 'elektronnym puchkom //Pis'ma v Zh'ETF. – 1997. – № 65. – P. 618-622.
13. Rempel'S.V., Gusev A.I. Poverhnostnaya segregaciya v raspadayuschihsya karbidnyh tverdyh rastvorah//Pis'ma v Zh'ETF. – 2008. – № 88. – P. 508-513.
14. Krause-Rehberg R., Leipner H.S. Positron Annihilation in Semiconductors: Defect Studies. – New York: Springer-Verlag Berlin Heidelberg, 2003. – 387 p.
15. Pogrebnjak A.D., Il'yashenko M.V., Kaverin M.V., Shypylenko A.P., Pshyk A.V., Beresnev V.M., Kirik G.V., Erdybayeva N.K., Makhmudov N.A., Kolisnichenko O.V., Tyurin Yu.N., Shpak A.P. Physical And Mechanical Properties of The Nanocomposite And Combined Ti-N-Si / WC-Co-Cr/ and Ti-N-Si/$(Cr_3C_2)_{75}$-$(NiCr)_{25}$ Coatings//Journal of Nano- and Electronic Physics. – 2009. – Vol. 1. – P. 66-77.
16. Pogrebnjak A.D., Mahmud A.M., Karasha I.T., Kirik G.V., Tkachenko R.Y., Shypylenko A.P. Structure and Physical-Mechanical Properties of nc-TiN Coatings Obtained by Vacuum-Arc Deposition and Deposition of HF Discharg//Journal of Nano- and Electronic Physics.– 2011.–Vol. 3. – P. 97-105.
17. Pogrebnjak A.D., Ruzimov Sh.M., Alontseva D.L., Zukowski P., Karwat C., Kozak C., Kolasik M. Structure and properties of coatings on Ni base deposited using a plasma jet before and after electron a beam irradiation//Vacuum. – 2007. – Vol. 81. – P. 1243.
18. Sobol' O.V., Pogrebnjak A.D., Beresnev V.M. Effect of the Preparation Conditions on Phase Composition, Structure, and Mechanical Characteristics of Vacuum-Arc Zr-Ti-Si-N Coatings// Phys. Met. Metallogr.– 2011.– Vol. 112. – P. 188.
19. Pogrebnjak A.D., Shpak A.P., Beresnev V.M., Kolesnikov D.A., Kunitskii Yu.A., Sobol O.V., Uglov V.V., Komarov F.F., Shypylenko A.P., Makhmudov N.A., Demyanenko A.A., Baidak V.S., and Grudnitskii V.V.. Effect of Thermal Annealing in Vacuum and in Air on Nanograin Sizes in Hard and Superhard Coatings Zr–Ti-Si-N//Journal of Nanoscience and Nanotechnology. – 2012. – Vol. 12.

UDC 669.297

PURIFICATION OF HAFNIUM FROM OXYGEN AND NITROGEN

M.M. Pylypenko, A.A. Drobyshevskaya
National Science Center "Kharkov Institute of Physics and Technology"
Ukraine

Received 24.08.2013

Data on the influence content of interstitial impurities on the mechanical properties of hafnium are presented in this work. Investigations the purification of hafnium from oxygen at added of aluminum on the melting reduction stage with subsequent refining electron beam melting were performed. It is shown that vacuum thermal treatment of hafnium tetrafluoride before carrying out melting reduction reduces the nitrogen content in hafnium less than 0.005 wt.%.

Keywords: hafnium, reactor, refining, impurities, properties.

ОЧИСТКА ГАФНИЯ ОТ КИСЛОРОДА И АЗОТА

Н.Н. Пилипенко, А.А. Дробышевская

В работе приведены данные по влиянию содержания примесей внедрения на механические свойства гафния. Выполнены исследования по очистке гафния от кислорода при введении алюминия на стадии восстановительной плавки с последующей рафинирующей электронно-лучевой плавкой. Показано, что вакуум-термическая обработка тетрафторида гафния перед проведением восстановительной плавки обеспечивает снижение содержания азота в гафнии меньше 0,005 мас.%.

Ключевые слова: гафний, реактор, рафинирование, примеси, свойства.

ОЧИСТКА ГАФНІЮ ВІД КИСНЮ ТА АЗОТУ

М.М. Пилипенко, А.О. Дробишевська

В роботі приведені дані щодо впливу вмісту домішок проникнення на механічні властивості гафнію. Виконано дослідження з очищення гафнію від кисню при введенні алюмінію на стадії відновлювальної плавки з подальшою електронно-променевою плавкою. Показано, що вакуум-термічна обробка тетрафториду гафнію перед проведенням відновлювальної плавки забезпечує зниження вмісту азоту в гафнії менше 0,005 мас.%.

Ключові слова: гафній, реактор, рафінування, домішки, властивості.

INTRODUCTION

In WWER reactors as in similar foreign reactors PWR the clustered assemblies of absorber elements of control protection system (CPS) serve as regulators [1]. The clustered assemblies can be operated in automatic control regime of reactor power and in the emergency protection regime. In the standard absorber elements vibrocompacted boron carbide powder (B_4C) with a natural abundance of the ^{10}B isotope used as an absorbent material. Cladding of absorber element diameter of 8.2 mm and a wall thickness of 0.6 mm is made of steel 06X18H10T. Immersion depth in the core of auto regulation rods is from 1500 mm at the beginning of the campaign to 300 mm at the end of the campaign and emergency protection rods during normal operation of the reactor are in the raised position at a distance of 80 – 100 mm from the upper edge of the core. Thus during reactor operation all the rods of control protection system are in non-uniform neutron field resulting in an uneven burnup of the ^{10}B isotope in boron carbide range adjustment of the absorber element. Their lower parts are at greatest irradiation.

Rather small term the service of the standard absorber elements of WWER-1000 (2 years in automatic regime and 5 years in the emergency protection regime) is connected both with significant embrittlement of the steel cladding 06X18H10T and a swelling of the absorber due to the reaction $^{10}B + {}^{1}n \rightarrow {}^{7}Li + {}^{4}He$. At a burnup of the ^{10}B isotope mo-re than 40% the appreciable yield of free helium occurs and swelling of boron carbide particles and its force effect on cladding is beginning to affect. Containing ^{10}B isotopes (n, α)-absorbers are characterized by relatively low radiation resistance due to the accumulation of large amount of gas products and do not provide the operability in emergency situations related to overheating.

Visible progress in increasing service life the clustered assemblies of CPS can be achieved when using a combined (n,α)-(n,γ)-absorber in the absorber elements of CPS of pressurized water reactors [2, 3]. As a result developed an interest to hafnium relating to the number of (n, γ)-absorbers. Hafnium in the absorber elements of CPS can simultaneously perform functions the neutron absorber and construction material. Fig. 1 shows the absorber elements of various types.

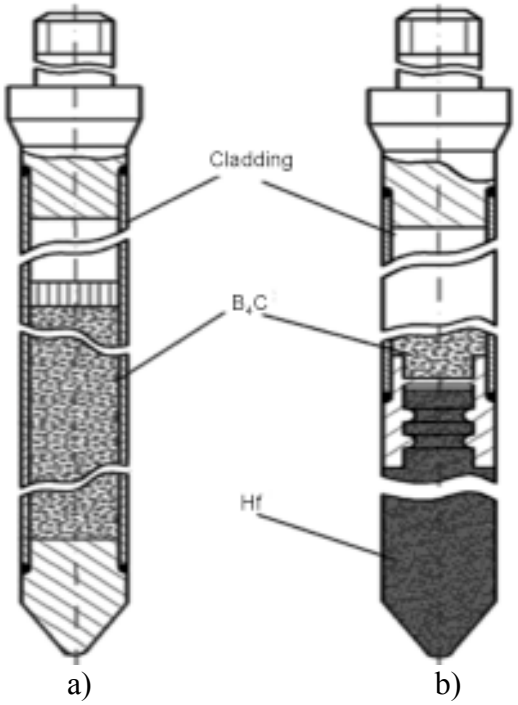

Fig. 1. Absorber elements with boron carbide (a) and combined (n, α)-(n, γ)-absorber (b).

Pure hafnium has a complex of physical-chemical and mechanical properties [4, 5] that allow using it for the production of regulators intended for long-term maintenance-free operation of nuclear reactors.

The cross-section of thermal neutron absorption of hafnium is slowly reduced when operating in the conditions of irradiation due to isotopic composition of natural hafnium. According to preliminary estimates service life of hafnium rods can be extended to 15 years or more due to the peculiarities of hafnium isotopes transmutation in the neutron flux [2]. The relative physical efficiency of Hf in respect to the core of WWER-1000 is ~80% of the efficiency of boron carbide [6].

According to foreign and domestic researchers [1, 6, 7] hafnium is an ideal material for control rods in pressurized water reactors and can be successfully used as an absorber rods of CPS WWER-1000 reactors.

In Ukraine the technology for obtaining of hafnium including hydrometallurgical repartition (the production of pure hafnium tetrafluoride – HfF_4) and metallurgical repartition (calcium thermal reduction of hafnium tetrafluoride and subsequent electron-beam melting (EBM)) is developed [8]. This technology allows getting a metal with low content of undesirable impurities influencing the metal plasticity, its corrosive and radiation properties. However in some cases there is also some local nonuniformity in content nitrogen, iron, oxygen and silicon.

On the hafnium properties influence the impurity contained therein. In particular this applies to the interstitial impurities especially oxygen and nitrogen. The data on the effect of oxygen content on the mechanical properties of hafnium are given in fig. 2 and

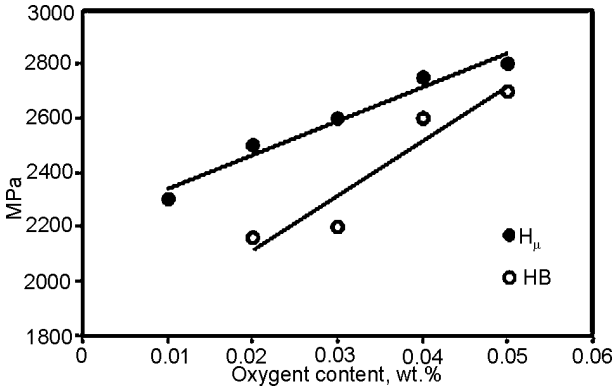

Fig. 2. The values of microhardness H_μ and Brinell hardness HB for hafnium with different oxygen content.

in tabl. 1 [9].

Table 1

The data of mechanical researches of hafnium with different oxygen content

Oxygen content, wt.%	$\sigma_в$, MPa	$\sigma_{0.2}$, MPa	δ, %
0.005	440.0	290.0	36.0
0.010	445.0	305.0	34.5
0.030	487.0	355.0	30.0
0.045	520.0	370.0	27.5

The necessary degree of hafnium purification from metal impurities is achieved within 2 – 3 EBM. Great difficulty in obtaining of nuclear grade hafnium is purification from interstitial impurities – nitrogen and oxygen.

At high oxygen and nitrogen content in hafnium it is almost impossible to mechanical treatment which greatly limits its application in the form of products for the nuclear power industry (rod, band, tube, wire).

PURIFICATION FROM OXYGEN

To remove oxygen from hafnium during EBM was suggested at a stage of reduction melting added into metal a third component which would formed a volatile oxide. This component should have a greater affinity for oxygen than hafnium and its gaseous suboxide should have greater volatility at the melting temperature of hafnium than hafnium monoxide.

Based on the analysis of literature data and taking into account obtained results of laboratory studies aluminum was chosen as a hafnium deoxidizer [10, 11]. The calculation of deoxidizing ability of aluminum showed that aluminum forms a volatile oxide which then desorbed from the hafnium at EBM by reaction $2Al_{Hf} + [O] \rightarrow (Al_2O)_{gas}$. Aluminum was added into hafnium on the reduction melting stage in an amount of 0.2 – 0.25 wt.% and then roughing metal subjected to remelting by electron beam in vacuum $1 \cdot 10^{-2} – 3 \cdot 10^{-3}$ Pa. According to the experimental results (tabl. 2) lower oxygen content is observed already on the reduction stage and significantly – after electron beam melting [10, 11]. The oxygen content is decreased almost three times (from 0.11 – 0.12 to 0.03 – 0.04 wt.%). The aluminum content in all samples of hafnium obtained after electron beam melting was $(2 – 3) \cdot 10^{-3}$ wt.% regardless of the aluminum additives were added or no.

Table 2

Oxygen content in hafnium after electron beam melting

Aluminum additive, wt.%	Oxygen content in hafnium, wt.%	
	roughing ingot	after EBM
–	0.15	0.045
–	0.17	0.050
–	0.18	0.055
0.20	0.10	0.035
0.20	0.11	0.030
0.25	0.12	0.030

Using the parameters obtained in laboratory researches in factory conditions the hafnium ingots purity of more than 99.94 wt.% were obtained at the addition of aluminum on the reduction melting stage after EBM with an impurity content: nitrogen – $3.0 \cdot 10^{-3}$ wt.%.; aluminum – $3.0 \cdot 10^{-3}$ wt.%.; tungsten – $1.0 \cdot 10^{-3}$ wt.%.; iron – $3.0 \cdot 10^{-3}$ wt.%.; oxygen – $4.0 \cdot 10^{-2}$ wt.%.; silicon – $3 \cdot 10^{-3}$ wt.%.; manganese – $3.0 \cdot 10^{-4}$ wt.%.; copper – $2.0 \cdot 10^{-3}$ wt.%.; nickel – $3.0 \cdot 10^{-3}$ wt.%.; niobium – $2.0 \cdot 10^{-3}$ wt.%.; carbon – $3.0 \cdot 10^{-3}$ wt.%.; chrome – $1.0 \cdot 10^{-3}$ wt.%. Hafnium obtained by using of aluminum additives on the reduction stage after refining by EBM can be successfully used as the construction material of a nuclear reactor core.

REDUCING THE CONCENTRATION OF NITROGEN IN HAFNIUM

One of the undesirable rigidly limited impurities at obtaining hafnium is nitrogen. Its content in the metal in accordance with the technical conditions should not exceed 0.005 wt.%. Analysis of statistical data about the behavior of nitrogen at obtaining hafnium indicates that nitrogen content in the melting products is always higher of its content in the starting materials [12].

Comparison of the nitrogen content in the starting materials and melting products allows concluding that to 30% of nitrogen adsorbed goes into hafnium from the unsublimated hafnium tetrafluoride. This fact dictates the need for reduce the amount of nitrogen adsorbed by hafnium tetrafluoride. To determine of the character process of gas separation from the sublimated and unsublimated hafnium tetrafluoride experiments were carried out in the temperature range 20 – 700 °C at a residual pressure $1.3 \cdot 10^{-1} – 1.3 \cdot 10^{-6}$ Pa.

Analysis of the residual gases spectra showed that the main gases which desorbed during heating hafnium tetrafluoride are nitrogen, carbon oxide, water vapor, hydrogen fluoride and other gases [13, 14]. Change of the general pressure in the chamber during heating of the unsublimated and sublimed hafnium tetrafluoride is shown in fig. 3. It is noted that amount of the gases desorbed from the sublimated and unsublimated hafnium tetrafluoride is significantly different. From unsublimated hafnium

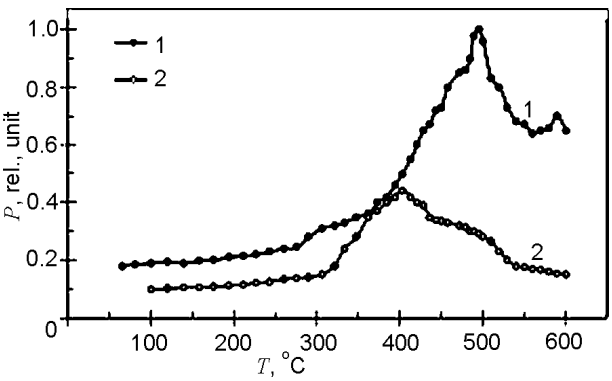

Fig. 3. Change of the total pressure in the chamber during heating of unsublimated (1) and sublimed (2) hafnium tetrafluoride.

tetrafluoride a greater number of gaseous impurities is desorbed (up to 3 wt.%) than from sublimated (up to 0.5 wt.%). With increasing temperature the maximum on curves of the total pressure change of unsublimated hafnium tetrafluoride approximately one hundred degree higher than of the sublimated.

The process of gas separation from unsublimated hafnium tetrafluoride is more complex due to the high content of the gas impurities in it and desorption of gas impurities with mass numbers 36 (HFO) and 38 (HF H_2O) (fig. 4). A comparison of the normalized composition of gases desorbed from unsublimated hafnium tetrafluoride with the composition of gases desorbed from of sublimated hafnium tetrafluoride shows that content of water, nitrogen, carbon oxide and fluorine-containing impurities of the unsublimated products is about 25%. The main gas impurity desorbed from sublimated hafnium tetrafluoride is water.

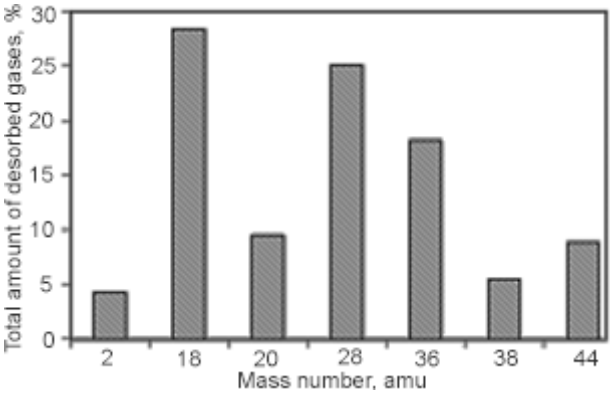

Fig. 4. Percentage of the desorbed gases with different masses from the unsublimated hafnium tetrafluoride in the temperature range 20 – 600 °C.

The results obtained allow to conclude that for reducing the nitrogen content in hafnium when using sublimed hafnium tetrafluoride the preliminary operation of vacuum thermal treatment in the temperature range 300 – 600 °C is desirable and for unsublimated hafnium tetrafluoride is necessarily.

Efficiency the use of vacuum thermal treatment was shown in practice during the laboratory melting. Nitrogen content in the obtained hafnium ingots without the use of vacuum thermal treatment of hafnium tetrafluoride was varied in the range 0.005 – 0.019 wt.%. After vacuum thermal treatment the nitrogen content in alloys does not exceed 0.005 wt.%.

CONCLUSION

The results of studies on the hafnium refining presented in this paper show that the developed methods of refining are highly effective for reducing the amount of gas impurities. The use of aluminum as a deoxidizing component on the reduction melting stage of hafnium results in essential decrease the oxygen content in the metal (to 0.03 – 0.04 wt.%) on the electron beam melting stage. Carrying out of vacuum thermal treatment of hafnium tetrafluoride before the reduction melting in the temperature range of 300 – 600 °C provides a nitrogen content in the metal less than 0.005 wt.%.

Thus the research results of refining hafnium allow carrying out the scientific approach to obtaining of hafnium with low oxygen and nitrogen content for modern technologies and creating of construction materials for nuclear reactors of the new generation and other responsible applications.

REFERENCES

1. Risovany V.D., Zaharov A.V., Klochkov E.P. Absorbent materials and regulators of nuclear reactors. – M.: Publishing House of MEI, 2012. – 392 p.
2. Ponomarenko V.B., Poslavsky A.O., Chernyshov V.M. and others. Regulators and BAR of nuclear reactors WWER-1000 and ways of their improvement//Problems of atomic science and technology. – 1994. – Issue 2(62) 3(63). – P. 95-113.
3. Ryahnovsky V.M., Shmelev S.V., Chernyshov V.M., Scheglov A.V. Present state of development and production of the nuclear reactors WWER-1000 regulators//Problems of atomic science and technology. – 1997. – Issue 1, 2. – P. 110-119.
4. Tihonov L.V., Kononenko V.A., Prokopenko G.I., Rafalovsky V.A. Structure and properties of metals and alloys. Mechanical properties of metals and alloys. – K.: Naukova Dumka, 1986. – 568 p.
5. Risovany V.D., Klochkov E.P., Kosenkov V.M., Ostrovsky Z.E. Structural damages of the metal hafnium at reactor irradiation//Radioactive Materials Science: Proceedings of the International Conference. – Kharkov. – 1990. – T. 8. – P. 118-124.
6. Afanasyev A.A., Konotop Yu.F., Odeychuk N.P. Hafnium is a promising absorber for absorbing elements of CPS WWER-1000 rectors of nuclear power plant Ukraine//Problems of atomic science and technology. – 2000. – № 4. – P. 80-85.
7. Risovany V.D., Varlashova E.E., Zaharov A.V. The absorbing materials based on dysprosium and hafnium for pressurized water reactors//Proceedings of the RIAR. – Dimitrovgrad: SSC SRIAR. – 2000. – Issue 2. – P. 49-62.

8. Shatalov V.V., Fedorov V.D., Kotsar M.L. and others. Extraction calcium thermal technology of obtaining hafnium//Problems of atomic science and technology. – 1999. – № 2. – P. 9-13.
9. Pylypenko M.M. Physical and technological basis of the zirconium materials and hafnium creation technology for the cores of nuclear power plants. – Diss. Doct. Tech. Sciences: 01.04.07. – Kharkov, 2012. – 313 p.
10. Azhazha V.M., Vjugov P.N., Lavrinenko S.D., Pylypenko M.M., Muhachev A.P., Lindt K.A., Lakhov A.M., Popov V.I. Investigation of the refining process of calcium thermal hafnium with the introduction of additives//Problems of zirconium and hafnium in the nuclear industry: proceedings of the international conference. – Alushta. – 1999. – P. 38-40.
11. Dmitrenko A.E., Pelykh V.N., Pylypenko M.M. Refining of hafnium by electron-beam melting// Problems of atomic science and technology. – 2004. – № 3. – P. 112-115.
12. Kotsar M.L., Azhazha V.M., Borisov M.I. and others. The obtaining of pure zirconium and hafnium// High-Purity Substances. – 1992. – № 4. – P. 85-92.
13. Azhazha V.M., Bobrov Yu.P., Vjugov P.N., Lavrinenko S.D., Pylypenko M.M. and others. Improving the process and equipment sublimation of zirconium and hafnium tetrafluoride//Problems of atomic science and technology. – 2006. – № 4. – P. 138-143.
14. Azhazha V.M., Bobrov Yu.P., Vjugov P.N., Lavrinenko S.D., Pylypenko M.M., Onischenko L.V. Investigation of gas phase composition in the sublimation chamber during heating of zirconium and hafnium tetrafluoride//Obtaining of high-purity metals and alloys: materials Kharkov Scientific Assembly (ISPM-8). – Kharkov. – 2002. – P. 13-16.

UDC: 539.21: 621.315.592

DEFINITIONS OF LOCALIZED ENERGY STATES ON THE QUASI-FERMI LEVEL WITH CHANGING TIMES

G. Guliamov[1], N.Y. Sharibaev[1,2], U.I. Erkaboev[1]

[1]Namangan Engineering Pedagogical Institute
Uzbekistan
[2]Namangan Engineering Institute of Technology
Uzbekistan

Received 04.09.2013

Studies of the generation-recombination process of electrons from the filled localized surface states at the time of their lives. The applicability of the derivative of the Dirac distribution as δ-function at low temperatures in order to study the temperature dependence of the spectrum of the density of surface states. To improve the accuracy of the results in the paper, a method of discrete states spectroscopy on quasi-Fermi level with the changing times.

Keywords: low temperature localized state spectroscopy of discrete states, increasing the accuracy of the results, the discrete spectrum of the density of states.

ОПРЕДЕЛЕНИЕ ЛОКАЛИЗОВАННЫХ ЭНЕРГЕТИЧЕСКИХ СОСТОЯНИЙ ПО КВАЗИУРОВНЯМ ФЕРМИ С ИЗМЕНЕНИЕМ ВРЕМЕНИ

Г. Гулямов, Н.Ю. Шарибаев, У.И. Эркабоев

Исследован генерационно-рекомбинационный процесс электронов из заполненных локализованных поверхностных состояний по их времени жизни. Показана применимость производной функции распределения Дирака как δ-функции при низких температурах для исследования температурной зависимости спектра плотности поверхностных состояний. С целью повышения точности получаемых результатов в работе предложен метод спектроскопии дискретных состояний по квазиуровням Ферми с изменением времени.

Ключевые слова: низкотемпературное локализованное состояние, спектроскопия дискретных состояний, повышение точности результатов, дискретный спектр плотности состояний.

ВИЗНАЧЕННЯ ЛОКАЛІЗОВАНИХ ЕНЕРГЕТИЧНИХ СТАНІВ ЗА КВАЗІРІВНЯМИ ФЕРМІ ЗІ ЗМІНЮВАННЯМ ЧАСУ

Г. Гулямов, Н.Ю. Шарібаєв, У.І. Еркабоєв

Досліджено генераційно-рекомбінаційний процес електронів із заповнених локалізованих поверхневих станів за часом їх життя. Показано застосовність похідної функції розподілу Дірака як δ-функції за низьких температур для дослідження температурної залежності спектру густини поверхневих станів. З метою підвищення точності одержаних результатів у роботі запропоновано метод спектроскопії дискретних станів за квазірівнями Фермі зі змінюванням часу.

Ключові слова: низькотемпературний локалізований стан, спектроскопія дискретних станів, підвищення точності результатів, дискретний спектр щільності станів.

INTRODUCTION

Standard relaxation spectroscopy density of surface states is based on the generation of thermal electrons, which can be easily observed only at high temperatures. This and the limited resolution of the method. To improve the resolution of the used method of expanding the range of density of surface states in a row, the derivative of the ionization of an electron from the surface level of energy [1 – 3].

$$Nss\left(E\right)=\sum_{i=1}^{n}Nss_i(E_i)\frac{\partial\rho_i\left(E,t\right)}{\partial E_0\left(T,t\right)}, \qquad (1)$$

where $\rho\left(E\right)=1-\exp\left(-\frac{t}{\tau}\right)$ [4] τ – the electron lifetime in the place he used the relation

$$\tau\left(E,T,t\right)=\tau_0\exp\left(\frac{E}{kT}\right). \qquad (2)$$

As a result, it was found that when

$$\frac{\partial\rho(E,T,t)}{\partial E_0}=\delta\left(E-E_0\right). \qquad (3)$$

The resulting delta function is asymmetric, so in this situation, it took into account the additional requirements [5].

The purpose of this paper to show the suitability of the derivative of the Fermi-Dirac distribution for quasi-Fermi level from time to time as a delta function for the discrete spectrum of the density of surface states and thus increase the resolution of the method.

QUASI-FERMI TIME

The density of surface states can be determined from the loss of charge in a charge-coupled device [1, 2]. At time $t = 0$ from the surface layer completely go all the free electrons. After starting generation of thermal trapped electrons. Given the statistics of the Shockley-Read-Hall process can be described as follows [1, 2, 4]:

and $$\rho(t, \tau) = 1 - \exp(-t/\tau), \quad (4)$$

where $$\tau = 1/\gamma_n N_c \quad (5)$$

electron lifetime. Equation (4) can be represented as follows:

$$\rho(t,\tau) = 1 - \exp\left(-\exp\left(\frac{kT\ln(t) - kT\ln(\tau)}{kT}\right)\right). \quad (6)$$

If we consider that in this process each time the surface layer is cleaned from the released electrons generated from the traps, the changes over time energy of the Fermi level E_{ft}. In the future, this value depends on the time t is denoted as the quasi-Fermi level.

We introduce the notation:

$$E_\tau = kT\ln(\tau) \quad (7)$$

electron energy of the lifetime τ and

$$E_{ft} = kT\ln(t) \quad (8)$$

quasi-Fermi energy by the time t.

Considering (7) and (8) may be (6) in the form:

$$\rho\left(E_{ft}, E_\tau\right) = 1 - \exp\left(-\exp\left(\frac{E_{ft} - E_\tau}{kT}\right)\right). \quad (9)$$

One can easily imagine the derivative $\rho(E_{ft}, E_\tau)$ on E_{ft} as a delta function at $T \to 0$

$$\frac{\partial\rho(E_{ft}, E_\tau)}{\partial E_{ft}} = \delta\left(E_{ft}, E_\tau\right). \quad (10)$$

SPECTROSCOPY OF QUASI-FERMI CHANGE IN TIME

The distributions function of the Fermi-Dirac distribution for the generation of electrons:

$$f = \left[\exp\left(\frac{E_{ft} - E_\tau}{kT}\right) + 1\right]^{-1} \quad (11)$$

step function is known energy [6]. It is also known that the derivative of the energy function of speed is the Dirac delta function (see fig. 1) in $T \to 0$ [6]. In this case, the delta function is as follows:

$$f = \frac{1}{kT}\exp\left(\frac{E_{ft} - E_\tau}{kT}\right)\left[\exp\left(\frac{E_{ft} - E_\tau}{kT}\right) + 1\right]^{-2}. \quad (12)$$

The resulting function (12) we substitute in (1) and get:

$$Nss\left(E\right) = \sum_{i=1}^{n} Nss_i(E_i)\frac{1}{kT}\exp\left(\frac{E_{fti} - E_\tau}{kT}\right) \times \times\left[\exp\left(\frac{E_{fti} - E_\tau}{kT}\right) + 1\right]^{-2}. \quad (13)$$

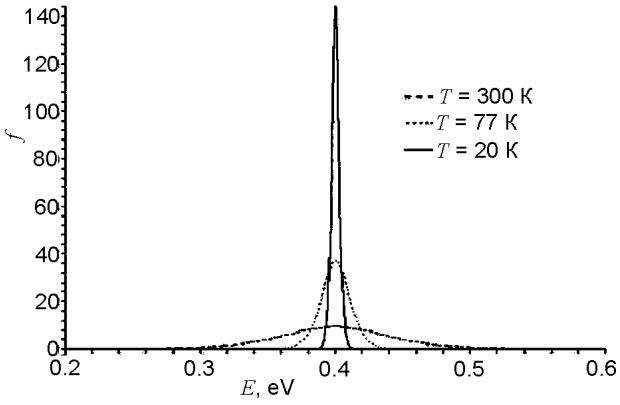

Fig. 1. The derivative of a step function at the Fermi-Dirac distribution of energy at different temperatures.

If we imagine that the quasi-Fermi E_{ft} level changes throughout the segment gap in each relevant electron energy E_τ generated from the trap life time τ, we get a peak delta function. Scanning energy E_{ft} for each specific temperature, perhaps because it is theoretically possible to set the appropriate time τ $E_{ft} \in [E_c, E_v]$. Fig. 2 shows a range where the shaded area are 10 discrete levels at different temperatures. It is easy to notice that for the discrete spectrum as in [1 – 4], we can use the derivative of the Fermi-Dirac distribution on E_{ft} a delta function.

TEMPERATURE DEPENDENCE OF THE DENSITY OF SURFACE STATES AND DISCRETE SPECTRA

We turn to the treatment of the density of surface states. Fig. 3 shows the density of surface states of [7], which shows the graphs of experimental and theoretical fitting the density of states $N_{ss}(E, T)$

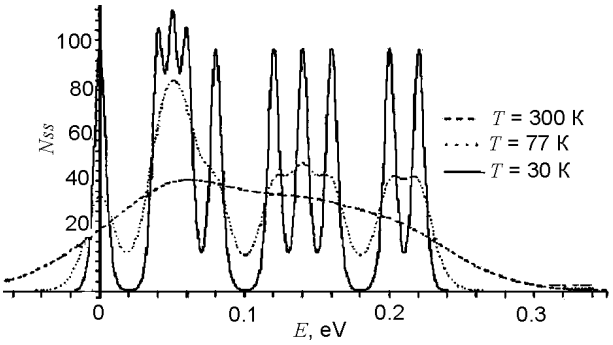

Fig. 2. The spectrum of the density of surface states at different temperatures.

obtained by the decomposition of the experimental curve in a series of functions (12).

Analysis of fig. 3 $N_{ss}(E, T)$ shows that the experimental plot at $T = 300$ K is easily decomposed into a series of functions (12). Fig. 4 is a graph theoretical model density of states that for $T = 5$ K. From these figures one can see that even at a low temperature in the graph clearly distinguish the individual peaks.

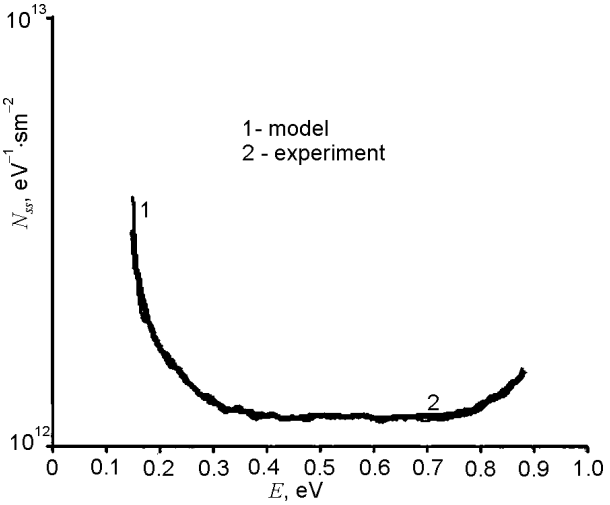

Fig. 3. Experimental [7] and the model spectrum density of surface states at $T = 300$ K.

When the temperature tends to zero, these peaks are transformed into discrete levels, and the continuous line $N_{ss}(E, T)$ in the discrete energy spectrum (see fig. 4). These changes $N_{ss}(E, T)$ are due to the fact that the temperature is lowered by reducing the thermal broadening of the energy levels (12) becomes the Dirac delta function $\delta(E - E_0)$.

Based on the study, it can be concluded that the experimental continuous spectrum density of surface states $N_{ss}(E, T)$ at a certain high temperature relaxation method at low temperatures becomes a discrete energy spectrum. Such a strong temperature dependence of the density of surface states due to

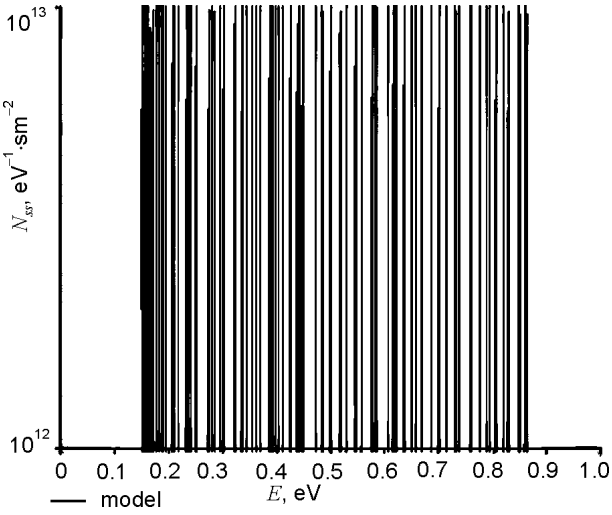

Fig. 4. Model discrete spectrum of the density of surface states at $T = 5$ K.

the fact that the derivative of the Fermi-Dirac distribution becomes a Dirac delta function.

The present method of determining the density of the surface low-temperature conditions increases the resolution of the transient spectroscopy and surface levels of relaxation techniques used to measure the energy spectrum of the density of states.

CONCLUSION

According to the study of surface electrons recharge levels in their lifetime based on the principle of CCD determined that the derivative of the ionization energy of the electron is a r-function at $T \to 0$. The applicability of the derivative of the Dirac distribution function of the energy of the quasi-Fermi level with the time change as a δ-function at low temperatures in order to study the temperature dependence of the spectrum of the density of surface states. This was possible because the derivative of a step function is a δ-function. We propose a method of spectroscopy of discrete states by quasi-Fermi level with the change of time to improve the accuracy of the results.

REFERENCES

1. Guliamov G., Sharibaev N.Yu. The temperature dependence of the density of surface states, determined by transient spectroscopy//Physical Engineering surface. – 2010. – Vol. 8, No. 1. – P. 53-68.
2. Guliamov G., Karimov I.N., Sharibaev N.Yu. Erkaboev U. Determination of the density of surface states at the semiconductor dielectric structures in Al-SiO2-Si and Al-SiO2-n-Si <Ni> at low

temperature//Uzbek Journal of Physics. – 2010. – Vol. 12, No. 3. – P. 143-146.
3. Guliamov G., Sharibaev N.Yu. Determination of the density of surface states of the interface, the semiconductor-insulator in the MIS structure// FTP. – 2011. – Vol. 45, No. 2. – P. 178-182.
4. Nosov Y.R., Shilin V.A. Fundamentals of Physics, charge-coupled devices. – M.: Nauka, 1986.
5. Guliamov G., Sharibaev N.Yu. X-ray, synchrotron and neutron research//Surface. – 2012, No. 9. – P. 13-17.
6. Zeldovich J.B., Myshkis A.D. Elements of applied mathematics. – M.: Nauka, 1972. – 592 p.
7. Karimov I.N. Basics of optimization of the physical processes at the semiconductor-insulator. – Dis . doc., Sci. Science, Tashkent, 1995. – 232 p.

UDC: 621.039.736

ANALYSES OF FLUORAPATITE PREPARED BY BOTH CHEMICAL PRECIPITATION AND SOLID PHASE REACTION METHODS

S.Yu. Sayenko, V.A. Shkuropatenko, R.V. Tarasov, K.A. Prudyvus, S.A. Savina, A.V. Zykova

NSC "Kharkov Institute of Physics and Technology"
Ukraine

Received 05.09.2013

At the present study the possibility of obtaining two compositions of $Ca_{10}(PO_4)_6F_2$ and $Ca_9Sr(PO_4)_6F_2$ fluoroapatites by both chemical deposition from solutions of the initial components and reaction in the solid phase was investigated. Using X-ray diffraction (XRD) method was shown that the fluorapatite synthesis based on calcium pyrophosphate with the addition of strontium takes place at lower temperatures. Fluoroapatite formation obtained by precipitation process is the result of the reaction between initial component solutions. At the process of heat treatment of obtained powders by XRD method was found that compared with fluorapatite obtained by solid phase reaction, fluorapatite obtained by precipitation method include less content of TCP phase. Maximum density (~92 % of the theoretical value) is reached for the sample heat treated at 1250 °C with the exposure time up to 6 hours for fluorapatite obtained by precipitation and at a temperature 1200 °C with the exposure time up to 10 hours for fluorapatite prepared by reaction in the solid phase.

Keywords: structure modification, fluorapatite, X-ray diffraction, differential thermal analysis, radioactive wastes immobilization

АНАЛИЗ ФТОРАПАТИТА, ПОЛУЧЕННОГО МЕТОДАМИ ХИМИЧЕСКОГО ОСАЖДЕНИЯ И ТВЕРДОФАЗНОЙ РЕАКЦИИ

С.Ю. Саенко, В.А. Шкуропатенко, Р.В. Тарасов, Е.А. Прудывус, С.А. Савина, А.В. Зыкова

В данной работе исследовалась возможность получения фторапатита двух составов $Ca_{10}(PO_4)_6F_2$ и $Ca_9Sr(PO_4)_6F_2$ методом химического осаждения растворов исходных компонентов и реакцией в твердой фазе. С помощью рентгенофазового анализа (РФА) показано, что с добавлением стронция синтез фторапатита на основе пирофосфата кальция проходит при более низких температурах. Образование фторапатита, полученного осаждением происходит в результате реакции между растворами исходных компонентов. При термообработке полученных порошков методом РФА установлено, что по сравнению с фторапатитом, полученным с помощью твердофазной реакции, фторапатит, полученный осаждением содержит меньшее количество ТКФ. Максимальное значение плотности (~92% от теоретической) достигнуто для образцов термообработанных при температуре 1250 °С и времени выдержки 6 часов для фторапатита, полученного осаждением и при температуре 1200 °С и времени выдержки 10 часов для фторапатита, полученного реакцией в твердой фазе.

Ключевые слова: радиоактивные отходы, иммобилизация, фторапатит, рентгенофазовый анализ, дифференциально-термический анализ.

АНАЛІЗ ФТОРАПАТИТУ, ОТРИМАНОГО МЕТОДАМИ ХІМІЧНОГО ОСАДЖЕННЯ ТА ТВЕРДОФАЗНОЇ РЕАКЦІЇ

С.Ю. Саєнко, В.А. Шкуропатенко, Р.В. Тарасов, С.О. Савіна, К.А. Прудивус, А.В. Зикова

У даній роботі досліджувалася можливість отримання фторапатиту двох складів $Ca_{10}(PO_4)_6F_2$ та $Ca_9Sr(PO_4)_6F_2$ методом хімічного осадження розчинів вихідних компонентів і реакцією в твердій фазі. За допомогою рентгенофазового аналізу (РФА) показано, що з додаванням стронцію синтез фторапатиту на основі пірофосфата кальцію проходить при нижчих температурах. Утворення фторапатиту, отриманого осадження відбувається в результаті реакції між розчинами вихідних компонентів. При термообробці отриманих порошків методом РФА встановлено, що у порівнянні з фторапатитом, отриманим реакцією в твердій фазі, фторапатит, отриманий осадженням містить меншу кількість ТКФ. Максимальне значення щільності (~92% від теоретичної) досягнуте для зразків термооброблених при температурі 1250 °С і часі витримки 6 годин для фторапатиту, отриманого осадженням і при температурі 1200 °С і часі витримки 10 годин для фторапатиту, отриманого реакцією в твердій фазі.

Ключові слова: радіоактивні відходи, іммобілізація, фторапатит, рентгенофазовий аналіз, диференціально-термічний аналіз.

INTRODUCTION

The surface and bulk material structure modifications are effective methods of modern innovative material development. Various technologies such as sintering, hot pressing, chemical precipitation and others are used for obtaining new materials with tailored properties.

The problem of radioactive waste accumulation is one of the long-term and hazardous consequences of nuclear programs. The most dangerous for the biosphere are high-level wastes (HLW). The concept of fractionation of HLW is developed according to the fact that the half-life, biological hazards and chemical properties of the HLW components vary greatly. The concept of radioactive waste immobilization into the crystalline matrices is based on a matrices using such as mineral phases, which have a natural analogs stable over long geological time.

Recently experts from different countries carried out multidisciplinary research of more than 30 such crystalline compounds for immobilization of HLW. There are durable and chemical stable minerals such as zircon, pyrochlore, magnesium-aluminum spinel, rare earth garnets, zirconolite, apatite, monazite, etc. [1]. In different countries, the application of a variety of rocks for geological disposal of the immobilized HLW is expected, so often, for the same radionuclides different waste forms were used for next compatibility with the disposal mineral phases and the immobilization matrices.

The immobilization waste forms based on apatite ceramic are considered as promising materials for the immobilization of high-level waste due to a wide range of iso- and heterovalent substitutions, high chemical and radiation resistance. Minerals and synthetic compounds with apatite structure type form a large family: $A_{10}(BO_4)_6X_2$ (A – Ca, Sr, Ba, Pb, Na, Cd, Fe, K, Li, rare earth elements; B – P, Si, As, Cr , V, S; X – F, Cl, OH, O, Br, CO_3) [2].

One of the famous examples showing the chemical and radiation resistance of apatite in nature is uranium deposit in Oklo (Gabon, Africa). The chain reaction of uranium fission in the mineral formation took place some two billion years ago. The crystals of apatite are located in this place, characterized by abnormal enrichment of ^{235}U and fission products. Consequently, the apatite-like compounds can maintain the crystalline structure within a very long time.

Apatite materials have also found an application in many other fields, including biology, medicine, electronics, etc. There are various technologies of fluorapatite synthesis such as solid phase reactions, precipitation from solution, sol-gel, hydrothermal methods, and others. The aim of the present study was to obtain calcium fluorapatite and fluorapatite with strontium content by means of the solid phase reaction and the precipitation of initial components solutions

MATERIALS AND METHODS

For fluoroapatite $Ca_{10}(PO_4)_6F_2$ preparation by means of the solid phase reaction the following components such as calcium pyrophosphate $Ca_2P_2O_7$, calcium fluoride, CaF_2, calcium carbonate $CaCO_3$, phosphoric acid H_3PO_4 were taken in the required stoichiometry. Process of preparation of fluorapatite was made by the following reaction [3]:

$$2Ca_2P_2O_7 + CaF_2 + 2H_3PO_4 + 3SaSO_3 \rightarrow \rightarrow Ca_{10}(PO_4)_6F_2 + 3H_2O + 5SO_2\uparrow. \quad (1)$$

To obtain fine powder of calcium pyrophosphate grinding carried out in a planetary mill Mono "Pulverisette 6" with isopropyl alcohol.

Calcium pyrophosphate, calcium carbonate and calcium fluoride were mixed in a mill environment in isopropyl alcohol and dried at a temperature of 100 °C to a residual moisture content 3 – 5%. Fluoroapatite dried mixture was screened through a sieve with a mesh size of 100 microns. For strontium adding in the fluorapatite mixture the strontium nitrate $Sr(NO_3)_2$ as an aqueous solution was used. Thus, an uniform distribution of strontium nitrate in the fluorapatite mixture was provided. Strontium fluorapatite $Ca_9Sr(PO_4)_6F_2$ was obtained by reaction:

$$2Ca_2P_2O_7 + CaF_2 + 2H_3PO_4 + 4CaCO_3 + +Sr(NO_3)_2 \rightarrow Ca_9Sr(PO_4)_6F_2 + 3CO_2\uparrow + 4H_2O + + 2NO_2 + (1/2)O_2. \quad (2)$$

For fluorapatite preparation by solutions precipitation method the following components such as calcium nitrate $Ca(NO_3)_2 \cdot 4H_2O$, disodium hydrogen phosphate $(NH_4)_2HPO_4$, ammonium fluoride NH_4F were taken in the required stoichiometry. The preparation of $Ca_{10}(PO_4)_6F_2$ was performed according to the following reaction:

$$10Ca(NO_3)_2 + 6(NH_4)_2HPO_4 + 2NH_4F + NH_4OH + (1/2)O_2 \rightarrow Ca_{10}(PO_4)_6F_2 + + 14NN_4NO_3 + +5{,}5H_2O + 7NO_2\uparrow. \quad (3)$$

The process of calcium fluoroapatite preparation by chemical precipitation method comprises the following steps [4]:

– Preparing of the aqueous solutions of the initial components required concentration. A sample of $Ca(NO_3)_2 \cdot 4H_2O$ in distilled water was dissolved. Separately, the samples of $(NH_4)_2HPO_4$ and NH_4F in distilled water were dissolved.

– Mixing the initial solutions. A solution of $(NH_4)_2HPO_4$ (0.3 M) and NH_4F by drops, with constant stirring, was poured in warm $Ca(NO_3)_2 \cdot 4H_2O$ (0,5 M) (50 °C) solution with pH = 9 – 9.5 adjusted by adding ammonium hydroxide NH_4OH.

– Preparing of a calcium fluorapatite powder. Flushing the precipitate, drying in air, grinding and heat-treating of the obtained powder was carried out in the temperature range 900 – 1250 °C for 1 hour.

The strontium incorporation into fluorapatite structure was made by strontium nitrate $Sr(NO_3)_2$ adding to a solution of $Ca(NO_3)_2 \cdot 4H_2O$. The preparation of strontium containing fluorapatite was carried out analogously to the preparation of calcium fluorapatite:

$$9Ca(NO_3)_2 + Sr(NO_3)_2 + 6(NH_4)_2HPO_4 + 2NH_4F + NH_4OH + (1/2)O_2 \rightarrow \rightarrow Ca_9Sr(PO_4)_6F_2 + 14NN_4NO_3 + 5.5\ H_2O + 7NO_2\uparrow. \quad (4)$$

The heat treatment of the powders was made in air furnaces SUOL–0.25.1/12 – M1 and MP – 2U. Thermogravimetric and differential thermal analysis (TGA/DTA) was performed on derivatograph Q – D 1500 at a temperature range 20 – 1000 °C, with heating rate about 12 °C/min and termoanalizatore SDT Q600 V20.9 Build 20 in the temperature range 50 – 1300 °C, with heating rate about 10 °C/min. The phase analysis was made by the phase X-ray diffraction method (XRD) (DRON – 1.5 with Cu radiation using a nickel selective filter). Samples were prepared in the form of tablets with diameter of 14 mm and height of 5 – 7 mm by double-side axial fluorapatite powder cold pressing method in a hydraulic press. Pressing was carried out in the pressure range 124 – 247 MPa.

The sintering of synthesized fluorapatite samples in air was performed in the temperature range 900 – 1250 °C. The apparent bulk density (ρ_{ap}) of the samples after sintering was determined by hydrostatic GOST 2409 – 95.

RESULTS AND DISCUSSION

Fluoroapatite obtained by solid phase reaction. According to results of XRD analysis, only lines of calcium pyrophosphate $Ca_2P_2O_7$ after mixing of the initial components were found (fig. 1a).

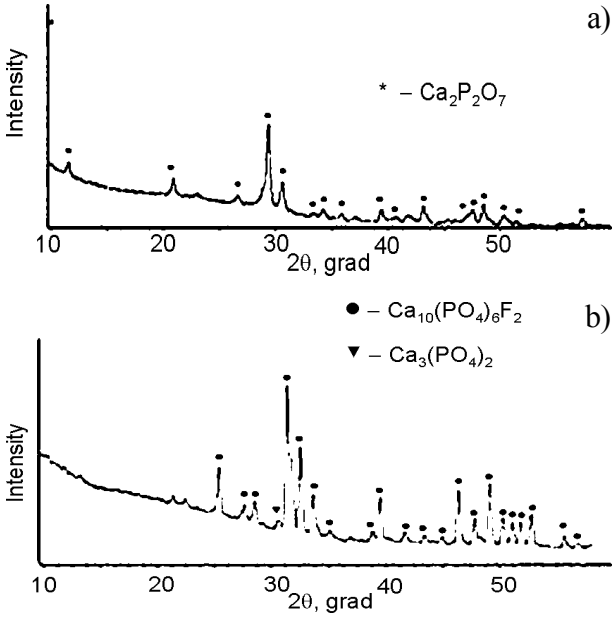

Fig. 1. Diffraction peaks of $Ca_{10}(PO_4)_6F_2$ obtained by solid phase reaction: a) – initial mixture; b) – termal treatment at: T = 1000 °C, τ = 1 hour.

The results of thermal analysis of the fluoroapatite $Ca_{10}(PO_4)_6F_2$ mixture are shown in fig. 2.

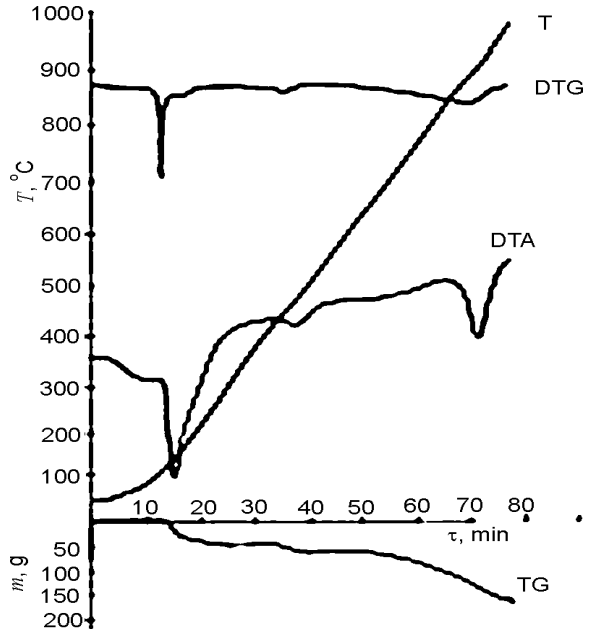

Fig. 2. TG/DTA analysis of $Ca_{10}(PO_4)_6F_2$.

Heat treatment of the original mixture up to 500 °C, according to X-ray studies, does not change the phase composition. According to TG/DTA analysis in the temperature range 120 – 280 °C there

is a strong endothermic effect, which is associated with the removal of adsorbed water and evidenced by weight loss in the TG curves, and also lack of visible change in the phase composition. Second small endothermic peak in the DTA curve in the temperature range 440 – 520 °C, apparently associated with the start of decomposition of calcium carbonate which is in a small amount in the mixture. At the difractogram of the powder, which was heat-treated at 600 °C, there is the appearance of lines fluorapatite. At temperature about 700 °C, there is a significant number of lines of fluorapatite, and reducing the intensity of the lines $Ca_2P_2O_7$. Total synthesis of the fluorapatite with $Ca_2P_2O_7$ destruction proceeds in the temperature range 900 – 1000 °C (fig. 1b). On the DTA curve at such temperature range there is a fairly strong endothermic effect. Furthermore the line of tricalcium phosphate $Ca_3(PO_4)_2$ (TCP) appears in addition to the lines of the synthesized fluorapatite in the diffraction peaks.

The research of phase formation of fluorapatite with strontium content demonstrate that heat treatment of fluorapatite mixture up to 500 °C similar to the case of the calcium fluoroapatite, does not affect on the mixture phase composition. Also, similar to the case of calcium fluoroapatite, on the DTA curve endothermic peaks were observed, which associated with removal of adsorbed water and the start of decomposition of calcium carbonate. Intensive synthesis of fluorapatite runs at 600 °C. Total synthesis of fluorapatite with the initial phases destruction occurs in the temperature range 800 – 900 °C (fig. 4) and is accompanied by the endothermic effect at the DTA curve. Similar to the calcium fluoroapatite case the diffraction lines of TCP appear, and its intensity decreases with increasing temperature up to 1000 °C (fig. 3).

The sintering in air at the temperature range 1100 – 1200 °C for 600 minutes residence time is performed. The data of the relative density measurements of the sintered samples in air are shown in fig. 4.

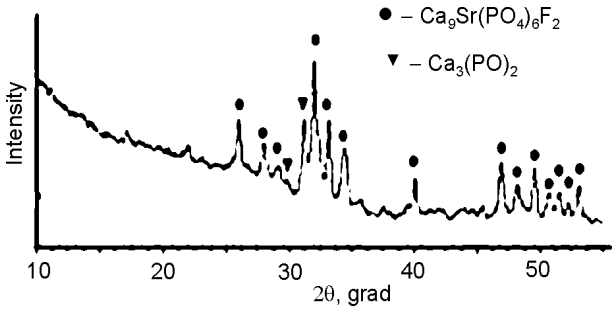

Fig. 3. Diffraction peaks of $Ca_9Sr(PO_4)_6F_2$ obtained by solid phase reaction T = 1000 °C, τ = 1 hour.

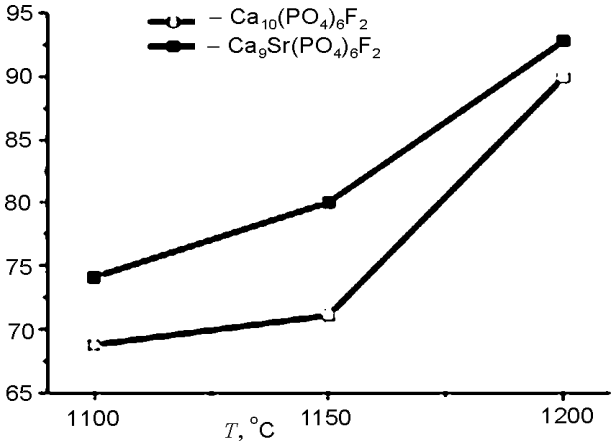

Fig. 4. The dependence of relative density of fluorapatite samples obtained by solid phase reaction on sintering temperature (τ = 600 min).

The results demonstrate that the sintering temperature increasing in air leads to increase in density and there is the maximum value of relative density for all investigated fluorapatite compositions at the temperature 1200 °C.

Fluoroapatite obtained by chemical precipitations method. Fig. 5 shows XRD data of powders obtained by co-precipitation of solutions of the initial components, $Ca_{10}(PO_4)_6F_2$ calcium and $Ca_9Sr(PO_4)_6F_2$ with strontium content fluorapatites. At all diffraction lines are present only one phase – $Ca_{10}(PO_4)_6F_2$ (fig. 1a) and $Ca_9Sr(PO_4)_6F_2$ (fig. 1b), respectively. Previously the necessity of heat treatment of resulting powder at 800 – 1000 °C for 1 hour for fluorapatite solid-phase synthesis by calcium pyrophosphate $Ca_2P_2O_7$ using, as a main component, was shown. In contrast to fluorapatite, obtained by reaction in the solid phase, the formation

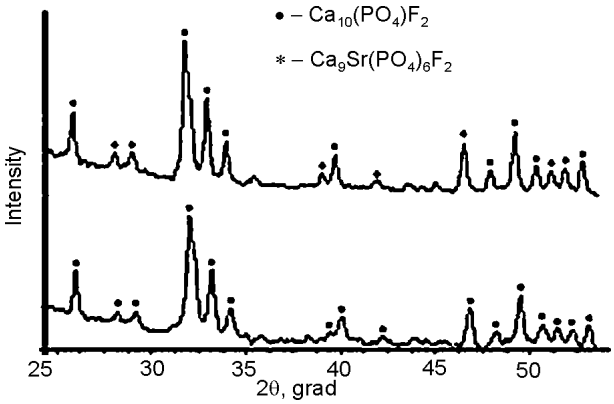

Fig. 5. Diffraction peaks of initial powders $Ca_{10}(PO_4)_6F_2$ (a) and $Ca_9Sr(PO_4)_6F_2$ (b) obtained by chemical precipitation method.

of fluorapatite by chemical precipitation is directly resulting of the reaction of the initial component solutions.

The only endothermic peaks with minimum at 100 °C which correspond to remove adsorbed water was observed at the DTA curve obtained by chemical precipitation of powders $Ca_{10}(PO_4)_6F_2$ and $Ca_9Sr(PO_4)_6F_2$.

A small endothermic peak at the temperature range 900 – 1000 °C in fig. 6 is observed and probably associated with the start of thermal decomposition reaction for fluoroapatite [5]:

$$Ca_{10}(PO_4)_6F_2 \rightarrow 3Ca_3(PO_4)_2 + CaF_2. \quad (5)$$

DTA data are confirmed by XRD data of fluorapatite heat-treated powders obtained by chemical precipitation from solutions The line of tricalcium phosphate with low intensity was observed after heat treatment of the powder of calcium fluoroapatite at 900 °C.

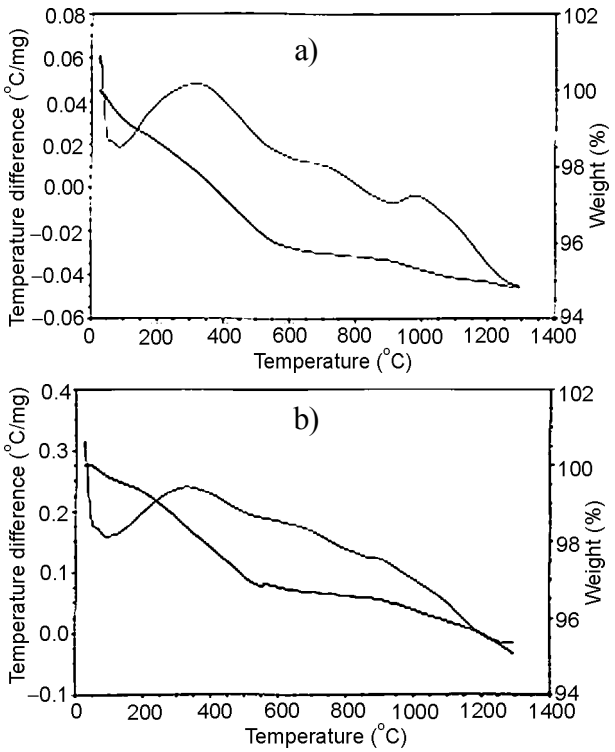

Fig. 6. TG/DTA analysis of $Ca_{10}(PO_4)_6F_2$ (a) and $Ca_9Sr(PO_4)_6F_2$ (b).

The increasing of the thermal treatment temperature up to 1150 °C does not affect on the phase composition of calcium fluoroapatite. In contrast to the diffractogram of strontium containing fluorapatite which has demonstrated the increasing of the $Ca_3(PO_4)_2$ lines number as compared to $Ca_9Sr(PO_4)_6F_2$, heat-treated at 900 °C. The next temperature increasing up to 1250 °C leads to the disappearance of the tricalcium phosphate lines in the diffraction pattern of calcium fluorapatite and the reducing of intensity and number of lines in the diffraction pattern of strontium containing fluorapatite (fig. 7). It is known that chemical durability of phosphate materials decreases during process of fluoroapatite → hydroxyapatite → tricalcium phosphate transformation [6].

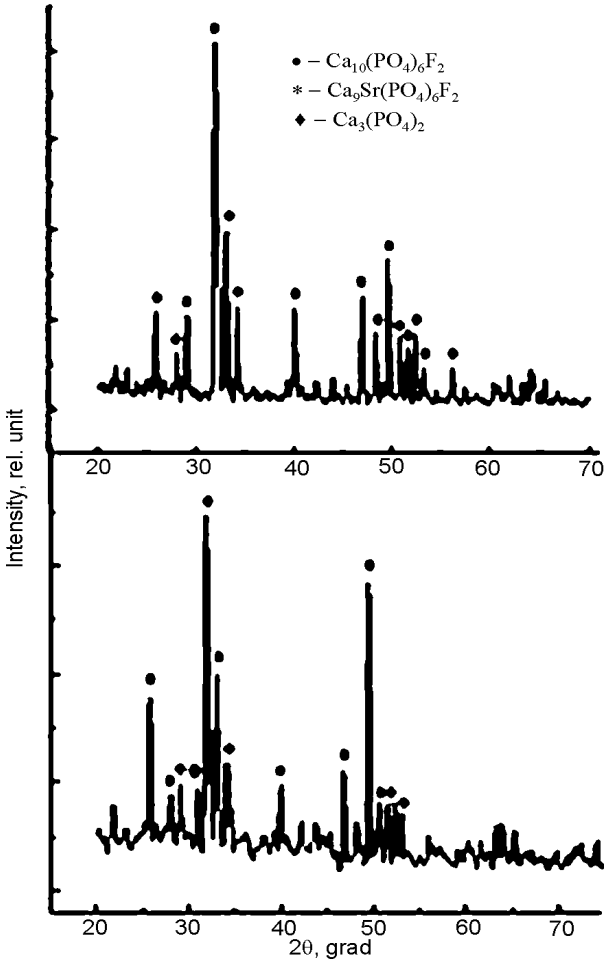

Fig. 7. Diffraction peaks of $Ca_{10}(PO_4)_6F_2$ (a) and $Ca_9Sr(PO_4)_6F_2$ (b) $T = 1250$ °C, $\tau = 1$ hour.

Therefore, the content of TCP in the fluorapatite matrices materials for next HLW immobilization should be minimal. The samples were sintered in the temperature range 1000 – 1250 °C for 6 hours in air. Fig. 8 shows the relative density fluoroapatite $Ca_{10}(PO_4)_6F_2$ (a) and $Ca_9Sr(PO_4)_6F_2$ depending on the sintering temperature.

The density measurement results found that at the temperature 1250 °C the maximum value of the relative density (90 – 92%) was observed both for calcium fluoroapatite and fluorapatite containing strontium.

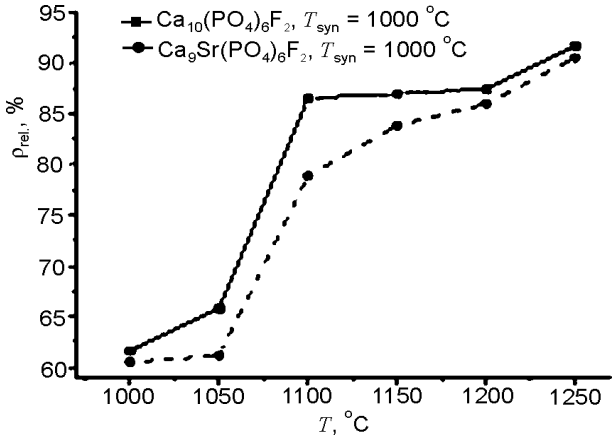

Fig. 8. The dependence of relative density of $Ca_{10}(PO_4)_6F_2$ (a) and $Ca_9Sr(PO_4)_6F_2$ on the sintering temperature.

CONCLUSIONS

1. The fluoroapatite compositions $Ca_{10}(PO_4)_6F_2$ and $Ca_9Sr(PO_4)_6F_2$ were prepared by both the reaction in the solid phase and chemical precipitation methods.
2. Found that in contrast to solid phase synthesis, the formation of fluorapatite by chemical precipitation method is directly resulted on the initial component solutions reaction.
3. According to XRD and DTA/TG analysis using was shown that heat treatment of obtained by precipitation from solutions fluorapatite at a temperature above 900 °C leads to formation of a small amount of TCP.
4. By sintering in air at temperatures of 1200 – 1250 °C the samples of calcium fluoroapatite and strontium containing fluoroapatite with low content of TCP and acceptable relative density of 90 – 92% both in the case of solid phase reaction and chemical precipitation were prepared.
5. The resulting material based on fluoroapatite structures may be used as effective matrices for strontium radionuclide immobilization.

REFERENCES

6. Omelyanenko B.I., Yudintsev S.V., Nikonov B.I., etc. Mineralogy and geochemistry of matrices preserving high-level waste//Geol. ores. deposits. – 1997. – T. 39, № 3. – P. 211-228.
7. Shpak A.P., Karbovskiy V.L., Trachevsiky V.V. Apatites. – K.: Academperiodika, 2002.
8. Shkuropatenko V.A., Tarasov R.V., Prudyvus E.A., etc. Synthesis of strontium fluorapatite on the basis of calcium pyrophosphate//Problems of Atomic Science and Technology. Series: physics of radiation damage and radiation material. Issue – 2012. – Vol. 5 (81). – P 98-105.
9. Hossein Eslami. Synthesis and characterization of nanocrystalline fluorinated hydroxyapatite powder by a modified wet-chemical process. Mehran Solati-Hashjin and Monhammadreza Tahriri//J. of Ceramic Processing Research 3. – 2008. – Vol. 9. – P. 224-229.
10. Chaikin M.V. Mechano-chemical processes and the mechanism of energy conversion indentation of single crystals//Chemistry for Sustainable Development. – 2009. – Vol.17. – P. 653-666.
11. Kanazawa T. Inorganic phosphate materials. – K.: Naukova Dumka, 1998. – 98 p.

UDC: 666.762.11:666.762.52

APPLICATION OF ELECTROCONSOLIDATION OF POWDER COMPONENTS FOR PRODUCTION OF ULTRADENCED CERAMICS Al_2O_3 AND ZrO_2 (3% Y_2O_3)

S.Yu. Sayenko, Eu.O. Svitlychniy, K.V. Lobach

National science center Kharkov Institute of Physics & Technology

Ukraine

Received 05.09.2013

The possibility of application of electroconsolidation for production of ultradenced ceramics based on Al_2O_3 and ZrO_2 (3% Y_2O_3) compounds is studied. As a result of the conducted researches optimum values of process temperature at which the best parameters of Al_2O_3 and ZrO_2 (3% Y_2O_3) ceramic properties are reached: the apparent density – 3.98 and 6.08 g/cm^3, bending strength – 350 and 800 MPa, fracture toughness – 4.0 and 8.0 MPa·m$^{0.5}$ respectively are established. The researches of a ceramics microstructure are found that high parameters of Al_2O_3 and ZrO_2 (3% Y_2O_3) properties are defined by dense and fine-crystalline structure.

Keywords: electroconsolidation, ceramic materials, mechanical properties, thermal shock resistance, microstructure, SEM analysis.

ПРИМЕНЕНИЕ ЭЛЕКТРОКОНСОЛИДАЦИИ ПОРОШКОВЫХ КОМПОНЕНТОВ ДЛЯ ПОЛУЧЕНИЯ ОСОБОПЛОТНОЙ КЕРАМИКИ Al_2O_3 и ZrO_2 (3% Y_2O_3)

С.Ю. Саенко, Е.А. Светличный, К.В. Лобач

Изучена возможность применения электроконсолидации для получения особоплотной керамики на основе Al_2O_3 и ZrO_2 (3% Y_2O_3). В результате проведенных исследований установлены оптимальные значения температуры процесса, при которых достигаются наибольшие показатели свойств керамики на основе Al_2O_3 и ZrO_2 (3% Y_2O_3) кажущаяся плотность 3.98 и 6.08 г/см^3, предел прочности при изгибе 350 и 800 МПа, коэффициент интенсивности напряжений 4.0 и 8.0 МПа·м^{0,5} соответственно. Исследованиями микроструктуры керамики установлено, что высокие показатели свойств Al_2O_3 и ZrO_2 (3% Y_2O_3) определяются плотной и мелкокристаллической структурой.

Ключевые слова: электроконсолидация, керамические материалы, механические свойства, термостойкость, микроструктура, SEM анализа.

ЗАСТУСОВАННЯ ЕЛЕКТРОКОНСОЛІДАЦІЇ ПОРОШКОВИХ КОМПОНЕНТІВ ДЛЯ ОТРИМАННЯ ОСОБЛИВОЩІЛЬНОЇ КЕРАМІКИ Al_2O_3 та ZrO_2 (3% Y_2O_3)

С.Ю. Саєнко, Є.О. Світличний, К.В. Лобач

Вивчена можливість щодо використання електроконсолідації для отримання особливощільної кераміки на основі Al_2O_3 та ZrO_2 (3% Y_2O_3). За результатами наведених досліджень встановлено оптимальні значення температури процесу, при яких досягаються найбільші показники властивостей кераміки Al_2O_3 та ZrO_2 (3% Y_2O_3): уявна щільність 3.98 та 6.08 г/см^3, міцність на вигин 350 та 800 МПа, коефіцієнт інтенсивності напруг 4.0 та 8.0 МПа·м^{0,5} відповідно. Дослідженнями мікроструктури було доведено, що високі показники властивостей Al_2O_3 та ZrO_2 (3% Y_2O_3) визначаються щільною та дрібнокристалічною структурою кераміки.

Ключові слова: електроконсолідація, керамічні матеріали, механічні властивості, термостійкість, мікроструктура, SEM аналізу.

INTRODUCTION

Recently the technologies of constructional ceramics production for the solution of various technical tasks are widely developed all over the world. One of leading position among studied materials possess ceramic materials based on Al_2O_3 and ZrO_2 (3% Y_2O_3) compounds [1 – 4].

Traditionally ceramic materials are produced from powder materials by various methods using such as formation and sintering. Depending on a form and the size of products, their purpose and the set properties apply different types of pressing, slip casting in plaster molds, extrusion, casting under pressure from thermoplastic slips, etc. [5].

The last operation of ceramics production is high-temperature sintering at which there is a process of consolidation of the formed samples. This process is accompanied by density increase, and also shrin-

kage of a green body. The kinetics of sintering and final properties of the solid body significantly depends on both properties of original powder from which the product was formed and technology factors such as temperature of sintering, speed of temperature raising, exposure time at the maximum temperature [6].

Last time for production ceramics with high physicomechanical characteristics are using high-disperse powders and ways of high-speed heating which allow to optimize a combination of processes of the maximum consolidation and the minimum growth of grain during sintering process. There are new methods of consolidation of powder materials: the activated sintering under the influence of an external field, high-speed hot isostatic pressing, electropulse sintering under pressure, etc. [7, 8].

Among progressive methods of producing ceramic materials one of perspective is electroconsolidation process. At electroconsolidation heating is carried out by a direct transmission of an electric current through the graphite elastic squeezed medium in which one or several samples are placed. Purpose of the medium is transfer of pressure created by punches, and ensuring heating of preparations due to heat allocated at passing of current. The speed of heating of preparations can reach 200 °C/min. Thus this process allows to carry out quasiisostatic hot pressing of powder compositions for minimum short terms with necessary isothermal endurance at the maximum temperature up to 3000 °C. Means of effective control of process are necessary for the technology using.

In National science center Kharkov Institute of Physics & Technology the equipment for realization of process of electroconsolidation is developed. The equipment provides opportunity to realize technological process of sintering of powder materials of different structure, in the medium of inert gases and in vacuum [9].

The purpose of this work is studying the possibility of application of electroconsolidation for production of ultradenced ceramics on the basis of Al_2O_3 and ZrO_2 (3% Y_2O_3).

EXPERIMENTAL PROCEDURE

As the main raw materials were used powder of alumina (3000 SDP, "Almatis", Germany) with a size of particles of 0.5 microns; and the powder ZrO_2 (3% Y_2O_3) (PSZ-5.2 YB, Stanford Materials Corporation, USA), with a size of particles of 0.04 – 0.07 microns.

For research carrying out the powders were filled up in forms and formed samples by a method of unaxial cold pressing under pressure of 100 MPa. After formation alumina samples were sintered (electroconsolidation) at a temperature 1500 and 1600 °C, with a speed of heating 100 °C/min and endurance 30 minutes, and zirconia samples were sintered at a temperature 1400 and 1500 °C with similar values of speed of heating and exposure time.

Open porosity and apparent density of samples were defined according to GOST 2409-95.

Bending strength was determined by a standard method in compliance with DSTU 3716-98. Determination of fracture toughness k_{1c} was carried out according to ASTM Standard C 1421-99.

For determination of thermal shock resistance the EN 820-3:2004 standard was used, according to which thermal stability characterized by difference of temperatures ΔT, at which there was an emergence of cracks in samples.

The researches of microstructure were conducted on an electronic microscope of the translucent type.

RESULTS AND DISCUSSION

Properties of ceramic samples Al_2O_3 and ZrO_2 (3% Y_2O_3) produced at various temperatures, in comparison with analogous properties of import analogs are given in the table. From the provided data it is clear that the samples of Al_2O_3 produced at a temperature 1500 °C, possess open porosity – 3 – 5%, their density makes 3.78 – 3.80 g/cm^3. The samples of Al_2O_3 produced at a temperature 1600 °C, are characterized by smaller porosity and higher values of the density – 3.96 – 3.98 g/cm^3 that conforms to requirements for ultradenced ceramics.

The Al_2O_3 samples produced at a temperature of 1500 °C, possess rather high parameters of the main properties: σ = 260 – 290 MPa, k_{1c} = 3.0 MPa·m$^{0.5}$, ΔT = 300 °C, however is not compared well with parameters of the samples produced at a temperature 1600 °C. The Al_2O_3 samples produced at a temperature 1600 °C, possess properties which are compared well with the parameters of the samples of import ceramics: σ = 350 MPa, k_{1c} = 3.5 – 4.0 MPa·m$^{0.5}$, ΔT = 300 °C.

Table

Properties of ceramic samples Al_2O_3 and ZrO_2 (3% Y_2O_3) in comparison with import analogs

Ceramic brand	Properties of ceramic				
	Open porosity, %	Apparent density, g/cm^3	Bending strength, MPa	Fracture toughness k_{1c}, MPa·м$^{0.5}$	Thermal shock resistance ΔT, °C
Al_2O_3 (1500 °C) NSC Kharkov	3 – 5	3.78 – 3.80	260 –290	3.0	300
Al_2O_3 (1600 °C) NSC Kharkov	0	3.96 –3.98	350	3.6 – 4.0	300
Al_2O_3, Dynamic ceramic (Eng.)	0	3.95	350	4.0	–
NSC Kharkov ZrO_2 (3% Y_2O_3) (1400 °C)	2 – 5	5.80 – 5.86	680	6.0 – 6.4	400
NSC Kharkov ZrO_2 (3% Y_2O_3) (1500 °C)	0	6.04 – 6.08	800	7.6 – 8.0	400
ZrO_2 (3% Y_2O_3) Kyocera (Japan)	0	6.00	750	7.0 – 8.0	400

Similarly properties of ZrO_2 (3% Y_2O_3) samples are changed. With increase in temperature of electroconsolidation from 1400 to 1500 °C, open porosity of samples disappears, their density increases to 6.04 – 6.08 g/cm^3, and the main parameters of properties correspond to level of import ceramics: σ = 800 MPa, k_{1c} = 7.6 – 8.0 MPa·м$^{0.5}$, ΔT = 400 °C.

As properties of ceramics, substantially are defined by its structure, for an explanation of the received results the corresponding researches were carried out.

In fig. 1 and fig. 2 the microstructure of ultradenced ceramic Al_2O_3 and ZrO_2 (3% Y_2O_3) is respectively shown.

From fig. 1 it is visible that the ceramics Al_2O_3 represents very fine-crystalline structure, with a prevailing size of grains of 1 – 3 μm. Thus the minimum size of grains of corundum makes 0.5 μm and maximum – 6 μm. Grains have a crystallographic facet that testifies about completion of process of crystallization at a temperature of 1600 °C. Borders

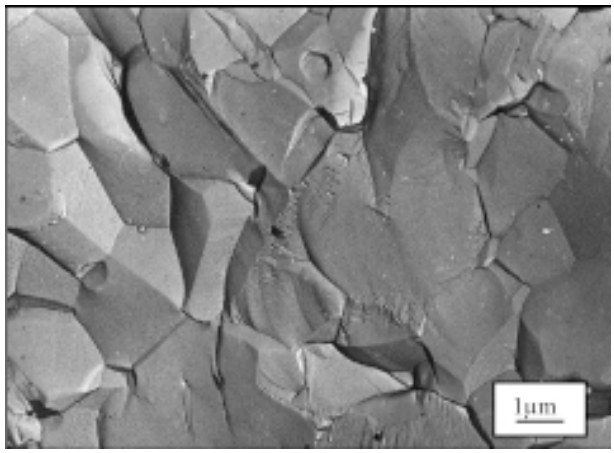

Fig. 1. Microstructure of ultradenced ceramic Al_2O_3.

of grains of corundum are very dense, thus on all volume of a ceramic sample are noticed fine-crystalline grains of spinel ($MgO·Al_2O_3$) with size ≤ 0,5 μm.

From fig. 2 it is visible that the ceramic sample of ZrO_2 (3% Y_2O_3) also has fine-crystalline structure which consists of well crystal grains of 0.2 – 2.6 μm in size, with a prevailing size of grains of 1.5 microns.

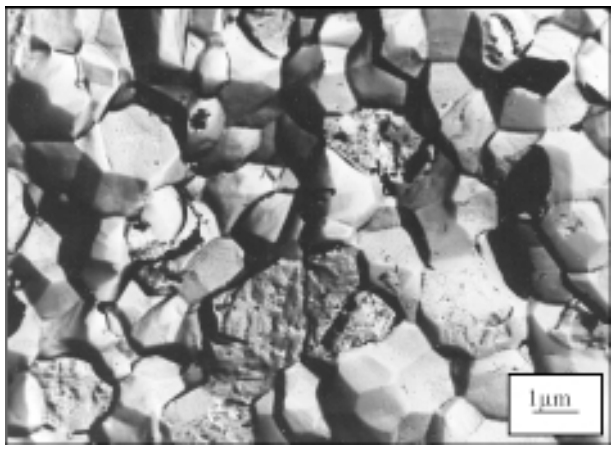

Fig. 2. Microstructure of ultradenced ceramic ZrO_2 (3% Y_2O_3).

As a result of the carried out researches, the possibility of application of electroconsolidation for production ultradenced ceramics Al_2O_3 and ZrO_2 (3% Y_2O_3) is established.

CONCLUSIONS

The possibility of application of electroconsolidation for production of ultradenced ceramics on the basis of Al_2O_3 and ZrO_2 (3% Y_2O_3) is studied. As a result of the conducted researches optimum values of process temperature at which the best parameters of properties of Al_2O_3 and ZrO_2 (3% Y_2O_3) ceramics are reached: the apparent density – 3.98 and 6.08 g/cm^3, bending strength – 350 and 800 MPa,

fracture toughness – 4.0 and 8.0 MPa·$m^{0.5}$ respectively are established. The researches of a microstructure of ceramics demonstrate that high parameters of properties Al_2O_3 and ZrO_2 (3% Y_2O_3) ceramics are defined by dense and fine-crystalline structure.

Developed ceramics are perspective for application as constructional materials for various spheres of science and engineering.

REFERENCES

1. Hannink R.H.J., Kelly P.M., Muddle B.C. Transformation toughening in zirconia- containing ceramics//J. Amer. Ceram. Soc. – 2000. – Vol. 83, № 3.– P. 461-487.
2. Medvedovski E., R.J. Liewellyn Oxide ceramics for abrasion and erosion resistance applications //Interceram.– 2002.– Vol. 51, № 2.– P. 120-126.
3. Svitlychniy Y.O. Corundum ceramics, modified zirconia, with increased strength and thermal shock resistance. – Avtoref. Cand. Tech. Sci.: 05.17.11. National Technological University "Kharkovskiy Polytechnical Institute". – Kharkiv, 2006. – 20 p.
4. Prokhorov I., Akimov G., Timchenko V. M Cold isostatic pressing as a way of receiving high-strength ceramic materials on the basis of ZrO_2 //Refractory and technical ceramics. – 1997. – № 8. – P. 12–17.
5. Garshin A.P., Gropyanov V. M., Zaytsev G.P., Semenov S.S. Machine-building ceramics. – SPb.: GTU, 1997. – 726 p.
6. Strelov K.K. Theoretical bases of technology of refractory materials. – M: Metallurgy, 1985. – 480 p.
7. Goldberger W.M., Fessler R.R. The development of Non-Intrusive Methods of Sensing and Control of Densification During Electroconsolidation// Advances In Process Measurements for the Ceramic Industry, Westerville, Ohio. – 1999. – P. 337.
8. Zhang J., Zavaliangos A., Groza J. R. Field activated sintering techniques: a comparison and contrast//P/M Science & Technology Brief. – 2003. – Vol. 5, № 3. – P. 17-21.
9. Project UNTC P-154. Htpp: //www.stcu.int.

UDC: 539.21: 621.315.592

THE TEMPERATURE DEPENDENCE OF THE BAND GAP Si

G. Guliamov[1], U.I. Erkaboev[1], N.Y. Sharibaev[1,2]
[1]Namangan Engineering Pedagogical Institute
Uzbekistan
[2]Namangan Engineering Institute of Technology
Uzbekistan
Received 07.09.2013

With the help of mathematical modeling of the thermal broadening of the energy levels studied the temperature dependence of the band gap semiconductors. In view of the temperature dependence of the effective mass of the density of states obtained graphs temperature dependence of the band gap. Investigated the effect of changes in the effective mass of charge carriers on the temperature dependence of the band gap semiconductors. The theoretical results of mathematical modeling are compared with experimental data for Si. The theoretical results satisfactorily explain the experimental results for Si.
Keywords: band gap, the effective density of states, the energy spectrum, the numerical simulation and experiment.

О ТЕМПЕРАТУРНОЙ ЗАВИСИМОСТИ ШИРИНЫ ЗАПРЕЩЕННОЙ ЗОНЫ Si

Г. Гулямов, У.И. Эркабоев, Н.Ю. Шарибаев

С помощью математического моделирования процесса термического уширения энергетических уровней исследована температурная зависимость ширины запрещенной зоны полупроводников. С учетом температурной зависимости эффективной массы плотности состояний получены графики температурной зависимости ширины запрещенной зоны. Исследовано влияние изменения эффективной массы носителей зарядов на температурную зависимость ширины запрещенной зоны в полупроводниках. Теоретические результаты математического моделирования сравниваются с экспериментальными данными для Si. Результаты теории удовлетворительно объясняют экспериментальные результаты для Si.
Ключевые слова: ширина запрещенной зоны, эффективная масса плотности состояний, энергетический спектр, численный эксперимент и моделирование.

ПРО ТЕМПЕРАТУРНУ ЗАЛЕЖНІСТЬ ШИРИНИ ЗАБОРОНЕНОЇ ЗОНИ Si

Г. Гулямов, У.І. Єркабоєв, Н.Ю. Шарібаев

За допомогою математичного моделювання процесу термічного розширення енергетичних рівнів досліджена температурна залежність ширини забороненої зони напівпровідників. З урахуванням температурної залежності ефективної маси густини станів отримані графіки температурної залежності ширини забороненої зони. Досліджено вплив змінювання ефективної маси носіїв зарядів на температурну залежність ширини забороненої зони в напівпровідниках. Теоретичні результати математичного моделювання порівнюються з експериментальними даними для Si. Результати теорії задовільно пояснюють експериментальні результати для Si.
Ключові слова: ширина забороненої зони, ефективна маса густини станів, енергетичний спектр, чисельний експеримент і моделювання.

INTRODUCTION

In [1 – 5] the temperature dependence of the density of states determined by relaxation spectroscopy of energy levels in semiconductors. It is shown that the surface state density is temperature dependent. The technique of determining the density of surface states. It is shown that due to the thermal broadening of the levels, the discrete spectrum with hanging temperature becomes a continuous energy spectrum. With the expansion of the energy spectrum of the density of states *GN* derivative function of the probability of energy required energy levels, it was shown that the magnitude of energy gap is temperature dependent. The temperature dependence of the band gap is determined by the temperature dependence of the density of the energy state of the conduction band and valence band of the semiconductor. Due to the thermal broadening of the density of states near the

bottom of the conduction band and valence band is reduced band gap. In the calculation of the temperature dependence of the forbidden assumed for simplicity that the density of states in the areas of constant edge of the conduction band and valence band are sharp and have a stepped shape. In these studies it was assumed that the effective mass of the density of states does not depend on the temperature. However, as shown by experiments [6], the effective mass of the density of states depends on the temperature. These changes are effective mass changes the temperature dependence of the band-gap.

However, in the real state of the semiconductor density is a function of speed and energy band structure of the sample is determined. Moreover, the density of states is so general that it can be used even when there is no Brillouin zone and sharp boundaries of permitted and prohibited zones [7, 8].

Thus, for analysis of experimental results for comparison between theory and experiment is necessary to consider the specific form of the band structure of the semiconductor and the dependence of the effective mass of the charge carriers of the temperature.

The aim of this work is to study the temperature dependence of the band gap semiconductor with the band structure and temperature dependence of the effective mass of carriers and comparison of theory with experiment.

THE TEMPERATURE DEPENDENCE OF THE DENSITY OF STATES

In determining the band gap values of the density of states corresponding to the energy band gap edges E_c and E_v denote by N_k the temperature dependence of the density of states can be studied by expanding the density of states in a series of $GN(E_i, E, T)$-functions of the derivative of the ionization energy of discrete states. The expansion has the following form: [1 – 5]

$$N_s(E,T) = \sum_{i=1}^{n} N_{si}(E_i) GN(E_i, E, T). \quad (1)$$

This is derived in turn from the integral expression:

$$N(E_0,T) = \int_{E_v}^{E_c} N(E)\rho(E_0, E, T)\, dE \quad (2)$$

$N(E_0, T)$ – the number of electrons generated from quantum states with energy less than E_0, with a continuous distribution in energy levels. We apply this method of expansion for the density of states in the conduction band of the semiconductor. For a quadratic dispersion law for the density of states of the conduction band is given by [9]

$$N(E) = N_{n0}\sqrt{E - E_c}\ ,\ N_{n0} = 4\pi\left(2m_n^* / h^2\right)^{3/2}. \quad (3)$$

Similarly, for the valence band

$$N(E) = N_{p0}\sqrt{E_p - E}\ ,\ N_{p0} = 4\pi\left(2m_p^* / h^2\right)^{3/2}. \quad (4)$$

As in the theory of non-crystalline semiconductors [7, 8] to determine the allowed and forbidden energy bands, we use the concept of density of states. Formulation (3) and (4) into (2) we obtain a model that describes the temperature dependence of the density of states near the band edges. With this in mind, we expand $N_s(E, T)$ in a series of $GN(E_i, E, T)$-functions. In the following form:

for the conduction band:

$$N_{sn}(E,T) = \sum_{i=1}^{n} N_{n0}\sqrt{E_i - E_c}\, GN(E_i, E, T)\Delta E$$

$$\text{at } E > E_c; \quad (5)$$

for the valence band:

$$N_{sp}(E,T) = \sum_{i=1}^{n} N_{p0}\sqrt{E_p - E_i}\, GN(E_i, E, T)\Delta E$$

$$\text{at } E > E_v; \quad (6)$$

for the gap:

$$N_{ss}(E) = 0 \text{ at } E_c > E > E_v,\ \Delta E = 1/n. \quad (7)$$

The values of the density of states corresponding to the energy band gap edges E_c and E_v is denoted by N_k. Then the energy position of the edges of the gap are determined by solving the following transcendental equations

$$\sum_{i=1}^{n} N_{sn}(E_i) GN(E_i, E, T)\Delta E = N_k,$$

$$\sum_{i=1}^{n} N_{sp}(E_i) GN(E_i, E, T)\Delta E = N_k, \quad (8)$$

where $\Delta E = 1/n$.

The solution of equation (8) determines the values at a given border gap $E_c(T)$ and $E_v(T)$, as a function of temperature T. N_k parameter of the problem and is determined experimentally. Then the band gap

$E_g(T)$ at a given temperature is defined as the difference between the values of $E_c(T)$ and $E_v(T)$ (9). Here $E_c(T)$ energy of the bottom of the conduction band, $E_v(T)$ – the energy of the valence band. It follows that the method of determining the accuracy of the experiment and the important factors in determining the width of the gap. Indeed the band gap, determined by optical methods – "optical width" of the band gap can not match the value of the band gap, determined by the temperature dependence of the resistance of the semiconductor. One of the reasons is that different values for N_k optical and electrical measuring techniques.

THE TEMPERATURE DEPENDENCE OF THE BAND GAP AND TO COMPARE THEORY WITH EXPERIMENT

In [6] established that the Si effective mass density of states depends on the temperature. Fig. 1 shows the temperature dependence of the effective mass of the density of states in Si m/m_0 from [6]. Using the data of fig. 1 using the model calculated the change in the band gap as a function of temperature.

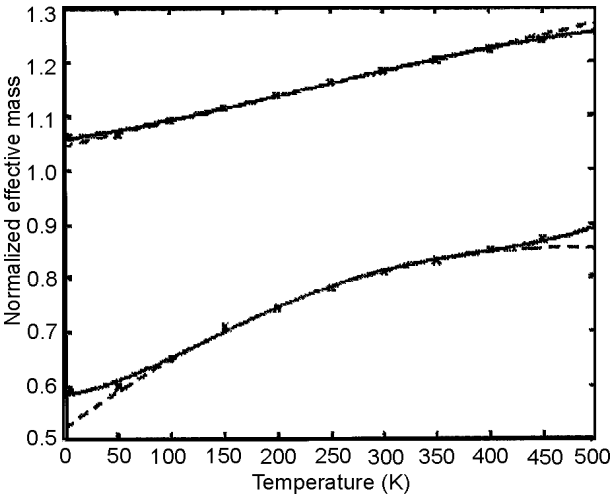

Fig. 1. The temperature dependence of the effective mass of the density of states in m/m_0 Si. [6]. ♦ – experiment [6]; — calculations for $m^*_n = m(T)$, $m^*_p = m(T)$; – – calculations for m^*_n = const; m^*_p = const.

Fig. 2 shows plots of the temperature dependence of the band gap of Si for the changes in the effective mass of the density of states taken from fig. 1 [6]. Fig. 2 shows that taking into account the temperature dependence of the effective mass significantly affect the results of the calculations.

Fig. 2 shows the results of the broken linear calculations and taking into account the temperature dependence of the electron effective mass. The same figure shows the theoretical linear continuous

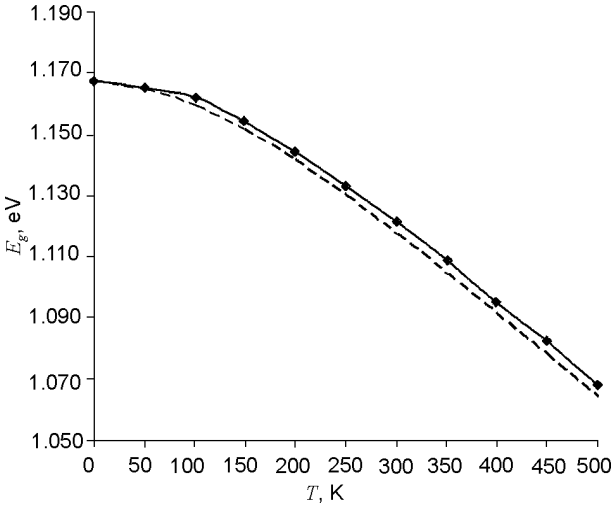

Fig. 2. Schedule - the temperature dependence of the band gap for Si. ♦ – experiment [6]; –– calculations for $m^*_n = m(T)$, $m^*_p = m(T)$; – – calculations for m^*_n = const; m^*_p = const.

temperature dependence of the band gap, taking into account the change in the effective mass of the electron and hole in the temperature range (0 K – 500 K). Experimental results for silicon taken from [6] are represented by dots. As can be seen from fig. 2 records the temperature dependence of the effective mass of electrons and holes are properly explain the temperature dependence of the band gap of silicon in the given temperature range. Thus, changes in the effective mass of the density of states with temperature can greatly affect the temperature dependence of the bandgap.

CONCLUSION

In this temperature range (0 K; 500 K) mathematical modeling of the temperature dependence of the band gap is satisfactorily described by a parabolic dispersion law. Experimental results of changing bandgap silicon [6] within the precision of the measurements with the theoretical calculations. Comparison of theory and experiment shows that the thermal broadening of the energy levels described by a *GN*-function satisfactorily describes the process of the temperature dependence of the band gap in Si. The temperature dependence of the energy spectrum of the density of states of semiconductors, taking into account the temperature dependence of the effective mass of the density of states. The temperature dependence of the band gap for the changes in the effective mass of the density of states. With the help of numerical experiments show that at temperatures $T > 50$ K change in the effective mass

of the density of states with increasing T a significant effect on the temperature dependence of the band gap.

REFERENCES

1. Gulyamov G., Sharibaev N.Yu.//FATA.– 2011. – Vol. 45, No. 2. – P. 178-182.
2. Gulyamov G., Sharibaev N.Yu.//Surface. – 2012, – № 9. – P. 13-17.
3. Gulyamov G., Sharibaev N.Yu., Erkaboev U.I.// PSE. – 2012. – Vol. 10, № 4. – P. 308-312.
4. Gulyamov G., Sharibaev N.Yu.//PSE. – 2012. – Vol. 10, № 2. – P. 221-225.
5. Gulyamov G., Karimov I.N., Sharibaev N.Yu., Erkaboev U.I.//Uzbek Journal of Physics. – 2010. – Vol. 12, № 3. – P. 143-146.
6. Caiafa X., Wang, Hudgins J.L., Santi E., and Palmer P.R. Cryogenic study and modeling of IGBTS IEEE. – 2003. – P. 1897-1903.
7. Bonch-Bruyevich V.B., and et.al. Electronic theory of non-crystalline semiconductors. – M.: Nauka, 1981. – 384 p.
8. Mott N., Devis E. Electronic Processes in Non-Crystalline Materials. Vol. 1. – New York: Wiley, 1982. – 664 s.
9. Shalimova K.V. Physics of semiconductors. – M.: Energoatomizdat, 1985. – 392 s.

UDC 669.017:620.186.

SILICIDE COATINGS STRUCTURE OPTIMIZATION BASED ON MULTISCALE APPROACH

S.V. Lytovchenko, V.M. Beresnev, V.A. Chyshkala, A.Ye. Dmytrenko, U.S. Nyemchenko, V.V. Burkovska

V.N. Karazin Kharkiv National University

Received 21.09.2013

This paper is an attempt to apply the multi-scale approach to the study of silicide coatings on molybdenum. Macro- and microstructure of silicide coatings largely determines mechanical and corrosion properties of molybdenum-protective coating composites. To prevent unacceptable changes, it is necessary to foresee the evolution of structure during formation of the coating and during operation of the composite. This paper analyzes the factors that determine degradation of properties of the coatings at different hierarchical levels. The requirements for the macro- and microstructure of the silicides with a view to achieving better thermal properties of the protective coating have been formulated.

Keywords: molybdenum, coatings, silicides, micro- and macrostructure

ОПТИМИЗАЦИЯ СТРУКТУРЫ СИЛИЦИДНЫХ ПОКРЫТИЙ НА ОСНОВЕ МУЛЬТИМАСШТАБНОГО ПОДХОДА

С.В. Литовченко, В.М. Береснев, В.А. Чишкала, А.Е. Дмитренко, У.С. Немченко, В.В. Бурковская

В работе предпринята попытка применения мультимасштабного подхода к изучению силицидных покрытий на молибдене. Макро- и микроструктура силицидного покрытия во многом определяет механические и коррозионные свойства композитов молибден – защитное покрытие. Для предотвращения недопустимых изменений необходимо предвидеть эволюцию структуры при формировании покрытия и в процессе эксплуатации композита. В работе проанализированы факторы, определяющие деградацию защитных свойств покрытия на разных иерархических уровнях. Сформулированы требования к макро- и микроструктуре силицидов с целью достижения более совершенных термических свойств защитного покрытия.

Ключевые слова: молибден, покрытия, силициды, микроструктура, макроструктура.

ОПТИМІЗАЦІЯ СТРУКТУРИ СИЛІЦИДНИХ ПОКРИТТІВ НА ОСНОВІ МУЛЬТИМАСШТАБНОГО ПІДХОДУ

С.В. Литовченко, В.М. Береснєв, В.О. Чишкала, О.Є. Дмитренко, У.С. Нємченко, В.В. Бурковська

У роботі зроблена спроба застосування мультимасштабного підходу до вивчення силіцидних покриттів на молібдені. Макро- і мікроструктура силіцидних покриттів багато у чому визначає механічні та корозійні властивості композитів молібден – захисне покриття. Для запобігання неприпустимих змін необхідно передбачити еволюцію структури при формуванні покриття і в процесі експлуатації композиту. У роботі проаналізовано чинники, що визначають деградацію захисних властивостей покриття на різних ієрархічних рівнях. Сформульовані вимоги до макро- і мікроструктури силіцидів з метою досягнення досконаліших термічних властивостей захисного покриття.

Ключові слова: молібден, покриття, силіциди, мікроструктура, макроструктура.

INTRODUCTION

Investigations of fundamental principles and basic mechanisms of structural phase transitions in solids are the most important component in development of new materials for use in modern high technology. Currently, a variety of composite materials, including those containing silicides of refractory metals, are increasingly replacing traditional structural and functional materials for the creation of new technologies, machines, mechanisms and devices in various fields of science and technology [1, 2]. This is largely due to the implementation of previously unattainable complex and/or the level of physical and mechanical, electro-physical, thermal, and other properties in such materials, which allows us to solve relevant technical and consumer problems: from reducing

weight and intake of metals to enhancing their durability, performance and efficiency.

Development of new and improvement of known materials is based on the results of two related areas of work – experimental and theoretical. In theoretical studies, the so-called cybernetic (experimental-statistical) and multilevel or multiscale approaches are distinguished. In the latter case, the material is represented in the form of a complex system – design, where the individual elements of the structure play a role of subordinate components (sub-systems, sub-structures), and conduct a direct simulation of the behavior of the material under the combined influence of external damaging factors including the internal geometry, properties, and interaction of elements. In this simulation, various approaches of continuum mechanics involving numerical or discrete techniques are used [3, 4].

In experimental studies of the mechanisms of formation and evolution of the structure of materials as well as structural phase transitions in them, it is of high importance to take into account the full range of external influences arising during operation (heat treatment, irradiation, corrosion, etc.). Combined external impact initiates the interference processes in materials, which can lead to the formation of quasi-stable states and can influence the formation of defects or other local irregularities in the original structure of the material [5, 6].

In this paper, a multiscale hierarchical approach is applied to the experimental studies of the possibility of raising long-term operational stability of the molybdenum-silicide coating composite material.

GENERAL CHARACTERISTICS OF SILICIDE COATINGS AND MULTI-SCALE ELEMENTS IN THEM

Silicide coatings are the most effective means of protection of refractory metals, particularly molybdenum from high-temperature oxidation [7, 8]. Silicides are used due to their heat resistance, ability to retain sufficient mechanical properties within a wide temperature range, higher conductivity and compatibility of silicide obtaining operation with a total production technology of the final products. Furthermore, silicides have a number of advantages, e.g. a high melting point, a wide range of resistivity, ability to form epitaxial layers forming the Schottky barrier of the predetermined value, possibility to grow the oxide film on the silicide. [9] At temperatures above 1500 °C in oxygenated atmospheres on the surface of the silicides the oxide film consisting of practically pure silicon dioxide SiO_2 is formed. This film provides a high heat resistance of silicide coatings, preventing penetration of oxygen to the metal surface.

Increased use of silicide coatings is constrained by a number of negative factors, significant of which is the lack of stability at high temperatures. This instability is caused by the initial thermodynamic instability of the substrate-coating system and its tendency for chemical reactions [10].

To achieve the best performance characteristics of molybdenum products with coatings, it is important to fully define the connection between the composition, structure and properties of the coatings, to simulate the optimal coating and develop a technology of its formation. At the same time, the simulation should take a large scale of object into account – from the macro-scale of the whole coating and its individual layers (with the size of hundreds of micrometers, fig. 1) to sub-micron elements (crys-

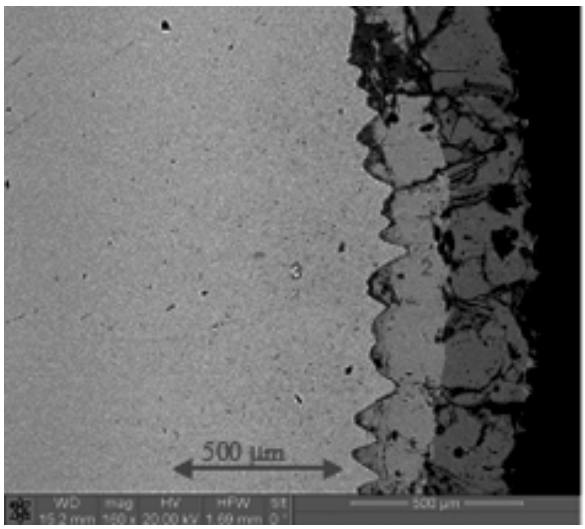

Fig. 1. Macroscale elements of the molybdenum substrate – two-phase silicide coating composition: 1 – $MoSi_2$; 2 – Mo_5Si_3, 3 – Mo.

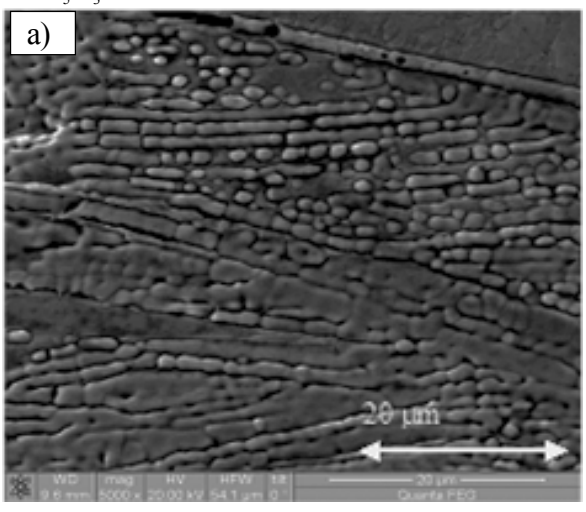

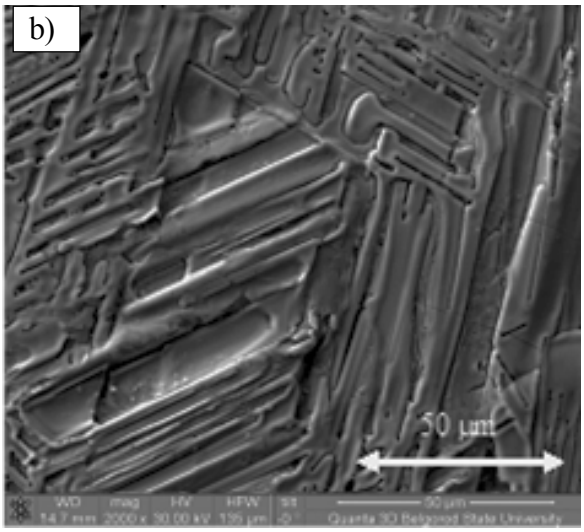

Fig. 2. Submicron elements of the $MoSi_2$-Mo_5Si_3 eutectic mixture.

tallites of eutectic mixtures, fig. 2) and the smallest nanoscale objects (pores, microcracks nucleus, interstitial atoms and molecules, vacancy clusters, fig. 3).

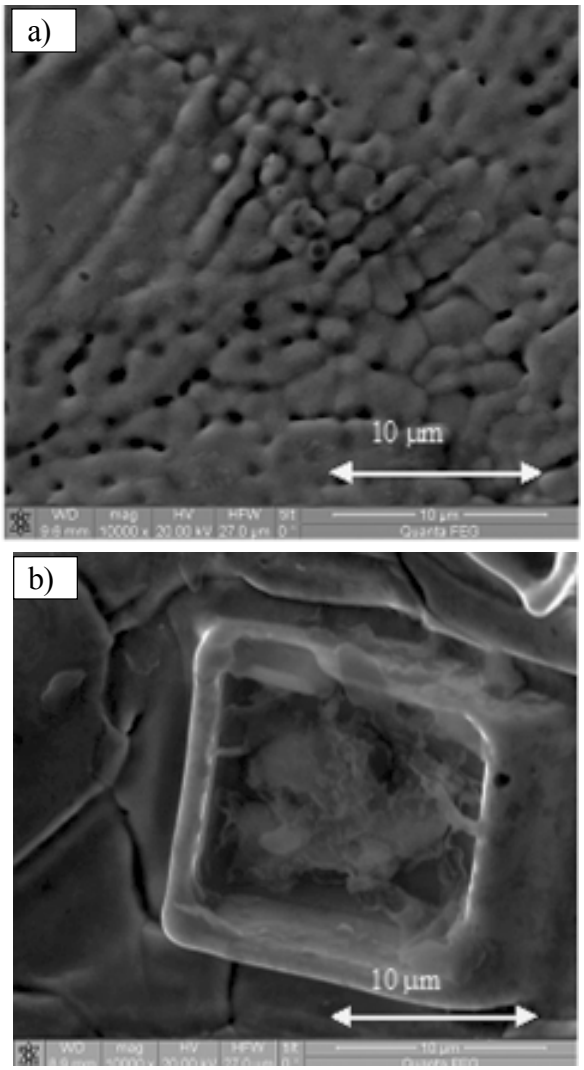

Fig. 3. Elements of the smallest scale in the silicide coating: a) – cluster of pores, b) – impurity.

It is known that the best coating from the perspective of uniform stress distribution, bonding strength and the greatest thermodynamic stability is a diffusion layer which is a continuous series of solid solutions [11]. Such a layer, for example, is formed in a place of contact of molybdenum and tungsten under high annealing (about 2000 °C) in vacuum. The same is observed while chromium-plating of molybdenum, tungsten and other metals. However, there is a relatively small amount of systems where due to the counter diffusion the monophase layer with continuously varying concentration of the doping component is implemented. This concentration continuously varies from the boundary value (at one boundary) to zero (at the other boundary).

OPTIMIZATION OF MACRO-AND MICROSTRUCTURE OF SILICIDE COATINGS

In many cases, including molybdenum siliconizing, multiphase compositions consisting of the layers of chemical compounds and sequentially arranged bounded solid solutions are formed.

When modeling a coating at macro level in systems with intermediate compounds (namely Mo-Si relates to such systems, where there are stable compounds of $MoSi_2$, Mo_5Si_3, Mo_3Si [12, 13]) it is necessary to strive for creating a composition the structure of which is very close to continuos series of solutions. This can be is achieved through meeting several requirements simultaneously.

Firstly, the greatest concentration of silicon must be on the surface of the coating. Implementation of this condition ensures rapid formation of an oxide film of SiO_2 and achievement of the desired protective effect.

Secondly, the concentration of silicon from the side of the molybdenum substrate should be the lowest, this will slow down the diffusive dissolution of the silicides inside it.

Thirdly, to achieve and maintain a reliable adhesive interaction between the coating and the substrate, it is necessary to relieve the mechanical stress in the system during formation of the coating as well as during the operation of the substrate-coating composite as much as possible.

Meeting the above requirements for the molybdenum-silicon system means that the silicide coating must be multiphase, and it is preferable to carry out its formation sequentially, starting from the lowest

silicide phases (phases with the less silicon atoms in the molecules of silicides).

The implementation of the proposed scheme to form a coating provides minimal changes in specific volumes on the phase boundaries and the lowest difference between the thermal expansion coefficients of the individual layers with a common boundary.

It should be noted that during the establishment of diffusion coatings the phase composition is often determined by the rate of their formation. In most cases, due to economic considerations, they traditionally tend to maximize the saturation velocity [14]. During siliconizing at high saturation speeds, the coating consists mostly from the higher silicide phase, i.e. the phase richest in silicon. In the studied system it is molybdenum disilicide $MoSi_2$. Since the specific volume ratio of this phase and the base metal (molybdenum) are significantly different, in the process of saturation, the coating is exposed to significant stresses relaxation of which leads to the formation of micro-and macro-cracks, pores and other defects. During operation of the coating, the amount of defects increases, they combine into larger formations, which leads to a rapid loss of protective effect of the coating. It is therefore extremely important to organize the technological process of coating deposition in a way to provide a gradual decrease of stress by the thickness of the coating. The stated comments also lead us to conclusion about the reasonability of forming a coating through the lower silicide phases [15].

Currently, lower molybdenum silicides are used mainly as individual additives in composite materials [16, 17], which is a consequence of rather widespread belief of their insufficient heat resistance. The standard approach to the formation of silicide coatings is the formation of sufficiently thick (500 microns or more) layers, the significant (most frequently – the major) part of which is represented by disilicide (fig. 4).

During the further use of the product with such coating, only its minor part is used as intended (i. e., to form an oxide layer of SiO_2 on the surface), and the rest turns into lower silicides as a result of diffusion reaction, which is activated by the high performance temperatures [18]. The process of redistribution of silicide phases in the coating is accompanied with the mechanical stress of alternating sign (tensile stress and compressive stress), which is due to the natural thermodynamic and structural properties of individual silicide phases [19]. These stresses can lead to a failure of uniformity of the coating.

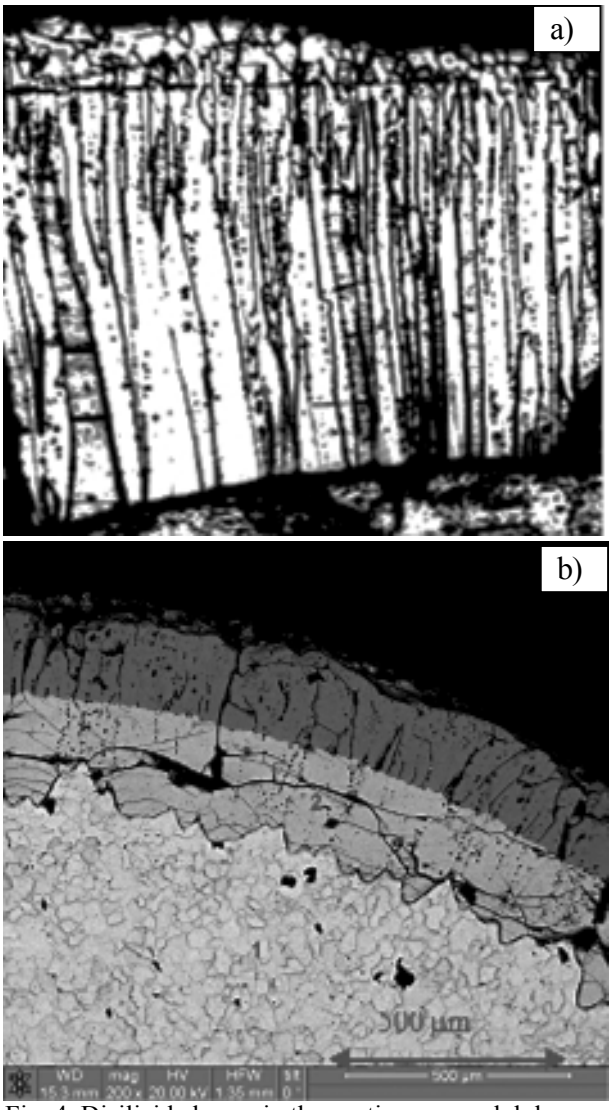

Fig. 4. Disilicide layers in the coatings on molybdenum: a) – almost entirely disilicide coating with the thickness of 450 microns, MIM-8 microscope; b) – complex coating on molybdenum (1) with an inner layer of silicide Mo_5Si_3 (2) and an outer layer of about 200 microns of molybdenum disilicide (3), Quanta 200 SEM.

The specific list of macroscale factors may be adjusted depending on the actual operating conditions (e.g., the case of coatings with different configuration and structure on different parts of the same product can be implemented in the presence of a temperature gradient on the surface of a product or different curvature of the surface on different areas).

Optimal modeling of the structure of the silicide coating on the microscale primarily requires creation of such a crystallite composition which can reduce

the grain boundary flow of silicon, slow down the diffusion phase dissolution and increase efficiency of the coating without significant phase transformations in it. In this sense, a coating with a fine-grained structure of the silicide formed by equiaxed (spherical or polyhedral) grains has the best potential. In our view, the better stability would be provided by a microstructure with grains elongated along the phase boundaries, and not oriented perpendicular to them (fig. 5).

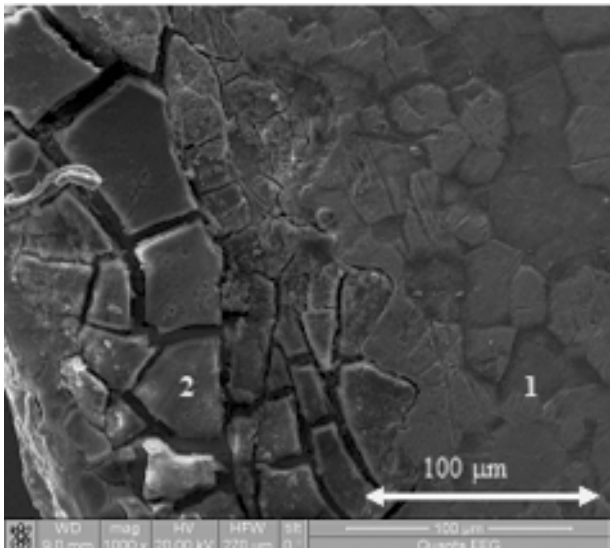

Fig. 5. Large-block silicide coating (2) on molybdenum (1), Quanta 200.

Much attention is paid to the fight against diffuse dissolving of disilicide phase and increase of the protective effect of the coating [20]. Attempts of insertion of additional elements to the composition of the coating, which form the barrier layers from the foreign substances to slow the diffusive dissolution of the higher phase, gave some positive result at moderate temperatures (up to 1650 – 1700 °C). At higher temperatures, the material of the barrier layer rapidly pollutes the protective film of silicon dioxide, and the heat resistance of the coating is sharply reduced [21].

Point insertion of additional chemical elements in the form of individual embedded or substituted atoms with formation of sub-micron inclusions of third phases of nanoscale inclusions of individual atoms will eliminate the negative factors that are inherent in conventional barrier layers, but the experimental data of such modification of the coating are practically absent. There is another model approach, viz. creation of chemically-related barrier layers in the coat submicron scale ing, which are obtained without the insertion of additional chemical elements. Examples of such layers are eutectic mixtures of nano- and submicron particles of various molybdenum silicides, as well as their solid solutions [22]. One of the options to obtain such compositions (fig. 6) can be contact melting of different silicide layers [23], co-sputtering of elements, f ollowed by condensation and reactionary diffusion or there can be some other methods.

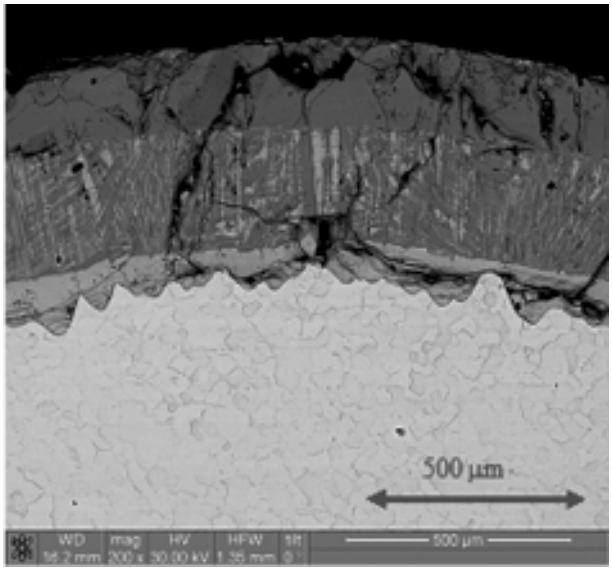

Fig. 6. The result of contact melting of silicides: $MoSi_2$ - Mo_5Si_3 eutectic layer in silicide coatings on molybdenum, Quanta 200.

CONCLUSION

Multi-level hierarchical approach (multiscale approach) is an important tool for optimizing the structure of composite materials. To achieve the best performance of materials in different operational conditions it is necessary to know the full range of both structural characteristics of the composite material, and environmental factors, which initiate evolution of the structure at each hierarchical level. Such knowledge allows to choose the acceptable level of degradation for each structural level and thereby simulate a coating with optimal structure-phase state.

The factors determining the implementation and changes in the structure of molybdenum silicides, are the initial structure of the substrate, material defect, stress-strain state of the material, method of processing, temperature, composition and the source of diffusion impurities. The requirements to the chemical composition of individual areas of the coating, to the sequence of phase layers and to the microstructure of the layers have been formulated.

The options of the construction of the coating with improved stability have been proposed.

For a system of molybdenum-silicide coating, practically in all cases, the best combination is a multilayer multi-phase silicide coating with a gradual decrease in the concentration of silicon from the surface to the substrate.

REFERENCES

1. Autar K. Kaw. Mechanics of Composite Materials, 2nd Ed. – Mechanical and Aerospace Engineering Series. – CRC Press: 2005. – 496 p.
2. Proceedings of the First High Temperature Structural Silicides Workshop. Gaithersburg, MD, USA /Ed. by H. Herman//Materials Science and Engi neering: A. – 1991. – Vol. 155, Iss. 1-2. – P. 278.
3. Moshev V.V., Svistkov A.L., Garishyn O.K, Yevlampiyeva C.E., Rogovoy A.A., Kovrov V.N., Komar L.A., Golotina L.A., Kozhevnikova L.L. Structural mechanisms of formation of the mechanical properties of granular polymer composites. – Yekaterinburg: Ural Academy of Sciences, Institute of Continuum Mechanics, 1997. –507 p.
4. Vakulenko A.A. About the effective properties and strength of ceramic composites//Proceedings of the Russian Academy of Sciences. Ser. Mechanics of solids. – 1998. – № 6. – P. 50-72.
5. Kirichok A.V., Kuklin V.M. Allocated Imperfections of Developed Convective Structures// Physics and Chemistry of the Earth Part A. – 1999. – № 6. – P. 533-538.
6. Kuklin V.M. The role of absorption and dissipation of energy in the formation of the spatial nonlinear structures in nonequilibrium media//Ukrainian Journal of Physics. Reviews. – 2004. – Vol. 1, № 1. – P. 49-81.
7. High-Temperature Silicides and Refractory Alloys /Ed. C.L. Briant, J.J. Petrovic, B.P. Bewlay, A.K. Vasudevan, H.A. Lipsitt//MRS Proceedings. – 1994. – Vol. 322. – P. 588.
8. Dzyadykevich Yu.V. Heat-resistant coatings for molybdenum and its alloys//Powder metallurgy. – 1988. – № 2. – P. 41-48.
9. Vasudevan A.K., Petrovic J.J. A Comparative Overview of Molybdenum Disilicide Composites //Pros. of the 1st HTSS. – 1992. – P. 1-17.
10. Lytovchenko S.V., Maslova T.S., Matviyenko D.S. and et. al. High-temperature stability of the silicide coatings based on molybdenum and other refractory metals//Bulletin of Kharkiv National University, № 529, physical series "Nuclei, particles, fields". – 2001. – Issue. 3(15). – P. 64-66.
11. Nechyporenko Ye.P., Petrychenko A.P., Pavlenko Yu.B. Protection of metals from corrosion. – Kharkiv: Higher school, 1985. – 112 p.
12. Samsonov G.V., Dvorina L.A., Rud B.M. Silicides. – M.: Metallurgy, 1979. – 271 p.
13. Gokhale A.B., Abbaschian G.J. The Mo-Si (Molybdenum-Silicon) System//J. Phase Equilibria. – 1991. – Vol. 12, № 4. – P. 493-498.
14. Zmiy V.I., Rudenky S.G. Reaction-activated diffusion and vacuum coatings. – Kharkiv: Kharkiv Institute of Physics and Technology, 2010. – 158 p.
15. Nechyporenko Ye.P., Petrychenko A.P., Pavlenko Yu.B., Lytovchenko S.V., Chyshkala V.A. Heat-resistant coatings based on molybdenum of the lower silicide phases//Heat-resistant inorganic coatings: Saint-Petersburg: Science. – 1990. – P. 183-186.
16. Patent. 2154122 Russian Federation, MPK C22 C29/02, C22C29/18, H05B3/14 The composite heat-resistant material [Text]/B.A. Gnesin.; B.M. Epelbaum.; P.A. Gurzhiyants.; applicant and patentee Institute of Solid State Physics. – № 98113544/02; application 07.07.1998; published 10.08.2000.
17. Yan J., Xu H., Zhang H., Tang S. $MoSi_2$ oxidation resistance coatings for Mo5Si3/$MoSi_2$ composites//Rare metals. - 2009. – Vol. 28, № 4. – P. 418.
18. Azarenkov N.A., Sobol O.V., Pogrebnyak A.D. and et. al. Materials science of the nonequilibrium state of the modified surface: Monograph. – Sumy: Sumy State university, 2012. – 604 p.
19. Samsonov G.V., Dvorina L.A., Rud B.M. Silicides. – M.: Metallurgy, 1979. – 271 p.
20. Byalobezhsky A.B., Krasilov B.I., Tsyrlin M.S. The modified silicide diffusion coatings for protection against oxidation of molybdenum//Protective coatings on metals. – 1973. – P. 90-93.
21. Burykina A.L., Dzyadykevich Yu.V., Epik A.L. and et. al. The use of boride coatings as barriers to diffusion of refractory metals//Organosilicate and inorganic coatings. – 1975. – Vol. 195. – P. 203.
22. Gnesin B.A., Gurzhiyants P.A., Borysenko Ye.B. Use of composite materials and some properties of eutectics of inorganic Materials $(Mo,W)_5Si_3$-$(Mo,W)Si_2$. – 2003. – Vol. 39, №7. – P. 827-836.
23. Nechyporenko Ye.P., Pavlenko Yu.B., Chyshkala V.A., Lytovchenko S.V. Formation of eutectic silicide coatings on molybdenum//Powder metallurgy. – 1993. – № 9-10. – P. 43-46.

UDC 539.2: 538.975

MAGNETRON SPUTTERING OF HIGH TEMPERATURE COMPOSITE CERAMICS AlN-TiB_2-$TiSi_2$

I.N. Torianik[1], V.M. Beresnev[1], A.D. Pogrebnjak[2], O.V. Sobol[3], Ye.V. Beresneva[1], I.A. Podcherniaieva[6], A.Yu. Kropotov[1,4], N.G. Stiervoiedov[1], P.V. Turbin[1,4], D.A. Kolesnikov[5], S.S. Grankin[1], U.S. Nyemchenko[1], P.A. Srebniuk[1], V.Yu. Novikov[5]

[1]V.N. Karazin Kharkiv National University, Ukraine

[2]Sumy State University, Ukraine

[3]National Technical University "Kharkiv Polytechnic Institute", Ukraine

[4]Scientific Center of Physical Technologies MES and NAS of Ukraine

[5]Belgorod National Research University, Russian Federation

[6]I.N. Frantsevich Institute for Problems of Materials Science, Ukraine

Received 24.09.2013

By means of the magnetron sputtering method using the DC and pulsed voltages applied to the target, the coatings based on AlN-TiB_2-$TiSi_2$ ceramics were obtained. An amorphous-like structure of the obtained coatings was revealed. It had the area of ordering ~ 1 nm and the viscoplasticity coefficient of 0.07. The hardness of the coatings reaches 15.3 GPa, and the modulus of elasticity is 206 GPa. The coatings are characterized by high adhesion strength to the substrate.

Keywords: ceramics, composite coatings, magnetron sputtering method, physical and mechanical properties.

МАГНЕТРОННОЕ РАСПЫЛЕНИЕ ВЫСОКОТЕМПЕРАТУРНОЙ КОМПОЗИЦИОННОЙ КЕРАМИКИ AlN-TiB_2-$TiSi_2$

И.Н. Торяник, В.М. Береснев, А.Д. Погребняк, О.В. Соболь, Е.В. Береснева, И.А. Подчерняева, А.Ю. Кропотов, Н.Г. Стервоедов, П.В. Турбин, Д.А. Колесников, С.С. Гранкин, У.С. Немченко, П.А. Сребнюк, В.Ю. Новиков

Магнетронным методом распыления, с применением постоянного и импульсного напряжений на мишень, получены покрытия на основе керамики AlN-TiB_2-$TiSi_2$. Выявлено аморфноподобную структуру сформированных покрытий с областью упорядочения ~ 1 нм и коэффициентом вязкопластичности 0,07. Твердость покрытий достигает 15,3 ГПа, а модуль упругости составляет 206 ГПа. Покрытия характеризуются высокой адгезионной прочностью по отношению к подложке.

Ключевые слова: керамика, композиционные покрытия, магнетронный метод распыления, физико-механические свойства.

МАГНЕТРОННЕ РОЗПИЛЕННЯ ВИСОКОТЕМПЕРАТУРНОЇ КОМПОЗИЦІЙНОЇ КЕРАМІКИ AlN-TiB_2-$TiSi_2$

І.М. Торяник, В.М. Береснєв, О.Д. Погребняк, О.В. Соболь, Є.В. Береснєва, І.О. Подченяєва, О.Ю. Кропотов, М.Г. Стєрвоєдов, П.В. Турбін, Д.О. Колесніков, С.С. Гранкін, У.С. Нємченко, П.А. Сребнюк, В.Ю. Новіков

Магнетронним методом розпилення, із застосуванням постійної та імпульсної напруг на мішень, отримані покриття на основі кераміки AlN-TiB_2-$TiSi_2$. Виявлено аморфноподібну структуру сформованих покриттів із областю впорядкування ~1 нм і коефіцієнтом в'язкопластичності 0,07. Твердість покриттів досягає 15,3 ГПа, а модуль пружності складає 206 ГПа. Покриття характеризуються високою адгезійною міцністю по відношенню до підкладинки.

Ключові слова: кераміка, композиційні покриття, магнетронний метод розпилення, фізико-механічні властивості.

INTRODUCTION

Ion-plasma deposition methods by means of sputtering targets, which consist of metals or their nitrides, carbides and borides, can generate a wide range of multi-component coatings. In many papers [1 – 3] various variants of such structures and their properties have been considered.

Prospects for the use of multi-component coatings containing wear-resisting and antifriction components are associated with the possibility of ob-

taining a new composite structures having the desired physical and mechanical properties. The most common and effective systems of coatings formation are systems based on magnetron sputtering techniques [4, 5]. During the deposition process, the amorphous structure can be formed along with the reduction of the size of the grain and obtaining new chemical compounds. This promotes a significant improve to the physical and mechanical properties of the coatings.

In the current work, the possibility of applying the method of magnetron sputtering of high-temperature composite ceramics and formation of coatings on their basis have been explored. The physical and mechanical properties of the coatings have been studied.

EQUIPMENT AND METHODS OF INVESTIGATION

Operational volume was a vacuum chamber made of stainless steel with a diameter of 75 cm and a volume of ~96 liters. The scheme of the installation is shown in fig. 1.

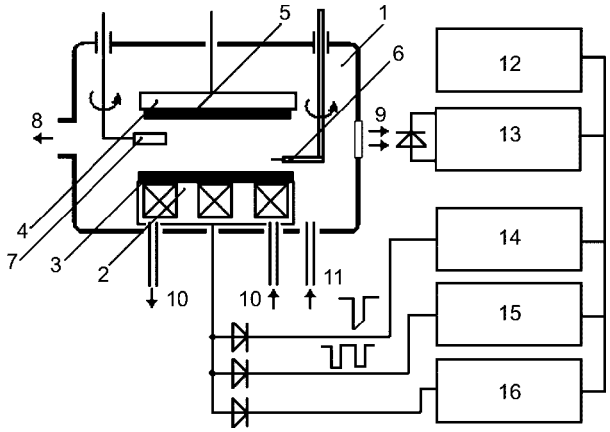

Fig. 1. Scheme of the installation for magnetron sputtering of multicomponent systems: 1 – vacuum chamber, 2 – planar magnetron, 3 – sputtering target, 4 – substrate holder, 5 – substrate, 6 – Langmuir probe, 7 – quartz thickness and the deposition rate measuring instrument, 8 – pumping, 9 – observation window, 10 – water cooling, 11 – operational gas buffing, 12 – system of control and data acquisition, 13 – photometer, 14 – ignition block, 15 – impulse power supply unit, 16 – constant power supply unit.

As the sputtered material we used ceramics (AlN-TiB_2-$TiSi_2$) with a diameter ~ 80 mm and thickness of 4 mm.

The coatings were deposited on the polished surface of the samples of steel 45 and on the surface of the silicon samples. Samples were fixed on the substrate, which was located above on a distance of 70 mm from the surface of the sputtering target. For comparison of the results of research, two modes of deposition have been used: at a constant voltage applied to the target and in pulsed mode.

DEPOSITION PARAMETERS

The DC voltage applied to the sputtering target was 400 V, current ~200 mA; deposition time 95 min; bias potential on the substrate was ~200 V. The partial pressure in the chamber during the coating deposition was P_{Ar} = 0.1 Pa. Before the deposition of the coatings, the cleaning of the samples in a glow discharge for 15 minutes at P_{Ar} = 0.08 Pa has been implemented.

The pulse voltage applied to the sputtering target was 700 V, current ~2.0 A; deposition time 35 min; potential bias on the substrate was ~200 V. The partial pressure in the chamber during coating deposition was P_{Ar} = 0.1 Pa. Before the deposition of coatings, the cleaning of the samples in a glow discharge for 15 minutes at P_{Ar} = 0.08 Pa has been implemented.

The surface morphology of the coated samples was studied using a scanning electron microscope FEI Quanta 600 FEG. Nanohardness measurements were carried out using NanoIndenter II (MTS Systems, USA) installation. It was equipped with a three-sided Berkovich pyramid. To study the structural elements, the method of atomic force microscopy (AFM) was used.

EXPERIMENTAL RESULTS AND DISCUSSION

Fig. 2 and fig. 3 show microphotographs of the surface of the coatings, as well as the fractorgaphy im-

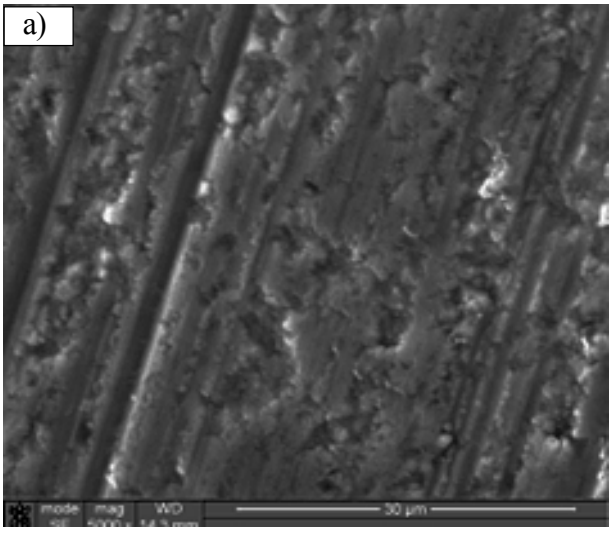

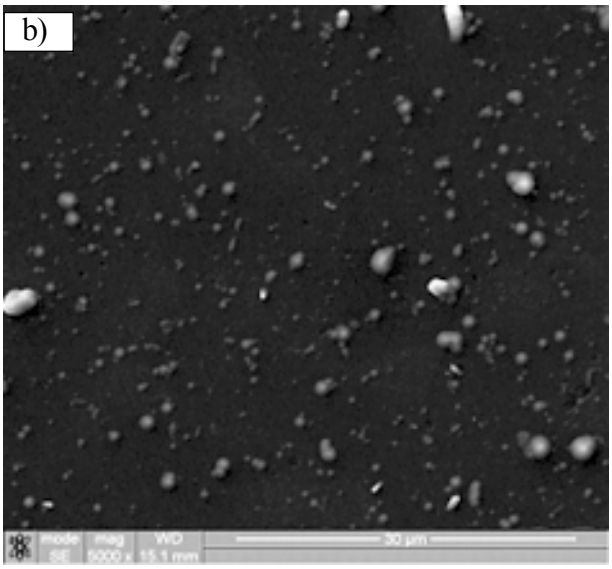

Fig. 2. Image of the surface topography of the AlN-TiB_2-$TiSi_2$ coating: a) – under DC, b) – pulsed magnetron sputtering.

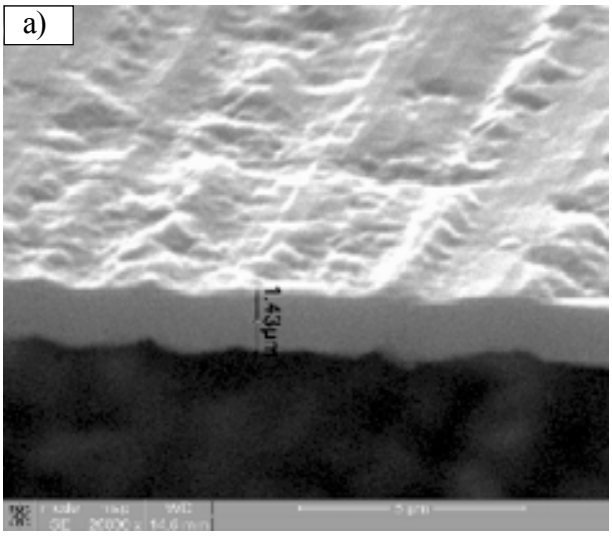

Fig. 3. Fractography images of the fractures of the AlN-TiB_2-$TiSi_2$ coatings: a) – obtained at a DC (t_{dep} = 95 min), b) – impulse magnetron sputtering (t_{dep} = 35 min).

ages of the fracture. The analysis of the images shows that the use of magnetron sputtering for the evaporation of the ceramic targets of compound composition leads to the fact of presence of a drop component in a small amount on the surface. The analysis of the published data suggests that the main factor determining the presence of the drop component is the low thermal conductivity of the vaporized components composing the target [6].

Even with intensive cooling of the target, the temperature of the evaporating surface increases because of the low thermal conductivity of the evaporable components: λ_{AlN} = 160 – 250 W/(m·K) [7]; λ_{TiB2} = 64,4 W/(m·K) [7]; λ_{TiSi2} = 45,9W/(m·K) [8], which leads to the generation of microdrops fraction [9]. Fig. 4 shows the results of energy dispersion microanalysis of the surface of the coatings based on AlN-TiB_2-$TiSi_2$.

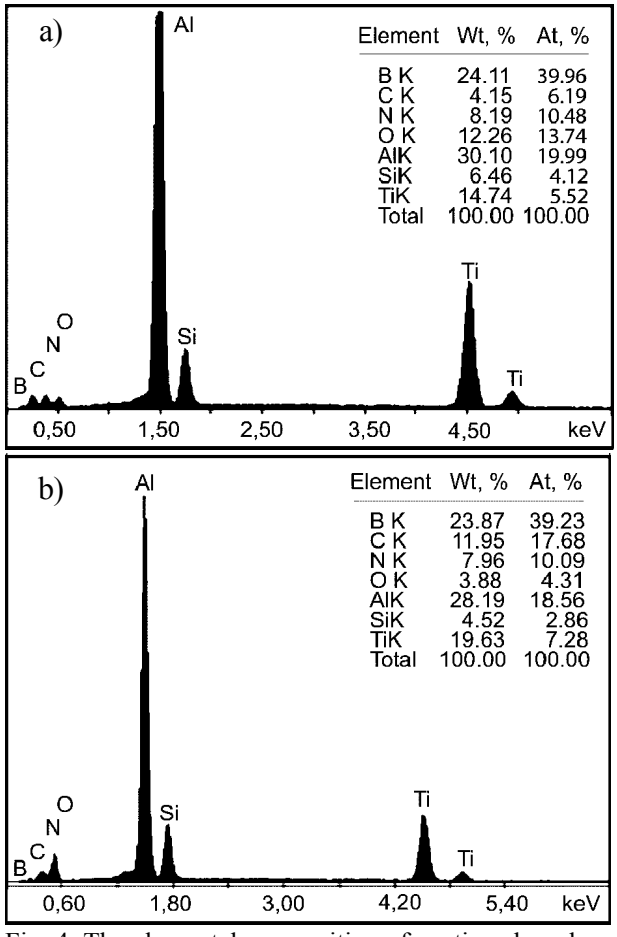

Fig. 4. The elemental composition of coatings based on AlN-TiB_2-$TiSi_2$: a) – in a DC voltage conditions, b) – in a pulsed voltage conditions.

The results of elemental microanalysis of the coating show that when applying a pulsed voltage to the sputtering target, the reduction of content boron, nitrogen, aluminum and silicon takes place (see fig.

5b). As for titanium, the selective sputtering of titanium atoms is less apparent compared with the coatings produced under conditions of DC applied to the target. The presence of oxygen and carbon in the coating is apparently due to the presence of the residual atmosphere in the vacuum system.

AlN-TiB_2-$TiSi_2$ coatings, obtained in this work, had an amorphous structure with a broad "halo" on the XRD spectra after the deposition. It had a center in the area of the diffraction angle $2\theta = 38°$. The size of the ordering area was about $R_m = 10$ Å = 1 nm, i.e., the obtained structure can be attributed to the amorphous cluster class.

Electron microscopy studies of the surface of the coating using reflection and transmission, confirm the presence of the ultrafine structure which is close to amorphous. This is evidenced by the nature of the diffraction pattern (fig. 5).

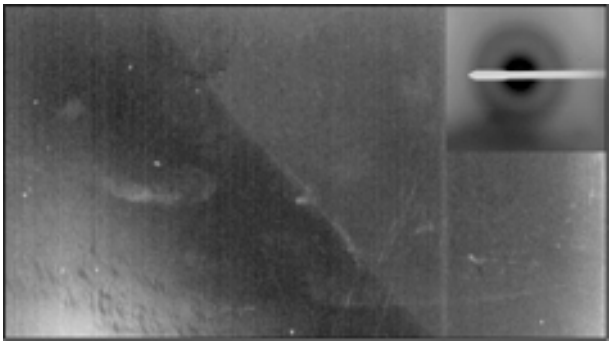

Fig. 5. Electron microscopic image of the coating AlN-TiB_2-$TiSi_2$.

Analysis of the mechanical characteristics, carried out by the nanoindentation method showed that in the initial state the obtained coatings have nanohardness $H = 15.3$ GPa and the elasticity modulus $E = 206$ GPa. The index of viscoplasticity [10] for the system we obtained the system was ~ 0.07, thus striving to the amorphous state of the material.

To obtain a high adhesive strength of the coating to the substrate, according to the literature [11], two factors are required: 1 – mechanical contact between the coating and the substrate, 2 – the chemical interaction on the border of two contacting surfaces. Mechanical interaction is determined by the roughness of the contacting surfaces, and the chemical interaction is determined by the interatomic interaction on the border of the contacting bodies. The high degree of activation can be obtained by surface treatment by the glow discharge and pulse processing before the deposition, which leads to the activation of the atoms interacting at the boundary of the contacting materials.

The adhesion of coatings based on ceramic system AlN-TiB_2-$TiSi_2$, obtained by the pulse magnetron sputtering, to a steel substrate is estimated [12] by the area of the chop which was obtained during the joint local plastic deformation of the coating and its substrate through the penetration of Rockwell indenter at a load of 1470 N. The quality of adhesion determined by this method indicates the presence of chops and peeling around the imprint (see fig. 6).

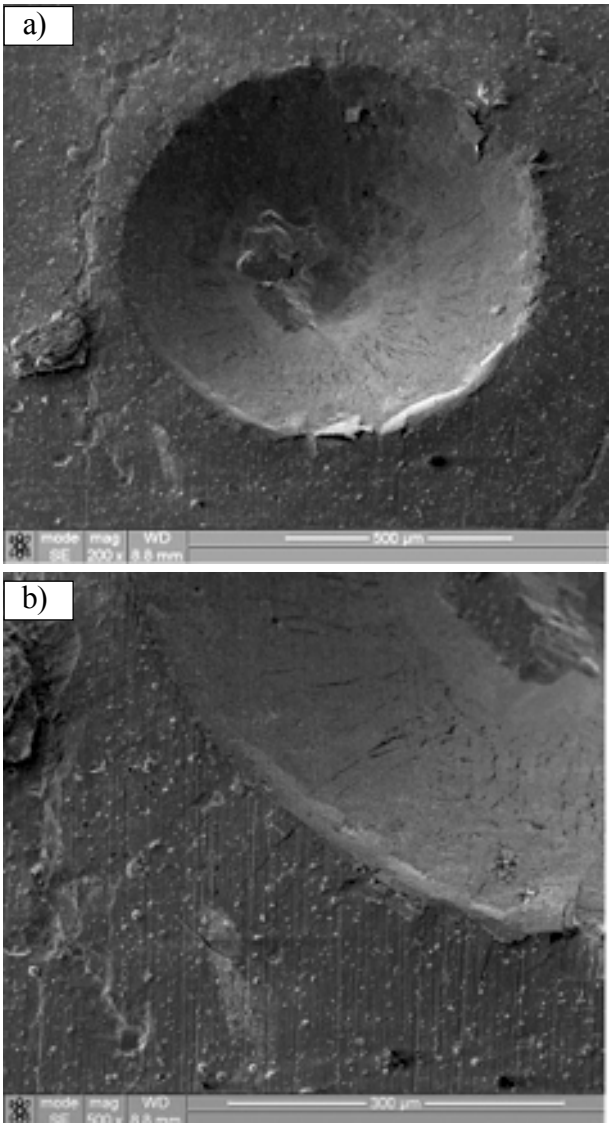

Fig. 6. Image of the area of the indenter imprint on samples of steel with a coating: a) – general view, b) – fragment of the imprint.

Coatings of the system AlN-TiB_2-$TiSi_2$, formed on a steel substrate, are characterized by the sufficient quality (see Fig. 6a) in the area around the imprint after the penetration of the indenter into the

deep. Peeling the coating from the substrate was not revealed. The obtained coatings based on ceramics AlN-TiB_2-$TiSi_2$, which have amorphous-like structure [13] can be effectively used to protect the surfaces of the rubbing details from the oxidation wear.

SUMMARY

1. In conditions of applying DC voltage and pulse voltage to the target, the composite coatings based on ceramic compounds AlN-TiB_2-$TiSi_2$ were developed.
2. X-ray diffraction analysis revealed an amorphous-like structure of the coating with the area of ordering about 1 nm and viscoplasticity coefficient of 0.07.
3. The mechanical properties of the coatings are characterized by the hardness of 15.3 GPa, modulus of elasticity of 206 GPa and a high adhesive strength with respect to the substrate.
4. Tribological properties of the obtained amorphous-like coatings based on the ceramic compounds AlN-TiB_2-$TiSi_2$ are promising for using them as protective coatings for the rubbing surfaces of machine details.

1. The work was done by the scientific research topics 0112U006974 and 0113U001079, funded by the Ministry of Education and Science of Ukraine. Part of the work was performed using the diagnostic equipment of the Center of Collective Using of scientific equipment of Belgorod National Research University, "Diagnostics of structure and properties of nanomaterials" under the state contract number 16 55211 7087 with the financial support of the Ministry of Education and Science of the Russian Federation.

REFERENCES

1. Nanostructured Coatings//Editors: Albano Cavaleiro, Jeff Th. M. De Hosson. – M.: Technosphere, 2011. – 792 p. (by Russian).
2. Kelly P.J., Arnell R.D. Magnetron sputtering: a review of recent developments and applications //J. Vacuum. – 2000. – Vol. 56. – P. 159-172.
3. Musil J., Baroch P., Vlиek J. et al. Reactive magnetron sputtering of thin films: present status and trends//Thin Solid Films. – 2005. – Vol. 475. – P. 208-218.
4. Berlin E.V., Seidman L.A. Ion-plasma processes in thin-film technology. – M.: Technosphere, 2010. – 528 p. (by Russian).
5. Azarenkov N.A., Sobol O.V., Pogrebnjak A.D., Beresnev V.M. Engineering of vacuum-plasma coatings. – Kharkiv: Karazin Kharkiv National University, 2011. – 344 p. (by Russian).
6. Lavrov V.N., Orlov I.I., Fedotov A.F. Thermal conductivity and temperature of vacuum-arc evaporation of multilayers of SVS-pressed cathode systems $TiS_{0.5}$-Al and $TiS_{0.5}$-Al-Si//Vestn. Samar. State. Tehn. Univ. Ser. Technical sciences. – 2013. – No. 1 (37). – P. 72-86. (by Russian).
7. Samsonov G.V., Vinnitskiy I.M. Refractory compounds: A handbook. – M.: Metallurgy, 1976. – 560 p. (by Russian).
8. Samsonov G.V., Dvorin L.A. PV Geld Silicide. – M.: Metallurgy, 1979. – 272 p. (by Russian).
9. Andreev A.A., Sabers L.P., Grigoriev S.N. Vacuum-arc coating. – Kharkiv: NSC "KhPTI", 2010. – 317 p. (by Russian).
10. Firsov S.A., Rogul T.G. Theoretical (limiting) hardness//Add. National Academy of Sciences of Ukraine. – 2007. – No. 4. – P. 110-114.
11. Shautsukov A.G. Contemporary conception about the possible mechanisms of adhesion of metallic films to different films//Applied Physics. – 2006. – No. 5. – P. 16-21. (by Russian).
12. Matsevity V.M. Coatings for cutting tools. – Kharkov: High School, 1987. – 127 p. (by Russian).
13. Musil J. Properties of hard nanocomposite thin films. (In book Nanocomposite Thin Films and Coatings: Processing, Properties and Performance). Ch. 5/Eds. S. Zhang, A. Nasar. – 2007. – London: Imperial College Press. – P. 281-328.

PACS:7350 Pz.7361 Le.7840 Fy

OPTICAL PROPERTIES OF DYSPROSIUM MONOANTIMONIDE THIN FILMS

I.G. Tabatadze, Z.U. Jabua, A.V. Gigineishvili

Department of Physics, Georgian Technical University (Tbilisi)

Georgia

Received 28.09.2013

A process has been developed for the growth of thin crystalline DySb films by thermal evaporation using Dy and Sb separate sourses. The room-temperature optical spectra (reflection and absorption, the real and the imaginary part of the dielectric constant, loss function) of DySb films have been studied at photon energies from 0.05 to 5.5 eV. The behavior and energy position of features in the spectra have been analyzed.

Keywords: film, substrate, the optical spectra, reflection, absorption, dielectric constant, loss function.

ОПТИЧЕСКИЕ СВОЙСТВА ДИСПОЗИИ ТОНКИХ ПЛЕНОК МОНОАНТИМОНИДОВ

И.Г. Табатадзе, З.У. Джабуа, А.В. Гигинейшвили

Разработана технология приготовления тонких кристаллических плёнок моноантимонида диспрозия методом вакуумно-термического испарения из двух независимых источников Dy и Sb. При комнатной температуре в области энергии фотонов 0.05 – 5.5 эВ исследованы оптические спектры (отражение и поглощение, действительная и мнимая части диэлектрических постоянных, функция потерь) приготовленных плёнок. Проанализировано поведение и энергетическое состояние спектральных зависимостей.

Ключевые слова: плёнка, подложка, оптические спектры, отражение, поглощение, диэлектрическая постоянная, функция потерь.

ОПТИЧНІ ВЛАСТИВОСТІ ДИСПОЗІЇ ТОНКИХ ПЛІВОК МОНОАНТИМОНІДІВ

І.Г. Табатадзе, З.У. Джабуа, А.В. Гігінейшвілі

Розроблена технологія приготування тонких кристалічних плівок моноантимоніду диспрозії методом вакуумно-термічного випару із двох незалежних джерел Dy і Sb. При кімнатній температурі в області енергії фотонів 0.05 – 5.5 еВ досліджені оптичні спектри (відбиття та поглинання, дійсна та уявна частини діелектричних постійних, функція втрат) приготовлених плівок. Проаналізовано поводження та енергетичний стан спектральних залежностей.

Ключові слова: плівка, підкладинка, оптичні спектри, відбиття, поглинання, діелектрична постійна, функція втрат.

INTRODUCTION

Rare-eart (RE) monoantimonides continue to receive a great deal of attention owing to their interesting properties which have not yet studied in sufficient detal [1 – 8]. These little-studied materials include dysprosium monoantimonide. In this work are presented the technology of preparation of DySb crystalline thin films and study of the optical properties at room temperature in the photon energy range 0.05 – 5.5 eV.

EXPERIMENT

Single-phase films DySb have been prepared by vacuum-thermal evaporation from two independent sources of Dy and Sb. As substrates we used glass-ceramic, fused silica and (111) oriented single-crystal Si plates. The sourse materials used were 99.9% DyM-1 dysprosium and 99.9999% antimony. During the growth process the vacuum in the deposition chamber was ~10^{-5} Pa. In the all of the growth runs, the substrate temperature was maintained from 1050 to 1110 K. The axis of the Dy and Sb evaporators made an angle of ~35° with the normal to the substrate surface. The source-substrate separation was 42 mm for Dy and 56 mm for Sb. Angles evaporators Dy and Sb against the normal of the substrate are the same and composes ~35°. The thickness of the prepared films varied in the range 1.2 – 2.1 μm, the deposition rate was ~68 Å/s

The phase composition and crystallinite of the films were cheked by by X-ray diffraction (XRD). XRD pattern were taken at CuKα radiation with a nickel filter, in the mode of recording a rate of

$4 \cdot 10^{-2}$ deg/s and eleqtron diffraction. Electron diffraction patterns were obtained in reflection at an accelerating voltage of $(75 – 100) \cdot 10^2$ V. The surface of the films was examined by X-ray fluorescence analysis (Camebax-Microbeam system). Their elemental analysis was determined by electron X-ray microanalysis.

Optical properties of dysprosium monoantimonide are studied poorly. In [9], only are researched reflection spectra of crystals and powder of DySb. In this paper, at room temperature in the photon energy of 0.05 eV – 5.5, reflection and absorption spectra are studied. By the Kramers-Kronig relations were calculated spectra of the main optical parameters such as real and imaginary parts of the dielectric constant, the loss function.

RESULTS AND DISCUSSION

By XRD and electron diffraction methods were investigated influence of temperature of a substrate in the range of 1050 to 1110 K and also the material of a substrate on crystallinity and phase structure of prefared films. Experiments have shown that the substrate material have no effect on the crystallinite and phase composition of the films. Films stay in the open air for 4 – 6 days causes change of color of films and the appearance of additional peaks on XRD pattern, not belong DySb, indicating the instability of films in air.

Fig.1 shows a typical the electronogramm and

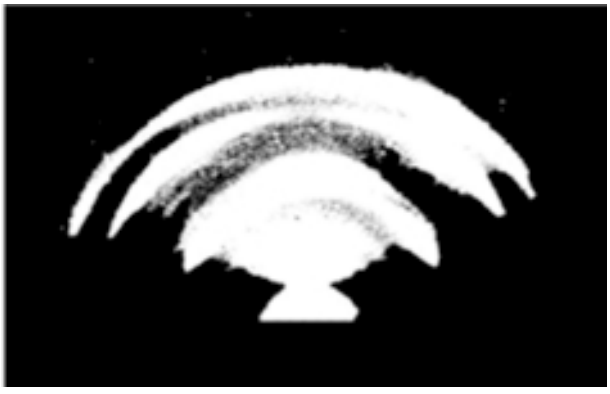

Fig. 1. Electron diffraction pattern of a thin DySb film (fused silica substrate, film thickness of 1.9 mm).

fig. 2 XRD pattern of an DySb film. Analysis of XRD and electron diffraction data indicated that the film grown at this temperature consisted DySb (cubic structure of NaCl-type) with lattice parameters 6.14 Å in good agreement with those of bulk DySb crystals 6.150 Å [9].

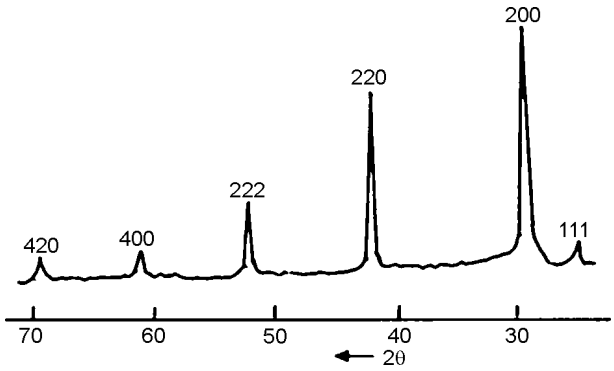

Fig. 2. XRD pattern of a thin DySb film (glass ceramic substrate, film thickness of 1.8 microns).

X-ray microanalysis showed that the film contained 49.8% Dy and 52.2% Sb.

In secondary X – rays the surface of the prepared films has been removed. The atoms of Dy and Sb are distributed on a surface of films in regular intervals enough at visible from fig. 3 (1) an (2) accordingly.

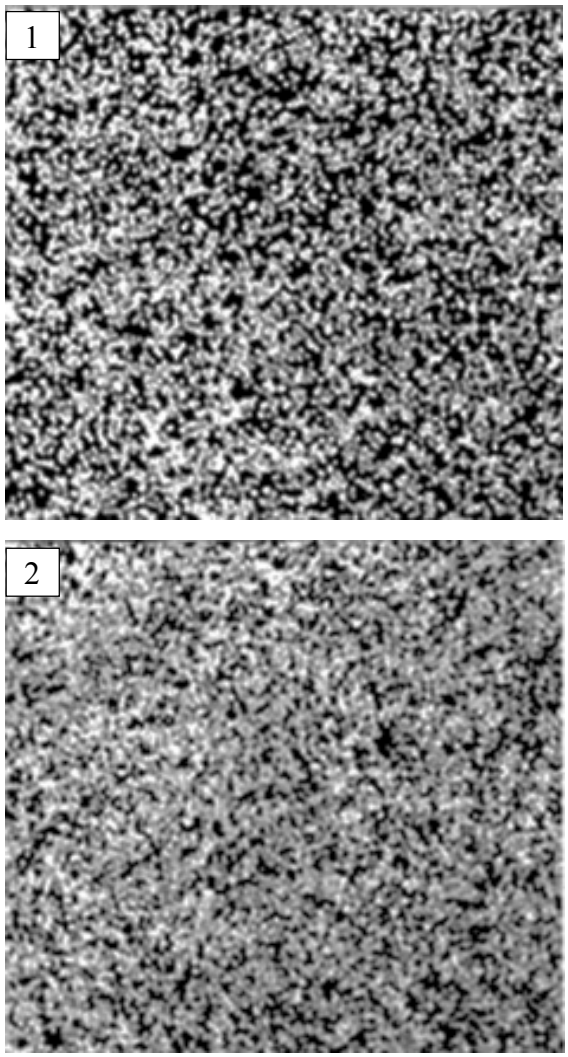

Fig. 3. The image of distribution of Dy (1) and Sb (2) atoms on a surface of a thin DySb film in secondary X-rays (×400).

On the reflection spectrum (fig. 4) are some features, such as: a deep minimum of about 0.28 eV which is accompanied with a pronounced long-wavelength edge of the reflection, well-formed reflection band with a maximum at 0.50 eV, a minimum at 0.22 eV and the structure at 1.67 eV. Depending on the spectral absorption coefficient (fig. 4.) strong absorption is observed in the region of relative transparency proximity 0.46 eV, 0.23 eV for the structure and the sharp increase in the absorption coefficient at energies below 0.12 eV.

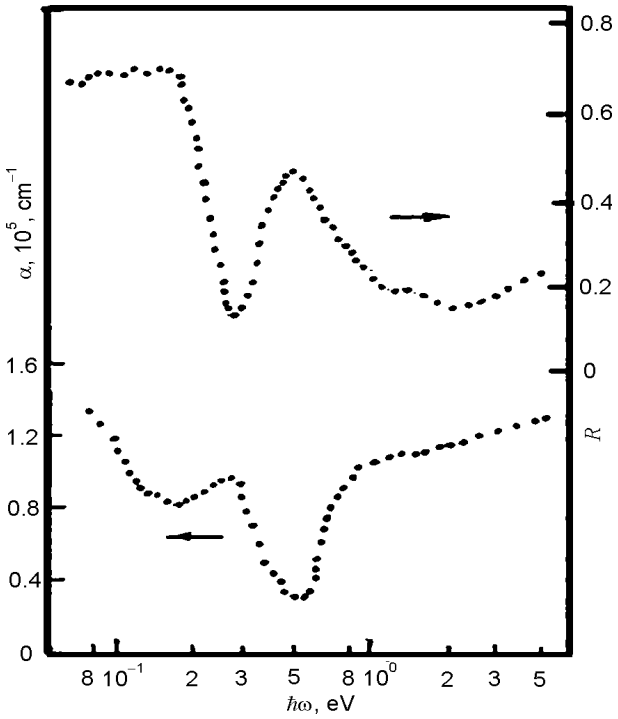

Fig. 4. Spectra of the reflection (R) and absorption (α) of a thin DySb film.

The interpretation of the optical spectra of DySb is difficult because there are no data on the energy band structure. It is possible to say only that a deep minimum of reflection and the associated increase in long-wave reflection is undoubtedly associated with plasma oscillations of charge carriers. Very difficult is interpret of the structural features of the spectra at energies close to 0.5 eV. On the one hand, we can assume that the same reflection spectra of crystals SmSb [10], in this region of the spectrum a decisive role plays the fundamental absorption with interband transition energy 0.50 eV. For an assessment of width of the forbidden zone it is necessary to consider the amendment connected with an arrangement of level of Fermi which corresponds to full regeneration. On the other hand, there are several objections to this explanation: when the carrier concentration is high ~$3 \cdot 10^{21}$ cm^{-3} and the effective mass of the order of the free charge carrier is m_0 (at X point of Brilyuen zone exists conduction d zone), the Fermi energy (0.75 eV) 1.5 times are more than energy of interzonal transitions and if in the trivalent rare earth elements compounds it is observed the reflection strip with a width few eV, in the DySb films half-width of the reflection strip which can be attributed with the electron interband transitions, is only 0.41 eV.

These remarks to some extent, may be rejected if interpretation of the optical spectra in the vicinity of the Fermi level admit the possibility of the existence of subbands d, f and f-d with very high density of states. In this case, apparently, the structure of the optical spectra of about 0.5 eV determined transitions of f and f-d nature.

On the basis of the spectral dependence of the coefficients of reflection and absorption spectra were calculated real μ_1 and imaginary μ_2 part of the permittivity (fig. 5) and the refractive n and absorption k index (fig. 6) and the loss function Imε^{-1} (fig. 7).

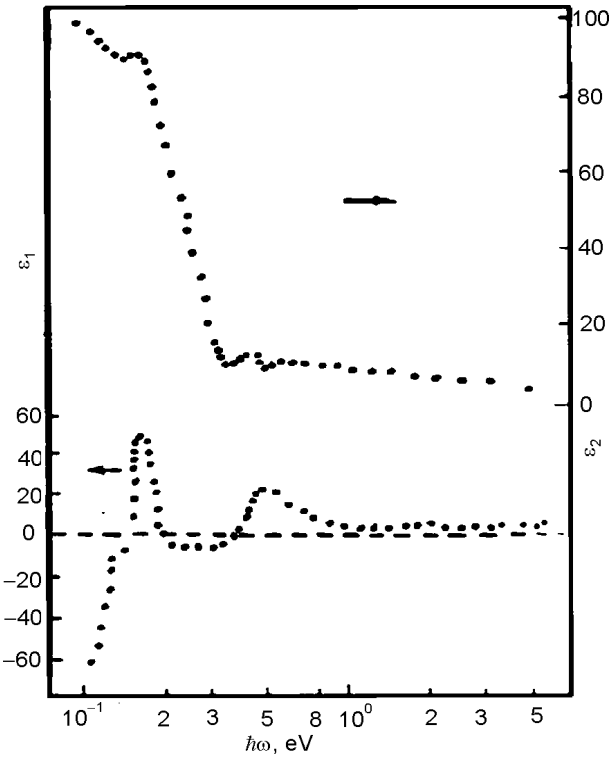

Fig. 5. Spectra of the real (ε_1) and imaginary (ε_2) part of the dielectric permitivity of a thin DySb films.

Fig. 5 shows that in the deep infrared region ε_1 aspires to very large negative values, which means that in the optical processes essential role played

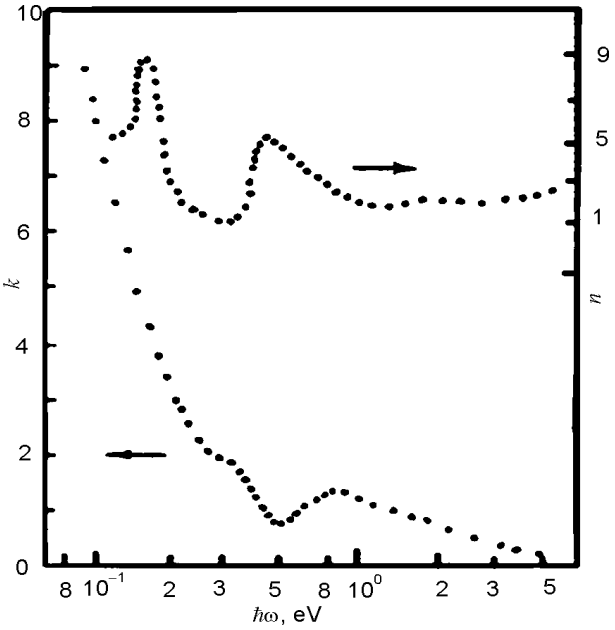

Fig. 6. Spectra of the reflectance (n) and absorption (k) of a thin DySb film.

free charge carriers. After that ε_1 changes a sign three times: twice with a positive slope ($d\varepsilon_1/d\omega > 0$) at 0.15 eV and 0.38 eV, that will well be coordinated with position of the maximum energy loss function accordingly, the energy of 0.38 eV probably corresponds to a plasma resonance. In the DySb films because of the proximity of this energy and energy of the band absorption, damping is large, excited plasma oscillations damped and the "true" plasma frequency should be higher than the estimated frequency.

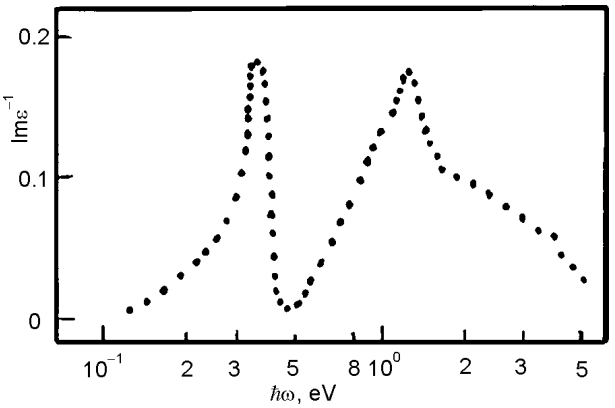

Fig. 7. Spectra of the loss function of a thin DySb film.

Characterized by relatively low-energy position of the main absorption band is clearly seen in the spectra of the absorption coefficient and the imaginary part of permittivity. In a place with that three factors: very sharp increase of the k and ε_2 in the long-wavelength part of the spectrum; the existence of a well-formed structure in spectrum of n and ε_1; the change of the sign of ε_1 with negative slope ($d\varepsilon_1/d\omega < 0$) at energy 0.18 eV suggest a significant contribution of intraband transitions and complex structure of the zone of DySb thin films.

CONCLUSION

The first process has been developed for the growth of thin crystalline DySb fiLms (cubic symmetry, NaCl structure, lattice parameters $a = 6.14$ Å) by vacuum-thermal evaporation of the two independent components. At room temperature in the photon energy range 0.05 – 5.5 eV spectra of reflection and absorption are measured. Are calculated spectra of the real and imaginary part of the dielectric constant, the loss function, the coefficient of reflection and absorption. It is shown that deep minimum on the reflection spectrum at 0.28 eV corresponds to the plasma energy minimum. It is suggested that the formation of the spectral dependence is dominated by intraband transitions.

REFERENCES

1. Nakane H., Yamazaki S., Fujishiro H., Yamaguchi T.,Yosizawa S., Numazava T., Okamura M. Low temperature properties of HoSb, DySb and GdSb//Cryocoolers. – 2002. – Part 11. – P. 443-448.
2. Daou R., Haase ., Doerr M., Rotter M., Weickert F., Nicklas M., Steglich F. Magnetoelastic quantum oscillation in GdSb to 55 T//J. Phys.: Conf. Ser. – 2011. – 273 012111 doi: 10 1088/ 1742-6596/273/1/012111.
3. Koiama K., Tomimatsu T., Yoshida M., Li D., Motokava M. Observation of cyclotron resonance on GdS// Physica B: Condensed Matter. – 2002. – Vol. 312-313. – P. 680-681/
4. Nakane H., Yamazaki T., Yosizawa S., Numazava T. Specific heat and magnetic properties of GdSb// Cryocoolers. – 2002. – Part 12. – P. 467-471.
5. Singh S., Singh R.K., Gour A. High pressure phase transition and stability of CeSb, LaSb and LuSb with NaCl-type structure//International J. of Modern Physics B(INMPB). – 2010. – Vol. 24. – P. 3543-3550.
6. Singh S., Bhartvaj P. Study of effect of covalency in heavy rare-earth monoantimonides up to 31 GPa // Journal of Alloys and Compunds. – 2011. Vol. 509. – P. 7047-7051.
7. Bhardwai P., Singh S. High pressure phase transition and elastic properties of covalent heavy

rare-earth antimonides//Journal os molecular modeling. – 2011. – Vol. 17. – P. 3057-3062.
8. Gasgnier M. Rare earth compounds, oxides, sulfides, silicides, boron… as thin films and thin crystals// Phys. Stat. Solidi A. – 1989. – Vol.114, № 11. P. 11-71.
9. Abdusalyamova M.N., Goryushko V.N., Ivanchenko L.A., Paderno Yu.B. Opticheskoe pogloschenie i parametry ‘elektroperenosa v antimonide disproziya/V kn.: Poluchenie i issledovanie svojstv soedinenii RZM. – K.: IPM, 1975. – P. 79-83.
10. Abdusalyamova M.N., Ivanchenko L.A., Paderno Yu.B., Shokirov H. Shirina zapreschennoj zony i parametry ‘elektroperenosa v monoantimonidah RZ‘E//Izv. AN SSSR. Neorganicheskie materialy. – 1978. – T. 14, № 12. – P. 2247-2251.

ПРАВИЛА ОФОРМЛЕНИЯ РУКОПИСЕЙ

В предоставляемой работе четко и последовательно излагаются оригинальные, не публиковавшиеся ранее результаты, полученные автором (авторами). Рукопись не должна находиться на рассмотрении к публикации в другом издательстве.

1. Распечатанная рукопись, с подписями всех авторов, предоставляется в 1 экз. на одном из следующих языков: украинский, русский, английский. Электронный вариант рукописи предоставляется на магнитном или оптическом носителе, либо (что предпочтительнее) направляется по E-mail.
2. К рукописи прилагаются следующие документы: направление от учреждения, где выполнена работа; заявление на имя главного редактора со сведениями об авторах; экспертное заключение о возможности опубликования работы в открытой печати (для граждан Украины); внешняя рецензия, подписанная доктором наук.
3. Последовательность размещения материала статьи: индекс по универсальной десятичной классификации (УДК); название статьи; инициалы и фамилия автора (авторов); полные почтовые адреса учреждений, в которых выполнена работа; аннотация; ключевые слова; текст; список цитируемой литературы; набор иллюстраций; подписи к рисункам и таблицам.
4. Название статьи, инициалы и фамилия автора (авторов), аннотации и ключевые слова подаются на трех языках: английском (для всех авторов), русском (для граждан СНГ) и украинском (для граждан украины). Объем аннотации не превышает 100 слов.
5. Текст рукописи желательно структурировать разделами: ВВЕДЕНИЕ, кратко формулирующее предысторию проблемы и цель данного исследования. Основная часть публикации, содержащая постановку задачи, экспериментальное и/или теоретическое описание исследований. Заключение, в котором приводятся результаты исследований, выводы, перспективы развития исследований и их возможные применения.
6. Полный объем обзорной статьи не должен превышать 60-ти страниц, оригинальной статьи – 20 страниц, краткого сообщения – 5-ти страниц.
7. Все физические величины следует представлять в единицах системы СИ.
8. Требования к оформлению рукописи. Параметры страницы: формат – А4 (210×297 мм). Поля: справа – 10 мм, остальные – 20 мм. Шрифт: Times New Roman, междустрочный интервал – полуторный. Название статьи – прописными, кегль 14. Авторы, аннотация, текст рукописи, формулы, список литературы, подписи к рисункам и таблицам – кегль 12.
9. Электронная версия рукописи представляется в формате Microsoft Office Word (версии – не выше MS Word 2003). Для записи формул следует использовать встроенный редактор Microsoft Equation с параметрами: основной математический символ – 12 пт, индекс – 6 пт. Формат переменных в тексте и формулах должен быть идентичным (желательно курсивом, греческие символы – прямые).
10. Электронный вариант иллюстраций представляется в отдельных файлах в одном из следующих форматов: tif, cdr (CorelDraw 11) черно-белые или с градацией серого, поименованные фамилией первого автора.
11. Иллюстрации к рукописи (рисунки, фото, таблицы), по какой-либо причине не предоставляемые в электронном виде, должны быть аккуратно выполнены на белой бумаге или представлены в виде качественных фотографий. Их размеры не должны превышать формат А4. На оборотной стороне каждой иллюстрации указывается ее порядковый номер, подрисуночная надпись и фамилия первого автора.
12. Перечень ссылок подается языком оригинала, составляется в порядке упоминания в тексте и в соответствии с требованиями ВАК Украины на библиографическое описание (см. приложение).
13. Авторы сообщают о себе следующие сведения: фамилию, имя, отчество, служебный и домашний адрес, телефон, факс, e-mail, указывают с кем из авторов предпочтительнее вести переписку.

Рукописи направляются по адресу:
Научный физико-технологический центр МОН и НАН Украины, пл. Свободы, 6, г. Харьков, 61022, а/я 4499, Украина,
E-mail: journal_pse@ukr.net

Приложение

1. Бизюков А.А., Луценко Е.И., Середа Н.Д., Фареник В.И., Юнаков Н.Н. Влияние электростатической неустойчивости на разрядные характеристики плазменного ускорителя с анодным слоем//УФЖ.– 1985.– Т.30, № 7. – С. 1030-1032.
2. Зыков А.В., Качанов Ю.А., Фареник В.И. Генерация потока ионов из пучкового фокуса// Письма в ЖТФ. – 1986. – Т. 12, вып. 10. – С. 593-596.
3. Zykov A.V., Dudin S.V., Farenik V.I. Low Energy Intense Ion Beams Space Charge Neutralization//Review of Scientific Instruments. – 1994. – Vol. 65, № 4. – P. 1451-1453.
4. Источник ионов: А.с. 1144548 СССР, МКИ 6 H01J 25/34C./А.В. Зыков, Ю.А. Качанов, В.И. Фареник, Н.Н. Юнаков (СССР). – № 3663766/25; Заявлено 16.11.83; Опубл. 20.06.95, Бюл. № 17. – 6 с. ил.
5. Егоренков В.Д., Лисовский В.А., Красников О.Б., Фареник В.И. Влияние растущих поли-мерных пленок на ВАХ ВЧЕ-разряда в технологических газах//Материалы IV международной конференции по физике и технологии тонких пленок. – Ивано-Франковск. – 1993. – С. 154.
6. Вербицкий В.Г. Ионные нанотехнологии в электронике.– К.: «МП Леся», 2002. – 376 с.

ПРАВИЛА ОФОРМЛЕННЯ РУКОПИСІВ

У поданій роботі чітко й послідовно викладаються оригінальні, отримані автором (авторами) результати, що раніше не публікувалися. Рукопис не не має перебувати на розгляді до публікації в іншому видавництві.

1. Роздрукований рукопис, з підписами всіх авторів, надається в 1 прим. однією з мов: українською, російською або англійською. Електронний варіант рукопису подається на магнітному або оптичному носії, або (що зручніше) надсилається по E-mail.
2. До рукопису додаються такі документи: направлення від установи, де виконана робота; заява на ім'я головного редактора з відомостями про авторів; експертний висновок про можливість опублікування роботи у відкритій пресі (для громадян України); зовнішня рецензія, підписана доктором наук.
3. Послідовність розміщення матеріалу рукопису: індекс за універсальною десятковою класифікацією (УДК); назва статті; ініціали й прізвище автора (авторів); повні поштові адреси установ, у яких виконана робота; анотація та ключові слова; текст; перелік посилань; ілюстрації; підписи до рисунків і таблиць.
4. Назва статті, ініціали та прізвище автора (авторів), анотація та ключові слова подається українською (для громадян України), російською (для громадян СНД) і англійською (для всіх авторів) мовами. Обсяг анотації не перевищує 100 слів.
5. Текст рукопису бажано структурувати розділами: ВСТУП, де коротко формулюються передісторія проблеми та мета даного дослідження. Основна частина публікації, містить постановку задачі, експериментальний і/або теоретичний опис досліджень. Висновок, у якому викладено результати досліджень, висновки, перспективи розвитку досліджень і можливі застосування.
6. Повний обсяг оглядової статті не повинен перевищувати 60-ти сторінок, оригінальної статті – 20 сторінок, короткого повідомлення – 5-ти сторінок.
7. Всі фізичні величини подаються в одиницях системи СІ.
8. Вимоги до оформлення рукопису. Параметри сторінки: формат – А4 (210×297 мм). Поля: праворуч – 10 мм, інші – 20 мм. Шрифт: Times New Roman, міжрядковий інтервал – полуторний. Назва статті – прописними, кегль 14. Автори, анотація, текст рукопису, формули, перелік посилань, підпису до рисунків і таблиць – кегль 12.
9. Електронна версія рукопису подається у форматі Microsoft Office Word (версії – не вище MS Word 2003). Для запису формул бажано застосовувати вбудований редактор формул Microsoft Equation з параметрами: основний математичний символ – 12 пт; індекс – 6 пт. Формат змінних у тексті й формулах мають бути ідентичними (бажано курсивом, грецькі символи – прямі).
10. Електронний варіант ілюстрацій подається в окремих файлах одним із форматів: tif, cdr (CorelDraw 11) черно-білі або з градацією сірого, пронумеровані та пойменовані прізвищем першого автора.
11. Ілюстрації до рукопису (рисунки, фото, таблиці), що якоїсь причини не можуть бути надані в електронному вигляді, мають бути акуратно виконані на білому папері або подані у вигляді якісних фотографій. Їхні розміри не повинні перевищувати формат А4. На зворотному боці кожної ілюстрації вказується її порядковий номер, підпис до рисунку і прізвище першого автора.
12. Перелік посилань подається мовою оригіналу, складається в порядку посилання в тексті й відповідно до вимог ВАК України на бібліографічний опис (див. додаток).
13. Автори повідомляють про себе такі відомості: прізвище, ім'я, по батькові, службова й домашня адреси, телефон, факс, E-mail, указують автора з ким з зручніше вести переписку.

Рукописи надсилаються на адресу:

Науковий фізико-технологічний центр МОН і НАН України, м. Свободи, 6, м. Харків, 61022, а/с 4499, Україна
E-mail: journal_pse@ukr.net

Додаток

1. Бизюков А.А., Луценко Е.И., Середа Н.Д., Фареник В.И., Юнаков Н.Н. Влияние электростатической неустойчивости на разрядные характеристики плазменного ускорителя с анодным слоем//УФЖ. – 1985. – Т. 30, № 7. – С. 1030-1032.
2. Зыков А.В., Качанов Ю.А., Фареник В.И. Генерация потока ионов из пучкового фокуса //Письма в ЖТФ. – 1986. – Т. 12, вып. 10. – С. 593-596.
3. Zykov A.V., Dudin S.V., Farenik V.I. Low Energy Intense Ion Beams Space Charge Neutralization//Review of Scientific Instruments. – 1994. – Vol. 65, № 4. – P. 1451-1453.
4. Источник ионов: А.с. 1144548 СССР, МКИ 6 H01J 25/34С./А.В. Зыков, Ю.А. Качанов, В.И. Фареник, Н.Н. Юнаков (СССР). – № 3663766/25; Заявлено 16.11.83; Опубл. 20.06.95, Бюл. № 17. – 6 с. ил.
5. Егоренков В.Д., Лисовский В.А., Красников О.Б., Фареник В.И. Влияние растущих полимерных пленок на ВАХ ВЧЕ-разряда в технологических газах/ Материалы IV международной конференции по физике и технологии тонких пленок. – Ивано-Франковск. – 1993. – С. 154.
6. Вербицкий В.Г. Ионные нанотехнологии в электронике.– К.: «МП Леся», 2002. – 376 с.

INFORMATION FOR AUTHORS

The paper should clearly represent original, unpublished earlier results obtained by the author (authors). The manuscript must not be considered elsewhere for publication.

Only for the citizens of Ukraine the article should have a direction from the institution, where the work was made, and sanction to its open publication.

The journal publishes reviews, original articles and brief reports. The length of the review article should not in general exceed 60000 words, original article – 15000 words and brief report – 5000 words.

The paper is signed by all the authors. The authors inform about: surname, name, patronymic, office and home addresses, tel./fax, E-mail and indicate the corresponding author.

The manuscript is represented in two hard copies in one of three languages: Ukrainian, Russian or English. It is desirable to prepare the manuscript in English and its electronic version on diskette or to send it by E-mail.

The paper copies should be prepared with sesquialteral line spacing and wide margins, on numbered sheets. The format of page is A4 (210×297 mm). The font is Times New Roman.

Structure of the paper. Classification codes (UDS or PACS). Article title. Authors. Affiliations. Abstract and keywords. Main text. Acknowledgements. Appen-dices. References. Figures. Figure captions. Tables.

Abstract. Abstract and keywords is represented in two languages: English and the paper language. Abstract is submitted in Ukrainian for the citizens of Ukraine. The length of Abstract does not exceed 100 words.

Main text. It is desirable to divide the Main text in the following sections: 1) Introduction. 2) Main part (Theoretical methods. Experimental details. Results. Discussion.). 3) Conclusion.

References. References should be numbered consecutively (in square brackets) through out the text and listed by number in the reference list. Listed references should be complete in all details including article titles. Please refer to the first issue of the journal or see: http://www.pse.scpt.org.ua, Appendix for examples.

Illustration. Illustrations are submitted in two copies. Illustrations should be prepared on white paper or can be photographs. The line drawing should be prepared in black Indian ink. The photographs should be originals with somewhat more contrast than is required in the printer version. The size of illustrations should not exceed the A4 format.

Electronic version. The electronic version of the article is represented in the format of Microsoft Word. It is desirable to use the editor of Microsoft Equation for printing mathematical equations and formulae. The electronic form of the illustrations is represented in graphics files: tif, cdr (CorelDrow 11) – black-white , for the microphotographs – with a grey gradation named by the surname of the author on a diskette or via E-mail. The electronic form of illustration (in graphic files) should be kept separately from the text files. The graphic files must be prepared with resolution 300 dpi and above.

Please write to the Publisher for details.

The paper should be sent to the Publisher, Editorial office, Scientifical Center of Physics and Technology, MES and NAS Ukraine, 6 Svobody sq, Kharkiv, 61022, box 4499, Ukraine.

E-mail: journal_pse@ukr.net

Appendix

1. Zykov A.V., Dudin S.V., Farenik V.I. Low Energy Intense Ion Beams Space Charge Neutralization//Review of Scientific Instruments. – 1994. – Vol. 65, № 4. – P. 1451-1453.
2. Baglin V., Bojko J., Grobner O., Henrist B., Hilleret N., Scheuerlein C., Taborelli M. The secondary electron yield of technical materials and its variation with surface treatment//7th European Particle Accelerator Conference.– Vienna (Austria). – 2000. – P. 217.
3. Raizer Y.P., Shneider M.N., Yatsenko N.A. Radio-Frequency Capacitive Discharges. – CRC Press: Boca Raton, 1995. – 300 p.

Тематичні напрямки:

- фізика поверхні – модифікації, покриття, плівки, приповерхні і перехідні шари різних видів, як результат впливу плазми, корпускулярно-фотонних потоків і випромінювання;
- взаємодія різноманітних видів випромінювання з поверхнями металів, напівпровідників, діелектриків;
- фізика і техніка низькотемпературної плазми;
- фізика і техніка лазерів;
- фізичні властивості плівок і покриттів;
- нанофізика, мікро- і нанотехнології, мікро- і наноелектроніка;
- фізичні та технічні аспекти сучасних технологій обробки поверхні, діагностики і контролю технологічних процесів.

Тематические направления:

- физика поверхности – модификации, покрытия, пленки, приповерхностные и переходные слои различных видов, как результат воздействия плазмы, корпускулярно-фотонных потоков и излучения;
- взаимодействие разнообразных видов излучения с поверхностями металлов, полупроводников, диэлектриков;
- физика и техника низкотемпературной плазмы;
- физика и техника лазеров;
- физические свойства пленок и покрытий;
- нанофизика, микро- и нанотехнологии, микро- и наноэлектроника;
- физические и технические аспекты современных технологий обработки поверхности, диагностики и контроля технологических процессов.

Topic directions:

- surface physics - modification, coating, film, near-surface and transient layers of different kinds, as outcome of influencing of plasma, corpuscular - photon flows and radiation;
- interaction of miscellaneous kinds of radiation with surfaces of metals, semiconductors, dielectrics;
- physics and engineering of low-temperature plasma;
- physics and engineering of lasers;
- physical characteristics of films and coatings;
- nanophysics, micro and nanoelectronics, micro and nanotechnologies;
- physical and engineering aspects of modern technologies of surfacing, diagnostic and control of technological processes.

Наукове видання

Фізична інженерія поверхні
Том 11, № 3, 2013

Українською, російською та англійською мовами

Комп'ютерне верстання Бєляєва Т.М., Бурштинська Л.В., Дудіна Н.Г.
Макет обкладинки Дончик І.М.

Підписано до друку 28.10.2013 р. Формат 60×84/8. Папір офсетний. Друк ризографічний.
Ум. друк. арк. 9.2. Обл-вид. арк. 10,6. Тираж 100 пр. Ціна договірна.

61022, м. Харків, майдан Свободи, 6.
Харківський національний університет імені В.Н. Каразіна
Інститут високих технологій

Надруковано: ХНУ імені В.Н. Каразіна
61077, Харків, майдан Свободи, 4.
Видавництво
Тел. 705-24-32
Свідоцтво суб'єкта видавничої справи ДК № 3367 від 13.01.09

2013
Физическая инженерия поверхности
Vol. 11, No. 3
Фізична інженерія поверхні
Том 11, № 3
Physical surface engineering

Виповнилося 85 років Національному науковому центру «Харківський фізико-технічний інститут» Національної академії наук України

Харківський фізико-технічний інститут (ХФТІ, раніше називався Українським ФТІ), один з найстаріших і найбільший центр фізичної науки в Україні, був створений у 1928 році з метою розвитку актуальних наукових напрямів (у той час - ядерної фізики та фізики твердого тіла). Вже через чотири роки, 10 жовтня 1932 року, був отриманий видатний результат - здійснено розщеплення ядра атома літію. У наступні роки у ХФТІ отримані рідкі водень і гелій, побудована перша радіолокаційна установка. Інститут став родоначальником високовакуумної техніки, на основі якої згодом було розвинуто новий фізико-технологічний напрямок - вакуумна металургія. Тут працювали відомі радянські фізики І.В. Обреїмов, А.К. Вальтер, К.Д. Синельников, О.І. Лейпунський, Г.Д. Латишев, Л.В. Шубников, І.В. Курчатов, Л.Д. Ландау, Є.М. Ліфшиць, І.М. Ліфшиць, В.Є. Іванов та інші.

У післявоєнні роки ХФТІ - один із активних учасників робіт над проблемою використання атомної енергії в СРСР. У промисловість впроваджені нові матеріали, масштабні технологічні процеси і установки, зокрема: технологія виготовлення тепловиділяючих елементів для атомних реакторів нового типу; технологія виробництва високотемпературних нагрівачів; технологія нанесення жароміцних, твердих і надтвердих покриттів на матеріали, які працюють в агресивних середовищах; технології зміцнення металорізального інструменту і деталей машин; вакуумні прокатні стани і технологія гарячої прокатки багатошарових матеріалів у вакуумі; високочисті матеріали та сплави на їх основі; надпровідники; композиційні вуглець-вуглецеві матеріали; малогабаритні прискорювачі заряджених частинок та інші.

Після розпаду СРСР інститут активно включився в процес становлення науково-технічного комплексу України, а також у формування політики та відповідних інститутів України у галузі атомної промисловості, ядерної енергетики, у визначення подальшої долі ядерної зброї, яка дислокувалася в Україні, у розвиток матеріалознавства, прискорювальної техніки і нових джерел енергії для потреб держави. У ХФТІ є велика кількість унікальних експериментальних установок, у тому числі ряд електронних та іонних прискорювачів, включаючи найбільший на пострадянському просторі лінійний прискорювач електронів, сімейство термоядерних установок «Ураган», крупне дослідно-експериментальне виробництво.

Гордістю ННЦ ХФТІ завжди були наукові школи, які з покоління в покоління передавали безцінне надбання - наукові знання і досвід. Всьому світу відомі школи академіків Л.Д. Ландау, К.Д. Синельникова, А.К. Вальтера, І.М. Ліфшиця, В.Є. Іванова, Б.Г. Лазарєва, О.І. Ахієзера, Я.Б. Файнберга, Д.В. Волкова. Вся вищезазначена діяльність дала можливість зберегти ці наукові школи і створити привабливу атмосферу для вчених, що є необхідною умовою подальшого розвитку наукових і технологічних досягнень.